No. 314
June 1990

PREDICTING COMPLICATED DYNAMICS LEADING TO VESSEL CAPSIZING

Jeffrey M. Falzarano

THE DEPARTMENT OF NAVAL ARCHITECTURE AND MARINE ENGINEERING

THE UNIVERSITY OF MICHIGAN

COLLEGE OF ENGINEERING

PREDICTING COMPLICATED DYNAMICS LEADING TO VESSEL CAPSIZING

by

Jeffrey M. Falzarano

A dissertation submitted in partial fulfillment
of the requirements for the degree of
Doctor of Philosophy
(Naval Architecture and Marine Engineering)
in The University of Michigan
1990

Doctoral Committee:

Associate Professor A.W. Troesch, Chairperson
Associate Professor M.M. Bernitsas
Assistant Professor J.W. Grizzle
Professor M.G. Parsons
Associate Professor S.W. Shaw, Michigan State University

some relevant quotes

Data aequatione quotcunque fluentes quantitae involvente fluxiones invenire et visa versa...
(It is important to study differential equations...)
Sir Issac Newton (Arnold, (1978))

Ce qui nous rend ces solutions périodiques si précieuses, c'est qu'elles sont, pour ainsi dire, la seule brèche par où nous puissions essayer de pénétrer dans une place jusqu'ici reputée inabordable.
(What makes these periodic solutions so precious for us, is that they are, so to speak, the only breach through which we can try to penetrate a domain that, until now, had the reputation of being inaccessible.)
Henri Poincaré (Minorsky, (1962))

To my parents, who have supported me throughout my education

ACKNOWLEDGEMENTS

I would like to thank the US Coast Guard Office of Research and Development/Michigan Sea Grant for their financial support (NA89AA-D-SG083); specifically, our technical monitor on this project Mr. Jim White, for his interest in the work. I would also like to thank the US Coast Guard Office of Merchant Marine which sponsored a previous research project (DTCG23-86-F-01167) that inspired the current work. I would like to thank my the department of Naval Architecture and the Rackham School of Graduate Studies for their support, especially of my trip to Vienna but in many other ways too. I would like to thank the members of my dissertation committee whose advice and healthy skepticism made this work possible and assured its realism and accuracy. I would also like to thank the various other experts in nonlinear and ship dynamics who reviewed our original proposal for research and continued to provide us with assistance. These experts include Professors Robert Beck, Steven Wiggins, Jerrold Marsden, Vladimir Igororevich Arnold, Fotis Papoulias, Anthony Bloch, Noel Perkins, and Leon Chua. I would also like to thank Professor Hans Troger and Doctors Anton Stribersky and Alois Stiendl for arranging my visit and working with me before, during and since my visit to the Institute for Mechanics, of the Vienna (Austria) Technical University and for the invaluable knowledge that I obtained from them all.

Finally, I would like to thank my family and friends (some of whom are included above) for making my stay in Ann Arbor just a little more interesting and enjoyable than it would have otherwise been.

PREFACE

This thesis represents an effort by one naval architect to analyze the important and practical age-old problem of nonlinear ship rolling motion and motion stability using the most modern methods available from other fields. Although some of the methods used in this work may be unfamiliar to ship design naval architects, most of the methods used herein represent the best and most recent techniques available from applied mathematics, applied mechanics, mechanical engineering and electrical engineering for analyzing periodically forced nonlinear time-varying systems. In the recent past, when confronted with a highly nonlinear problem, one might be tempted to say "give me a big enough computer and I can integrate any system of differential equations, ordinary or partial..." This may not always be the most efficient or enlightening method of analysis. This thesis specifically addresses this problem and I hope will provide a convincing argument for the value of qualitative analysis of differential equations.

Clearly, the emphasis of this thesis is the qualitative analysis of nonlinear differential equations. The specific system to be analyzed is the periodically forced nonlinear roll equation in isolation or coupled with the other modes of motion. An important discovery of this work is the complicated dynamics which may occur when a vessel has an initially negative roll restoring moment and an eventual positive roll restoring moment at some small but finite loll angle. Such a situation may occur because of the presence of water trapped on the the deck of a small fishing vessel. Much of the emphasis of this work is devoted to analyzing this situation using an approximate model

and applying specialized techniques to predict and analyze the surprising dynamics that may occur. Although simulation of the approximate model is almost trivial to apply to this problem, its results are still interesting and enlightening. In addition to using simulation to analyze this problem, we also apply various qualitative or geometric analysis techniques. These methods include Melnikov's method, the study of invariant manifolds, lobe dynamics, Lyapunov exponents and bifurcation theory.

This work is meant to clarify and extend the simple analysis and realistic simulation that was performed as part of a previous project (Falzarano, (1988)). The material included in this thesis involves applying existing techniques to the specific problem at hand, clarification of certain aspects of existing techniques; explaining, reporting and condensing from several diverse sources existing techniques; and finally reporting some extensions of general theory and techniques to circumstances which have not been previously reported. It is my hope that, after reading this thesis, the reader will have a reasonably complete picture of what is available from other fields to analyze similar problems and what types of interesting dynamic behavior are possible for a small fishing vessel that is damaged or has water trapped on deck.

TABLE OF CONTENTS

DEDICATION ii

ACKNOWLEDGEMENTS iii

PREFACE iv

LIST OF FIGURES viii

LIST OF APPENDICES xii

LIST OF TABLES xiii

CHAPTER

I. INTRODUCTION 1

Summary of the coming chapters

II. BACKGROUND 7

Motivation
Previous work
Related studies
Other ship stability research

III. FORMULATION OF THE SHIP DYNAMICS PROBLEM 11

Equations of motion
Linearization of the equations of motion
The approximation to the water-on-deck force
The importance of nonlinear roll dynamics
The importance of chaotic dynamics in our ship dynamical systems
Overview of various approximations to be used

IV. LOCAL BIFURCATION AND STABILITY ANALYSIS OF THE SHIP DYNAMICAL SYSTEM 36

Numerical path following techniques

Stability of periodic solutions
Practical application of BIFPACK
Bifurcation theory and the slowly turning vessel

V. POINCARÉ MAPS AND INVARIANT MANIFOLDS OF MARINE DYNAMICAL SYSTEMS 46

Poincaré maps
Invariant manifolds
Invariant manifolds as boundaries of behavior

VI. MELNIKOV'S METHOD APPLIED TO THE SHIP DYNAMICAL SYSTEM 58

The homoclinic case
Consideration of heteroclinic orbits
Evaluation of approximations and more realistic systems
Alternative criteria for complicated dynamics
Relationship between transverse intersections and chaos

VII. LOBE DYNAMICS FOR THE SHIP DYNAMICAL SYSTEM 76

The relationship between vessel capsizing and lobe dynamics
Practical aspects of lobe dynamics
Basin boundary metamorphasis

VIII. APPLICATIONS AND RESULTS 88

Applications of geometric methods
Comparative simulation studies
Some qualitatively different motions
Parametric excitation

IX. OBSERVATIONS AND CONCLUSIONS 147

X. FUTURE WORK 153

Multi-frequency forcing
Parametric excitation and a bias

APPENDICES 156

BIBLIOGRAPHY 182

LIST OF FIGURES

Figure		
3.1	Ship coordinate system	13
3.2	Euler angles rotation sequence (Thelander, (1964))	14
3.3	Roll restoring moment curve unmodified and modified	24
3.4	Pitchfork bifurcation diagram and phase portraits	25
3.5	Phase portraits with a) homoclinic and b) heteroclinic connections	26
3.6	Pictorial comparison of various righting arms considered	35
4.1	Magnification diagram, bifurcations occur at vertical tangent	41
4.2	Invariant manifolds in the Poincaré map	43
5.1	The Poincaré section in the extended phase space (Thompson and Stewart, (1986))	48
5.2	The Poincaré section in the cylindrical phase space (Moon, (1989))	49
5.3	Phase portrait of undamped unforced pendulum (Guckenheimer and Holmes, (1986))	50
5.4	Phase portrait of unforced damped pendulum (Parker and Chua, (1989))	51
5.5	Invariant manifold of the Poincaré map (Parker and Chua, (1989))	55
5.6	Boundary between safe and unsafe region	57
6.1	Homoclinic orbits, a) unperturbed b) damped c)periodically forced	60
6.2	Regions of periodic and chaotic motion mixed (Moon, (1988))	63
6.3	Wire-frame plot of invariant manifolds in three-dimensions	70
6.4	Various cases for maximum amplitude (Rudowski and Szemplinska-Stupnika, (1989)	73
6.5	Poincaré maps of intersected manifolds	74
6.6	Poincaré maps of re-intersected manifolds and tangles	75
7.1	Multiple attractors and basins of attraction	77

B.1 Multi-dimensional manifolds a) before and b) after intersection . . . 168
C.1 Deviation of known solution with respect to time (Seydel, (1988)) . 170
C.2 Mechanisms for losing stability (Seydel, (1988)) 173
D.1 Evolution of an initial condition sphere with time (Moon, (1988)) . 175
D.2 Lyapunov exponent from a time series replacement (Wolf, et al., (1985)) 178
E.1 Derivation of modified righting arm curve from reference 181

LIST OF APPENDICES

Appendix

A. The Mathematical Details of the Melnikov Function 157

B. Discussion of the Melnikov Vector 164

C. Stability of Periodic Solutions and the Monodromy Matrix 169

D. Quantifying Complicated Ship Dynamics with Lyapunov Exponents . . . 174

E. Modification to the Righting Arm Curve 180

LIST OF TABLES

Table

3.1	Chapters where various approximations have been considered	35
8.1	Least stable eigenvalues for $\omega = .45$ and $\eta = .5'$	112
8.2	Most stable eigenvalues for $\omega = .45$ and $\eta = .5'$	112
8.3	Qualitatively different motions $\omega_o = .4$ rad/s, $\beta = 90$ deg	133
B.1	Possible intersections of two manifolds in R^4	168

CHAPTER I

INTRODUCTION

In this thesis we investigate the important naval architectural problem of vessel capsizing with a loll angle due to damage or water-on-deck. This focus has been motivated by a previous project (Falzarano, (1988)) in which a water-on-deck simulation program was developed (Dillingham and Falzarano, (1986a and b)) and used to investigate fishing vessel dynamics. However, the mathematical techniques we describe to analyze fishing vessel capsizing are by no means limited to vessels with a loll angle. On the contrary, we include the loll angle only because of the additional interaction that may occur with the larger amplitude dynamics near the angle of vanishing stability.

The techniques we describe are suitable for analyzing large amplitude vessel motions which may lead to capsizing. We consider the coupled roll (linearly coupled to sway and yaw) motion in regular waves (single-frequency periodic-forcing), and include a nonlinear roll restoring moment curve, and linear and quadratic damping. We investigate the various steady-state solutions and then analyze their phase space boundaries. These boundaries separate the transient behavior that determines whether one or another of these solutions will be the eventual steady-state. For a moderate forcing amplitude, the eventual behavior of a given initial condition is clear since the boundaries are simple. However, as the amplitude is increased beyond some threshold value, the eventual behavior is no longer clear. This threshold

value can be predicted in terms of the physical parameters, using Melnikov's method. Preliminary simulation studies using parameter values representing the twice capsized clam dredge *Patti-B*, exhibited aperiodic response of the periodically forced system. On further investigation, the mechanism leading to chaos was shown to be the transverse intersection of the behavior boundary curves. These boundary curves are called invariant manifolds. Therefore, in this work we investigate the effect of these intersections on the eventual behavior of the vessel.

Although the methods we describe are capable of analyzing the chaotic dynamics that may occur following transverse intersection of the invariant manifolds, these methods are not limited in being able to analyze only chaotic systems. Instead, these techniques are generally applicable to the analysis of any periodically time varying (periodically forced) nonlinear differential equation or system of equations, and the surprisingly complex behavior that can occur. With this as a background, we now describe the specifics. We begin with what we and others have done, and eventually describe a method which allows us to study the dynamics which occur after the manifolds have intersected.

Summary of the coming chapters

In Chapter II, we provide motivation for the current work by describing a few actual small fishing vessel capsizings where water-on-deck was believed to be an important factor. Next, we describe a previous ship stability project (Falzarano, (1988)). Finally, we describe how some of the other nonlinear ship dynamics research groups are analyzing similar problems.

In Chapter III, we describe the ship dynamics aspects of the problem. We begin with the dynamically exact Euler's equation of motion and the associated Euler angle kinematics. Because expressions for general hydrodynamic forces do not yet exist, we use linear, ideal flow hydrodynamics augmented by a nonlinear roll restoring moment,

and linear and nonlinear (quadratic) viscous damping. To be consistent, we linearize the dynamically exact equations, at which point, the roll, sway and yaw modes of motion, for a symmetric ship, decouple from the other modes. We next describe our water-on-deck or damaged approximation which may cause a loll angle. Throughout this chapter, we describe the current state-of-the-art in determining hydrodynamic forces, assess the various classic approximations, and relate this to what types of dynamics analysis are available and what types of dynamics are possible.

In Chapter IV, we describe a numerical path following, bifurcation analysis and stability analysis technique we used for analyzing periodic solutions of the *Patti-B* without water-on-deck or damage subjected to a regular wave train. The goal of using this technique was to assess the accuracy of the single degree of freedom constant (with respect to frequency) hydrodynamics approximation which is commonly used by other researchers of nonlinear ship rolling motion. In order to motivate this assessment, we consider the physical problem of a vessel slowly turning while traveling at a constant forward speed.

In Chapter V, we begin the description of the specialized techniques which are the focus of this work. We describe the procedure to obtain a Poincaré map from a periodically forced (time-varying) ordinary differential equation. Next, we describe the important, increasingly complex boundary curves for 1) the undamped (conservative) and unforced (autonomous), 2) the damped (dissipative) and unforced (autonomous) and finally, 3) the damped (dissipative) and periodically forced (nonautonomous) ordinary differential equations which are the successively more accurate approximations of the nonlinear roll equations of motion. The boundary curves are associated with the nonstable saddle fixed points of the differential equations. These boundary curves separate regions of qualitatively different dynamics. The boundaries in the Poincaré map of the periodically forced equation are called invariant manifolds. For a large enough forcing, these curves may intersect; in this case, simple boundaries

no longer exist and aperiodic dynamics can occur.

In Chapter VI, we describe the Melnikov technique which is used to predict when the previously described manifolds intersect. We begin by describing the simple Melnikov technique suitable for analyzing the manifolds associated with the zero roll (in the unforced system) angle saddle and small amplitude loll angle dynamics, and next apply the technique to the manifolds associated with the saddle at the angle of vanishing stability (in the unforced system) and possibly unbounded (capsizing) motion. We then describe successively more accurate Melnikov analyses including application to models with multiple degrees of freedom, and a more accurate description of the restoring moment curve. In order to approximately describe the multiple degrees of freedom dynamics, we obtain two characteristics which must be satisfied in order to be able to determine an equivalent single degree of freedom system from the multiple degree of freedom system. When employing the more accurate representation of the restoring moment curve, we need to numerically evaluate the Melnikov integral. Not limiting our analysis to the Melnikov technique, we next describe an innovative chaos criterion due to Szemplinska-Stupnicka, (198X) which uses the classic harmonic balance technique. Finally, we describe how the manifold intersections leads to horseshoe dynamics which are a necessary condition for chaos.

In Chapter VII, we describe an innovative technique developed by Wiggins, (1990), called lobe dynamics. After the manifolds have intersected, it is no longer easy to separate qualitatively different behavior. Lobe dynamics allows us to study the dynamics inside the regions bounded by the intersected manifolds, called lobes, in order to continue to predict whether or not an initial condition will eventually become unbounded (the vessel will capsize), or will remain bounded (the vessel is safe).

In Chapter VIII, we demonstrate the practical use of the previously described techniques by applying them to the twice capsized clam dredge *Patti-B*. We begin by

studying the bifurcation and stability of a vessel without a loll angle. We continue by studying the various modern methods previously described. First, we study the manifold intersections and evaluate the accuracy of using two different locally valid cubic approximations to the righting arm curve by comparing them to a numerically determined Melnikov function based upon a single globally valid quintic approximation. Next, we consider how to reduce the multiple degree of freedom system to an equivalent single degree of freedom system. Most importantly, we study the dynamics associated with the lobes in the plane and demonstrate the practical use of this theory to predict safety and capsizing. We continue by showing some simulations around the saddle for the vessel turning problem. Next, we show some qualitatively different types of motion including harmonic, subharmonic and aperiodic. Finally, we present some results for a combined externally and parametrically excited vessel.

In Chapter IX, we summarize the lessons learned during the course of the thesis. Specifically, we describe the appliciability of the results obtained and the generality of the techniques described.

Since no single study can completely answer all the questions associated with vessel stability, in Chapter X, we suggest extensions of the work previously described. As a first step in analyzing a random seaway, we describe how we might consider multiple (finite) frequency forcing. Next, we describe how we could extend the parametrically excited analysis to the case where the parametric and external forcing frequencies are incommensurate. Finally, we describe a suggestion by Troesch, (1990), on how we might use the previous techniques in a probabilistic ship stability criteria. In such a criteria, this work would be the conditional probability of capsize given probabilistically determined initial conditions.

The appendices are included so as to make this work relatively self-contained, yet not to break up the flow of ideas with side topics and excessive mathematics developed by others. Appendix A describes the derivation of the Melnikov function and

how the Melnikov function can be used to study the lobes. Appendix B describes the extension of the Melnikov theory to include additional phase variables. This extension is called the Melnikov vector. The Melnikov vector allows us to study additional phase variables when these variables are slowly varying functions of time as they are in our system. We also attempt to describe some of the geometric complexities of the more complete multiple degree of freedom problem which eludes simple analysis. Appendix C describes the details of the monodromy matrix, which is used to assess stability of periodic solutions and mechanisms for losing stability in such systems. Appendix D describes how to quantitatively describe chaotic dynamics and the associated strange attracting sets which may occur. These numerical techniques are called Lyapunov exponents, Lyapuonv dimensions and attractor reconstruction. Finally, Appendix E describes how a reference righting arm curve can be approximately modified for the effects of water-on-deck or external damage.

CHAPTER II

BACKGROUND

Motivation

The capsizing of small fishing vessels is a serious problem. It is one of the factors contributing to make commercial fishing the most dangerous occupation in the United States (Jons, Fuller, and Letorneau, (1987)). Of the many capsizing mechanisms, the effect of water trapped on deck may be the most important. It is known to have had a dominant effect in at least three capsizings. *Patti-B* is described to have had water-on-deck just before her first capsizing (NTSB, (1979)). Survivors describe the *Joan La Rie* as rolling in bad weather with water-on-deck, then suddenly being hit by an extremely large "freak" wave and capsizing (USCG, (1984)). Eyewitnesses describe the *Hellan-Hansen* in bad weather as heeled (lolled) to one side with water-on-deck after having been hit by a breaking wave, then suddenly being hit by another large wave, and finally capsizing (Dahle and Kjaerland, (1979)). These capsizings seemed to be ultimately linked to the de-stabilizing effect of water-on-deck. In addition, since the *Patti-B* seemed to have surpassed all existing stability recommendations and still capsized, her capsizing seems to be related to additional dynamic effects not considered in the current static criteria. In this work, we attempt to study nonlinear

ship dynamics in a rational and systematic fashion in order to uncover some of these previously neglected important effects.

Previous work

Given the importance of water-on-deck and its dominant effect in many vessel capsizings, an initial investigation (Falzarano, (1988)) was undertaken. Accurate prediction of forces and resulting motions from water-on-deck was a fundamental aspect of that previous work. Other investigators have stressed the importance of predicting water-on-deck effects, but have relied on experiments (e.g., Adee and Pantazopoulos, (1986)). These experiments suggested the importance of the so-called pseudo-static heel angle (loll angle) when water is trapped on deck. However, physical experiments involve unknowns due to scaling and are extremely costly. Thus, they are limited in the number of parameters that can be systematically studied. Numerical prediction is more cost effective because of the availability of large scale computers and the ease with which various parametric effects can be analyzed through simulation. However, numerical prediction techniques are limited by the speed and storage capacity of available computers so that fully solving a given problem, although theoretically possible, may be impractical. In addition, simulations rely heavily on accurate prediction of initial conditions.

Since water-on-deck is believed to be the cause of numerous capsizings, an important aspect of the previous investigation (Falzarano, (1988)) was to develop a realistic numerical model of the combined ship motion and water-on-deck problem for a small vessel in a seaway. This method is carried out in two computer programs that have different time-domain ship motions models (Falzarano, (1988)). The computer program COMBINE is essentially the US Coast Guard supplied computer program CAPSIZE (Paulling, (1979)) extended to include the numerical simulation

of the dynamic effects of water-on-deck. The water-on-deck effect is predicted by using the two-dimensional numerical method of Dillingham, (1979&1981), as extended by Dillingham and Falzarano, (1986a&b). The simulation includes a model for determining how water flows onto/off the deck over the bulwark top, and through the scuppers. The computer program SLOSH2D uses a linear time-domain approach to determine the hydrodynamic restoring forces and the same water-on-deck simulation procedure as COMBINE.

One aspect of the previous investigation (Falzarano, (1988)) was to analyze the twice capsized fishing vessel *Patti-B*. Extensive numerical experiments were carried out using the aforementioned computer programs. These numerical experiments demonstrated sensitivity to initial conditions and system parameters. Although these extensive numerical experiments yielded empirical criteria for the *Patti-B* capsizing, further insight into the causes of water-on-deck capsizing was sought; rationally derived criteria and guidance in undertaking these simulations was needed. In addition, simplified classical ship stability calculations and linear dynamic stability analysis were undertaken. The results of this analysis was also inconclusive and dissatisfying. The current effort draws on the experience gained from the previous work (Falzarano, (1988)), yet applies the most modern and best techniques available from other fields to analyze periodically time varying dynamical systems.

Related studies

Of the current world-wide research in nonlinear ship rolling dynamics, only two other research groups have considered the possibility of complex dynamics occurring. These are the research groups at University College of London (Virgin, (1987)), and Virginia Polytechnic Institute (Nayfeh and Khedir, (1986)). Both of these groups have observed chaotic dynamics due to regular wave excitation of the single frequency single degree of freedom roll equation with and without a static bias. This static bias

may, for example, be due to a steady wind or shifted cargo. Both have determined the route to chaos as the period doubling route. Our approach is unique in that the important practical effects of water-on-deck with multiple degrees of freedom have been investigated using Melnikov's method, in lieu of the empirically observed period doubling route to chaos used by others. This method results in an analytical expression or criterion in terms of the physical parameters of the system (bilge keel size and area of aft deck) to predict the possible occurrence of complicated dynamics.

Other ship stability research

Although the current engineering approach to analyze ship stability uses nonlinear statics, the idea of applying nonlinear dynamics is not new (Mosley, (1850)). Although the use of scale model experiments is common (e.g., Paulling, et al., (1979), Takezawa and Hirayama, (1986) and Grochowaloski, (1989)) using approximate time domain simulation models to analyze extreme (nonlinear) ship dynamics possibly leading to capsizing is also common (e.g., Paulling, et al., (1974), Elsimaillaway and Miller, (1986) and Brook, (1986)). Much work has been done using the idea of stability of motion using Lyapunov functions to predict the boundedness of motion (e.g., Odabassi, (1979), Ozkan, (1981) and Calderia-Saraiva, (1986)). In addition, approximate perturbation schemes have been applied to analyze nonlinear roll motion (e.g., Cardo, et al., (1986), Nayfeh and Sanchez, (1988) and Virgin, (1987)). However, ship stability and nonlinear rolling motion have somehow managed to stay outside the mainstream of ship dynamics (hydrodynamics) research with the exception of some primarily hydrodynamic works (e.g. Vinge and Brevig, (1982) and Braeethen, (1987)). Due to the uncertainty of the environmental conditions, in order to then apply any of these techniques to vessel design, they must then be incorporated into some type of probabilistic criteria which considers the randomness of the environment (Dahle and Myhaurg, (1986)).

CHAPTER III

FORMULATION OF THE SHIP DYNAMICS PROBLEM

Equations of motion

The equations of motion describing a floating body are in general nonlinear and time varying. Depending upon the assumptions and approximations made, these equations are difficult and possibly impossible to solve analytically. Therefore, approximations must be made in order to make any real progress. Many of these approximations are both accurate and realistic. Some classical approximations will be reviewed here. First, consider the zero frequency limit of the frequency dependent coefficients. The slow motion derivatives used in ship maneuvering result. If the motion is slow enough, the frequency dependent wave excitation and wave radiation forces may be neglected. The equations are time independent and possibly nonlinear. Second, consider small amplitude ship motion due to a single frequency wave train; the hydrodynamic properties are constant but the excitation is periodic. In the frequency domain, the sinusoidal time dependence factors out so that the resulting equations are linear and time independent. Third, consider ship motion in a following sea when the encounter frequency is very low; the response is dominated by hydrostatics, but the roll restoring coefficient is periodic so parametric excitation

occurs. The equations are linear but time-varying because of the periodically varying roll restoring moment coefficient. Finally, consider small amplitude time-dependent ship motion due to an arbitrary incident wave. This is transient ship motion. Since waves are met, created, and diffracted, the system has memory, and is accurately described by convolution integrals. The equations are linear but time-varying due to the time dependent convolution integrals. The equations are called linear functional or integro-differential equations. As the amplitude of the transient ship motion increases, the equations become nonlinear and may be described by a Volterra series (Bishop, (1978)).

The purpose of this research has been to gain a clearer practical understanding of what characteristics make a vessel safe or unsafe when exposed to extreme weather conditions. In order to accomplish this goal, the system of differential equations describing the motion has been studied using explicit simplified models, alternative representations of external forces, the methods of dynamical systems and nonlinear oscillations. Particular attention has been paid to the nonlinear and coupled aspects of the equations of motion.

The full nonlinear coupled equations of rigid body motion written in a body fixed axis system are derived in a variety of references (Vugts, (1970), Abkowitz, (1969)); these equations are as follows:

$$X = m[\dot{u} + qw - rv - x_G(q^2 + r^2) + z_G(pr + \dot{q})] \tag{3.1}$$

$$Y = m[\dot{v} + ru - pw + x_G(pq + \dot{r}) + z_G(qr - \dot{p})] \tag{3.2}$$

$$Z = m[\dot{w} + pv - qu + x_G(rp - \dot{q}) - z_G(p^2 + q^2)] \tag{3.3}$$

$$K = I_{44}\dot{p} - (I_{55} - I_{66})qr - I_{64}(\dot{r} + pq) - mz_G(\dot{v} + ru - pw) \tag{3.4}$$

$$M = I_{55}\dot{q} - (I_{66} - I_{44})rp - I_{64}(r^2 - p^2) + mz_G(\dot{u} + qw - rv) - x_G(\dot{w} + pv - qu) \tag{3.5}$$

$$N = I_{66}\dot{r} - (I_{44} - I_{55})pq - I_{64}(\dot{p} - qr) + mx_G(\dot{v} + ru - pw) \tag{3.6}$$

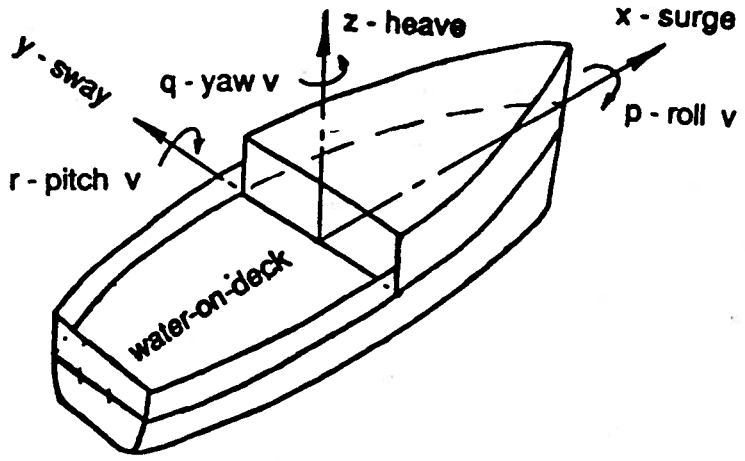

Figure 3.1: Ship coordinate system

Where (X,Y,Z,K,M,N) = $\underline{X}$ are the externally applied forces and moments in the body fixed system, and (u,v,w,p,q,r) = $\underline{u}$ are the translational and rotational velocities in the body fixed system, x_G and z_G are the coordinates of the ship center of gravity. In ship motions calculations, the origin of the coordinate system is usually placed at amidships and at the design waterline. The I_{ij} are the inertia about the specified axes ($i = j$) or cross products of inertia ($i \neq j$). Here, the subscripts are 4 = roll, 5 = pitch, and 6 = yaw. The dots indicate derivatives with respect to time.

When studying large amplitude motion, the supplementary equations in the form of a rotation matrix relating the inertial and body axis rotation rates (Thelander, (1964)) must be considered. To avoid changes in body inertial properties about the fixed axis system, it is standard (in all but infinitesimal motions such as linear ship motions) to adopt the procedure of solving the equations of motion in a body fixed axis system. When using a body fixed system, the rotating or body axis system must be continuously related to the fixed or inertial axis system. Since the rotations are now finite and not infinitesimal, Euler angles are introduced. The standard ship motions axis system (see Figures 3.1 and 3.2), in lieu of the equilibrium axis system commonly used in ship maneuvering, will be considered here. The following rotation order will be used:

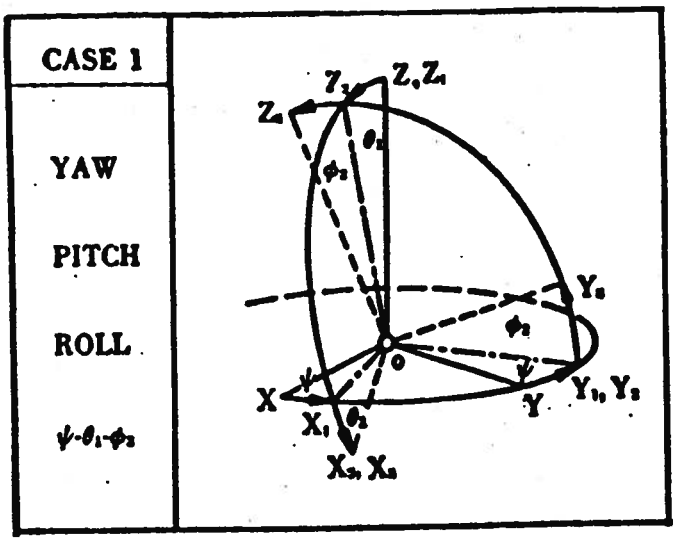

Figure 3.2: Euler angles rotation sequence (Thelander, (1964))

1: yaw ψ right-handed rotation about the inertial z-axis, bow to port is positive.

2: pitch θ right-handed rotation about the yawed y-axis, bow down is positive.

3: roll ϕ right-handed rotation about the yawed and pitched x-axis, starboard down is positive.

Furthermore, the supplementary system of differential equations relating the time derivatives of the Euler angles $(\dot{\psi}, \dot{\theta}, \dot{\phi})$ and angular velocities in the body fixed system (p, q, r) must be considered.

$$\begin{pmatrix} \dot{\phi} \\ \dot{\theta} \\ \dot{\psi} \end{pmatrix} = \begin{pmatrix} 1 & \sin(\phi)\tan(\theta) & \cos(\phi)\tan(\theta) \\ 0 & \cos(\phi) & -\sin(\phi) \\ 0 & \sin(\phi)\sec(\theta) & \cos(\phi)\sec(\theta) \end{pmatrix} \begin{pmatrix} p \\ q \\ r \end{pmatrix}$$

This implies that derivatives of the Euler angles are not exactly equal to body fixed angular velocities. Kinematically, the translational quantities in the body system (x_b, y_b, z_b) must be related to the inertial system (x,y,z).

$$\begin{pmatrix} x_b \\ y_b \\ z_b \end{pmatrix} = \begin{pmatrix} \cos(\psi)\cos(\theta) & \sin(\psi)\cos(\theta) & -\sin(\theta) \\ \sin(\phi)\sin(\theta)\cos(\psi) & \sin(\phi)\sin(\theta)\sin(\psi) & \\ \quad -\cos(\phi)\sin(\psi) & \quad +\cos(\phi)\cos(\psi) & +\sin(\phi)\cos(\theta) \\ \cos(\phi)\sin(\theta)\cos(\psi) & \cos(\phi)\sin(\theta)\sin(\psi) & \\ \quad +\sin(\phi)\sin(\psi) & \quad -\sin(\phi)\cos(\psi) & +\cos(\phi)\cos(\theta) \end{pmatrix} \begin{pmatrix} x \\ y \\ z \end{pmatrix}$$

It is important that the order of these rotations be followed, since finite rotations are not vectors as are infinitesimal rotations. Therefore, finite rotations do not commute. This fact can be easily demonstrated by considering two different rotation sequences. As an example, consider ψ, θ, ϕ, and ϕ, θ, ψ, rotations of 90 degrees each. After these two rotation sequences, the body will settle to two different orientations.

Linearization of the equations of motion

In order to obtain the linear seakeeping equations from Euler's equation of motion, a systematic linearization is performed (Vugts, (1970)). The nonlinear inertial terms drop out and the only nonlinear terms that are retained are the nonlinear roll restoring moment and the nonlinear viscous roll damping. Furthermore, the kinematic relationship between the body fixed rotation rates (p,q,r) and the derivatives of the Euler angles ($\dot{\psi}$, $\dot{\theta}$, $\dot{\phi}$) becomes an identity.

Following standard practice (Vugts, (1970)), consider all velocities to be small relative to some reference quantity, or alternatively, consider the motion to be restricted to a small neighborhood about the origin. This procedure can be generalized to consider non-zero equilibria. Following this procedure, the above nonlinear equations of motion become the linearized equations of motion and are as follows,

$$X = m[\dot{u} + z_G\dot{q}] \tag{3.7}$$

$$Y = m[\dot{v} + x_G\dot{r} - z_G\dot{p}] \tag{3.8}$$

$$Z = m[\dot{w} - x_G\dot{q}] \tag{3.9}$$

$$K = I_{44}\dot{p} - I_{64}\dot{r} - mz_G\dot{v} \tag{3.10}$$

$$M = I_{55}\dot{q} + m(z_G\dot{u} - x_G\dot{w}) \tag{3.11}$$

$$N = I_{66}\dot{r} - I_{64}\dot{p} + mx_G\dot{v}. \tag{3.12}$$

To first order, the rotation about a fixed or moving axis system become identical.

Determining the general (nonlinear) force vector $\underline{X}$ of equations 3.1-3.6 is difficult if possible at all. For general body motion, it has not yet been done. It requires solving the three-dimensional hydrodynamics problem of a body floating on the free surface. Although various representations of these forces are possible, for simplicity we follow Vugts (Vugts, (1970)) and consider small amplitude motion in an ideal fluid. These normal forces are obtained by integrating the pressure over the body surface. First order terms proportional to unit body motion (displacement, velocity and acceleration) and incident wave amplitude are obtained. Forces [1] proportional to unit body displacement are the hydrostatic forces **C**, forces proportional to unit body acceleration are called the added mass forces **A**, and forces proportional to unit body velocity are called damping forces **B**. The forces due to the incident wave are called wave exciting forces $\underline{F}(t)$. If the system is linear and the excitation is due to a single frequency wave (i.e., $\underline{F}(t) = \underline{F}_o e^{i\omega t}$), then the matrices **A** and **B** are constant. The matrix **M** is made up of the physical mass or inertias about the specific axis plus the inertial and coordinate coupling. The elements of the matrices A_{ij}, B_{ij}, and C_{ij}

---

[1] We note here that when we refer to forces and motions, we refer to generalized forces and motions which are forces and moments, and translational and rotational motions (displacements, velocities or accelerations), respectively.

are the forces in the ith mode of motion due to a unit motion (acceleration, velocity or displacement) in the jth direction of motion. The mass matrix M_{ij} contains the appropriate mass, inertial or coordinate coupling terms. The subscripts refer to the mode of motion and are: 1=surge, 2=sway, 3=heave, 4=roll, 5=pitch and 6=yaw (see Figure 3.1). Considering only these forces, the well-known frequency domain representation of the seakeeping equations are obtained,

$$(\mathbf{M} + \mathbf{A})\ddot{x} + \mathbf{B}\dot{x} + \mathbf{C}x = \underline{F}(t). \tag{3.13}$$

Note from the linearized equations that no inertial coupling exists between the symmetric (surge, heave and pitch) and the asymmetric (sway, roll and yaw) modes of motion. Moreover, owing to port-starboard symmetry of the underwater body of a typical ship, there is no hydrodynamic coupling either. Therefore, for the remainder of this work we will consider only the sway, roll and yaw equations. In order to concentrate on the linear coupling between the asymmetric modes and yet not ignore important ($O(1)$) nonlinear effects, we consider the linear seakeeping equations supplemented with an empirically derived linear and quadratic viscous roll damping and a calculated nonlinear roll restoring moment curve. We note here that other investigators (Marshall, Nayfeh, and Mook (1973)) have considered the possibility of a pitch-roll coupling when the roll and pitch natural frequencies are related by an integer ratio. In lieu of this, we consider the possibly more general effect which is realized when roll is parametrically excited by a passing wave. This is briefly discussed in the "Applications and Results" chapter (Chapter VIII). The viscous damping is calculated component-wise using the methods described by Himeno, (1981) and the nonlinear roll restoring moment curve is calculated using the ship hydrostatics computer program STAAF (InterCAD, 1983).

To express the system 3.13 in Cauchy standard form, multiply through by the inverse of the mass and added mass matrix $(\mathbf{M} + \mathbf{A})^{-1}$ and define $y = \dot{x}$. The

following equations are obtained,

$$\dot{y} = -\mathbf{B}^* y - \mathbf{C}^* x + \underline{F}^*(t) + g(x) \tag{3.14}$$

$$\dot{x} = y. \tag{3.15}$$

Here the matrices $\mathbf{B}^*$ and $\mathbf{C}^*$, and the vectors $\underline{F}^*(t)$ and $g(x)$, have already been multiplied by the inverse of the mass plus added mass matrix. We note here that the only phase variables of interest are sway velocity, roll velocity, yaw velocity and roll displacement since nowhere in the equations of motion do forces porportional to sway and yaw displacement appear. Therefore, our extra equation is one dimensional and merely defines the derivative of roll displacement as the roll velocity.

Next, define

$$\begin{pmatrix} z \end{pmatrix} = \begin{pmatrix} y \\ x \end{pmatrix}$$

and finally, the system below is obtained,

$$\dot{z} = \mathbf{K} z + h(z,t) \tag{3.16}$$

Where the matrix $\mathbf{K}$ contains all the linear time invariant force coefficients and the vector $h(z,t)$ are the nonlinear and time-varying forces. The calculation of the linear hydrodynamic restoring forces are performed using the linear frequency domain ship motions computer program SHIPMO (Beck and Troesch, (1989)). These coefficients are determined by solving a series of linear boundary value problem one at each frequency.

The frequency dependence of the hydrodynamic forces

The frequency dependence of the linear hydrodynamics is well-known (Newman, (1977))(Vugts, (1970)) in the ship dynamics field. The frequency dependence is easily demonstrated by considering the zero and infinite frequency limits of the linear combined free surface boundary condition. Recall, that the linear hydrodynamic coefficients are determined as the solution of a boundary value problem using the linear frequency domain ship motions computer program SHIPMO (Beck and Troesch, (1989)). One form of the boundary condition on the free surface for the velocity potential is the combination of the kinematic and dynamic free surface conditions, which results in,

$$\frac{\partial^2 \phi}{\partial t^2} + \frac{\partial \phi}{\partial z} = 0. \tag{3.17}$$

For a single frequency excitation, with $e^{i\omega t}$ time dependence, the above relationship (equation 3.17) becomes,

$$\omega^2 \phi + g \frac{\partial \phi}{\partial z} = 0. \tag{3.18}$$

In the limit as $\omega \rightarrow 0$, the above boundary condition (equation 3.18) approximately becomes:

$$\frac{\partial \phi}{\partial z} = 0. \tag{3.19}$$

This implies that we have no vertical fluid velocity at the free surface ($z = 0$); we get mirror image (opposite) double body motion for the heave, pitch and roll motions, and the same image double body motion for the surge, sway and yaw motions. Physically, we may consider the body motion to occur in a wall bounded infinite fluid.

In the limit as $\omega \rightarrow \infty$, the above boundary condition (equation 3.18) approximately becomes:

$$\phi = 0. \tag{3.20}$$

This implies that we have only vertical fluid velocity at the free surface ($z = 0$); we get following image (same) double body motion for the heave, pitch and roll motion and the opposite image body motion for surge, sway and yaw. Physically, we may consider the body motion to occur in an unbounded infinite fluid.

Since two very different double body motions result at the two respective limits, and a smooth transition must occur between these two limits, it is argued that the added mass must be a function of frequency. Furthermore, since the double body motions at the two limits correspond to motions in an unbounded fluid without waves, the linear hydrodynamic damping vanishes at these two limits. However, between these two extremes, waves are created and the linear hydrodynamic damping takes on finite values. Therefore, the hydrodynamic damping is a smoothly varying function of frequency, that is zero at zero and infinite frequency.

Empirically derived viscous roll damping

The viscous portion of the damping (linear and quadratic) is determined on a component basis as described in Himeno, (1981), and as refined and incorporated into SHIPMO (Beck and Troesch, (1989)). However, the viscous damping does not necessarily follow the simple limits described for the hydrodynamic damping. The mechanisms involved in viscous ship roll damping include:

B_F: The moment resulting from skin drag (friction).

B_E: The moment resulting from the bare hull arising from separation and eddies mostly near the bilge keels.

B_L: The moment resulting from lift forces due to an apparent angle of attack as the ship rolls while underway.

B_{BK}: The normal, flow modification and wave making moment components due to the pressence of bilge keels.

B_{BKN}: The bilge keel moment due to normal pressure.

B_{BKH}: The moment due to the flow around the hull being modified due to the presence of bilge keels.

B_{BKW}: The modification to the wave making moment due to the presence of bilge keels.

B_W: The moment due to wave making which is calculated using potential flow and modified.

These various components are functions of speed, encounter frequency and the presence and size of the bilge keels. According to Himeno's data, the B_F, B_L, B_W, B_{BKW}, are linear while the B_{BE}, B_{BKN}, B_{BKH} are nonlinear. The linear B_1 and nonlinear B_2 damping coefficients can, therefore, be expressed as follows,

$$B_1 = B_F + B_L + B_W + B_{BKW} \tag{3.21}$$

and

$$B_2 = B_E + B_{BKN} + B_{BKH}. \tag{3.22}$$

The total damping is therefore,

$$B(\dot{\phi}) = B_1\dot{\phi} + B_2\dot{\phi}|\dot{\phi}|. \tag{3.23}$$

In linear ship motions programs, the standard approach is to use an equivalent linearization which equates energy dissipation per cycle. This equivalent coefficient is a function of the amplitude of the resulting roll motion $\dot{\phi}_A{}^2$ and must therefore be

---

[2] The amplitude of the rolling velocity $\dot{\phi}_A$ is a constant with respect to time. However, the roll velocity $\dot{\phi}$ and the roll displacement vary as a function of time (i.e., $\dot{\phi} = \dot{\phi}(t)$ and $\phi = \phi(t)$).

determined in an iterative fashion. The formula is as follows,

$$B_e = B_1 + \frac{8}{3\pi} B_2 \dot{\phi}_A \dot{\phi}_A. \tag{3.24}$$

where, $\dot{\phi}_A$ is the amplitude of the roll velocity which may be harmonically approximated as,

$$\dot{\phi}_A \approx \sqrt{\dot{\phi}^2 + \phi^2 \omega^2}. \tag{3.25}$$

Finally, in order to avoid problems resulting from the absolute value function, Dalzell, (1978) suggests using an equivalent nonlinearization as follows,

$$|\dot{\phi}|\dot{\phi} \approx \frac{5}{16}\dot{\phi}_A + \frac{35\dot{\phi}^3}{48\dot{\phi}_A}. \tag{3.26}$$

Although some work (e.g., Braathen, (1987)) has been done on calculating the eddy making roll damping forces using vortex tracking schemes, the use of such methods is time consuming and still requires the other components to be empirically calculated.

From the above formulation, we obtain constant coefficients at each frequency. Although constant coefficients at the harmonic frequency is an approximation to the nonlinear problem, the above formulation allows us to evaluate the importance of the nonlinear roll restoring moment, nonlinear roll damping and the linear coupling between the asymmetric degrees of freedom (roll, sway and yaw).

The approximation to the water-on-deck force

In a previous investigation, Falzarano (1988) utilized a simulation model which simultaneously solved the ship motion and water-on-deck problem. The ship motion was modeled using a linear time-domain model and an approximate nonlinear model (time-varying hydrostatics). The water-on-deck was modeled by solving the shallow

water hydraulics (Dillingham and Falzarano, (1986a & b)) problem at each time step. Considering the importance of initial conditions and equation parameters in determining the eventual motion of a vessel with water-on-deck, and the impracticality of analyzing general nonlinear time-varying systems analytically, the study of an analytically tractable explicit simplified model exhibiting similar dynamics is appealing. By explicit, we mean a differential equation expressible in terms of simple functions of the phase variables and time. Because is is necessary to solve a nonlinear system of partial differential equations at each time step, the water-on-deck force is a general function of time and cannot be studied analytically. This investigation will focus on evaluating the effect of various simplifications to the nonlinearity and equation coupling and relating these dynamics to those of the more realistic, yet complicated and computationally intense simulation model. Therefore, in this investigation, we will study a simplified model, so that we can evaluate the effect of approximations by using analytical techniques to predict capsizing.

Description of explicit simplified model

The equation of motion describing the single degree of freedom vessel roll motion ϕ with water-on-deck is as follows,

$$(I_{44} + A_{44})\ddot{\phi} + B_{44}\dot{\phi} + B_{44q}\dot{\phi} \mid \dot{\phi} \mid + \Delta\, GZ(\phi) = F_{sea}\cos(\omega t + \gamma_4) + F_{wod}(t). \quad (3.27)$$

Where I_{44} is the moment of inertia (in air) about the roll axis, A_{44} is the roll hydrodynamic added mass coefficient, B_{44} is the linear roll hydrodynamic and viscous damping coefficient, B_{44q} is the quadratic viscous damping coefficient, Δ is the vessel displacement, and $GZ(\phi)$ is a polynomial approximation to the nonlinear roll restoring moment curve. The single frequency (ω) external wave exciting force has amplitude F_{sea} and phase angle γ_4 (with respect to wave crest amidships). The force due to the water-on-deck, $F_{wod}(t)$, can only be calculated in a simulation computer

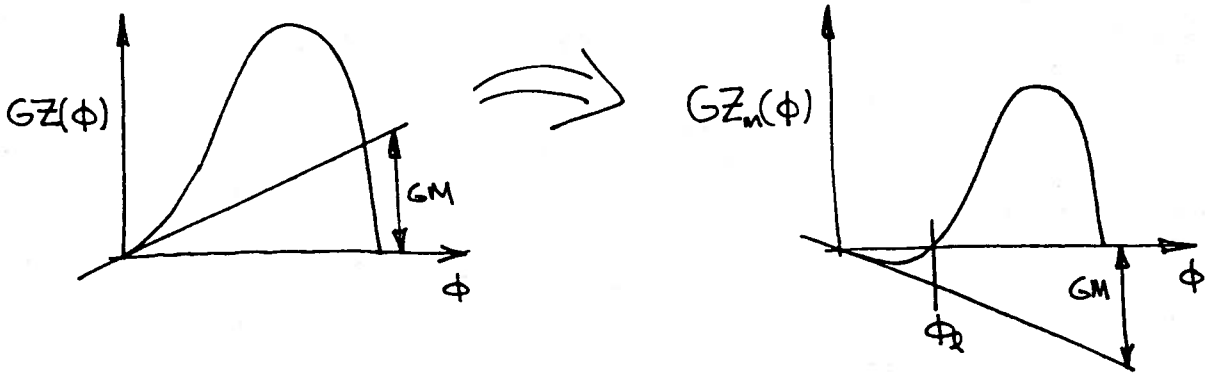

Figure 3.3: Roll restoring moment curve unmodified and modified

code (Dillingham and Falzarano, (1988a & b)) by solving a system of coupled nonlinear partial differential equations, it is not available in closed form. Caglayan, (1985) suggests that the dominant dynamics of the water-on-deck problem can be approximated by a fixed weight to achieve the same pseudo-static heel angle (loll angle). In order to evaluate the importance of the loll angle but to avoid a complicated implicit analysis involving the time simulation of a coupled system of nonlinear partial differential equations, the hydrostatic curve is modified due to the weight and moment of water-on-deck as follows,

$$(I_{44} + A_{44})\ddot{\phi} + B_{44}\dot{\phi} + B_{44q}\dot{\phi} \mid \dot{\phi} \mid + \Delta\, GZ_m(\phi) = F_{sea}\cos(\omega t + \gamma_4) \qquad (3.28)$$

The unmodified and modified hydrostatic curve $GZ_m(\phi)$ for a typical fishing boat (e.g., *Patti-B*) with water-on-deck might look like Figure 3.3.

It can be shown that for the unforced equation ($F_{sea} = 0$), the equilibria of this dynamical system correspond to roots of the function $GZ(\phi) = 0$. This is shown by writing the above equation in Cauchy standard form $\dot{x} = f(x,t)$, and setting $\dot{x} = 0$. When the GM is reduced through zero (from no water-on-deck to the static effect of water-on-deck), the stable upright equilibrium, $\phi = 0$ and $\dot{\phi} = 0$, bifurcates

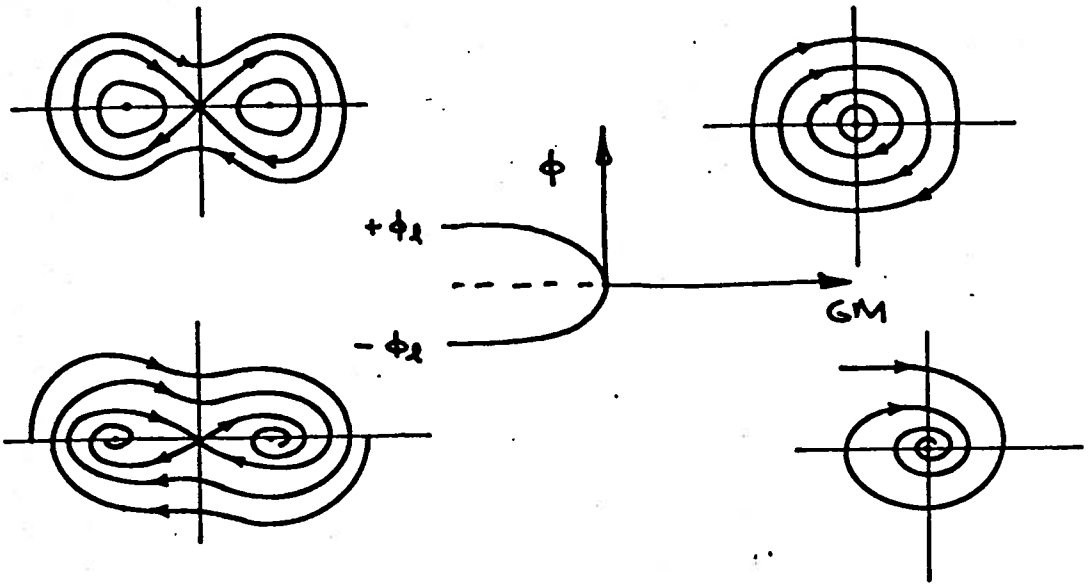

Figure 3.4: Pitchfork bifurcation diagram and phase portraits

into an unstable upright equilibrium and two stable equilibria at the plus and minus loll angles $\pm\phi_l$. Locally, this bifurcation is the classical pitchfork bifurcation and is illustrated below in its bifurcation diagram and corresponding phase portraits (Figure 3.4).

Global bifurcation is related to a type of stability called *structural stability* of trajectories (c.f., equilibria as in local bifurcation theory) which is caused by changes in a system's parameters and the resulting character of the phase plane trajectories near fixed points are affected by those changes. Examples of important parameters for our system include coefficients of the differential equations describing the vessel's motion. For the ship, important system parameters are the value or sign of the coefficients or derivatives of the righting arm curve. The qualitative features of the righting arm curve as affected quasi-statically by the vessel's motion should be studied, since they are important for the dynamics. Parameter values at which stability changes occur are called bifurcation points (Seydel, (1988), Guckenheimer and Holmes, (1986)). Local bifurcation theory attempts to study how the system

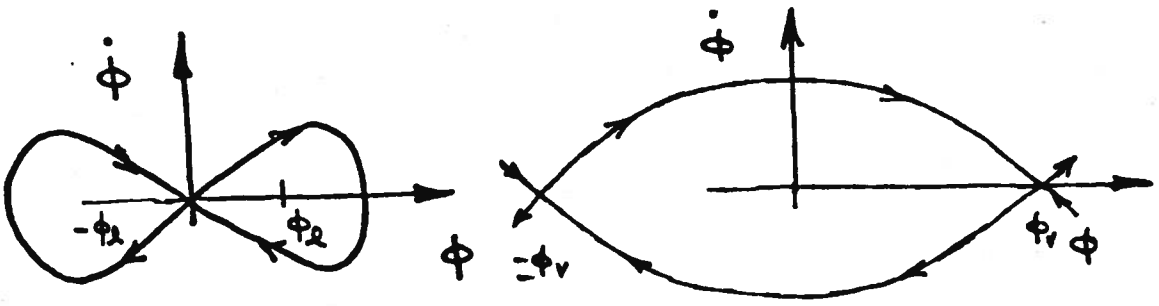

Figure 3.5: Phase portraits with a) homoclinic and b) heteroclinic connections

changes close to bifurcation points. Important changes in the system dynamics occur at or near the bifurcation points (Thompson and Stewart, (1986)). Although the qualitative aspects of the vessel's righting arm curve, and how changes in it affect the system's dynamics were originally discussed by Zeeman, (1977), he did not consider the possibility of a loll angle.

For the bifurcated (as a result of the loll angle) system described by equation 3.28 (one unstable and two stable equilibria) without damping or forcing, the phase portrait will have two homoclinic orbits, each connecting the unstable saddle at $\phi = 0$ and $\dot{\phi} = 0$ to itself (Figure 3.5a). For a typical ship (we do not consider self-righting lifeboats which have an angle of vanishing stability at ϕ_v= 180 degrees), the undamped unforced phase portrait will have a heteroclinic connection which connects the saddles at the plus and minus angle of vanishing stability to one another and visa versa (Figure 3.5b).

This phase portrait is described as structurally unstable, since once damping and forcing are added, the homoclinic manifold (the phase space evolves with time once forcing is added) breaks and may intersect itself. If this intersection occurs once transversally (non-tangent), it can be shown that the manifolds intersect one another

infinitely many times (Wiggins, (1990)). The intersection of these manifolds is a necessary condition for complicated (chaotic) dynamics to occur. Dynamical systems possessing homoclinic orbits [3] are among the few dynamical systems whose behavior may be studied globally. The Melnikov method is one of few analytical methods for the detection and study of chaotic dynamics in such systems (Guckenheimer and Holmes, (1986)).

The importance of nonlinear roll dynamics

From a vessel safety standpoint, the most critical aspect of ship dynamics is the roll motion, and it must be studied in great detail. Roll motion is highly nonlinear because of viscous damping and restoring forces. Uncoupled ship roll motion in regular waves may be described by an extended[4] periodically forced Duffing's equation No closed form solutions exist for this equation in general. Moreover, for certain parameter ranges, this equation is known to have subharmonic and even chaotic solutions (Guckenheimer and Holmes, (1986)). By subharmonic, we mean the period of the response is some integer multiple of the forcing period. By chaotic we mean the response is aperiodic; it never repeats itself. For examples of the various types of solutions see the "Applications and Results" chapter (Chapter VIII). Although, almost any system of nonlinear differential equations can be integrated numerically, differential equations with chaotic solutions may exhibit an extreme sensitivity to

---

[3] It should be pointed out here that once time dependent forcing is added we must consider an extended phase space, adding time. Since the time dependence is periodic, we may consider a Poincaré map sampled every period at the same phase of the forcing. The details of the procedure for obtaining a Poincaré map from periodically time-varying differential systems are described in the chapter on Poincaré maps and invariant manifolds (see Chapter VI).

[4] By extended, we mean a Duffing's equation with linear and nonlinear (quadratic) damping and perhaps a more complicated restoring force curve. By a more complicated restoring force curve, we mean one expressible by a polynomial of fifth order or higher.

initial conditions and simulation results should be interpreted cautiously. These and other characteristics are not usually encountered in linear systems. As Nayfeh and Khedir, (1986) have stated,

> These nonlinearities bring a whole range of new phenomena not found in linear analysis. These include multiple solutions, jumps, frequency entrainment, natural frequency shift, subharmonic, superharmonic, combination and ultrasubharmonic resonance, period doubling, bifurcations and chaos. It should be noted that not all of these resonance phenomena produced by the nonlinearity do occur often and are significant in ship motions. Some of them are probably uncommon and possibly not very significant. However, the practicing naval architect must be able to recognize all such phenomena when they do occur and should understand their consequences so that he/she will be able to avoid a design that promotes capsizing, and to evaluate the seaworthiness of a craft, and to recommend appropriate actions to control or minimize these large motions.

Approximate analytic techniques are useful in assessing the qualitative and quantitative behavior of solutions and in checking numerical methods. The only technique for obtaining solutions to general nonlinear ordinary differential equations is numerical integration. However, the inexperienced numerical analyst could integrate for a long time and never discover the most important or critical behavior. Therefore, guidance on what types of behavior to expect is of practical use. Classical qualitative analysis techniques usually apply to conservative autonomous systems, linearizations about equilibria or weakly nonlinear systems (local analysis). Modern geometric methods are continually being developed and refined, but consideration of time varying and dissipative systems is not common. Both classical perturbation techniques suitable for weakly nonlinear systems and modern global analysis techniques can be used in evaluating the effect of water-on-deck on the nonlinear roll

equation of motion; the emphasis of the qualitative analysis of this work will be on studying the strongly nonlinear effects, global effects and chaotic dynamics.

Considering what analysis techniques are available, a more appealing alternative to studying the exact equations, the solution to which may only be known as a result of simulation, is to consider explicit simplified dynamical equations. These equations should be embedded in the exact equations and exhibit behavior qualitatively similar to the more exact system. Considering simplified models exhibiting dynamics that are qualitatively similar to more complex systems is appealing because we can analyze these simple systems analytically. Modifying the ship righting arm curve to model the important effects of the weight and moment of water trapped on deck is the most simple model proposed to be analyzed.

These assumptions result in a single degree of freedom nonlinear oscillator with a hydrostatic restoring lever curve modified for the weight and moment of the water trapped on the deck and the moment induced by the asymmetric loading of the tank as the vessel is heeled. The details of how the modified roll restoring moment curve is determined are contained in Appendix E, Modification of the Vessel's Righting Arm Curve.

The importance of chaotic dynamics in our ship dynamical systems

Preliminary numerical simulation results suggested that the ship dynamical system with a lolled righting arm curve $GZ(\phi)$ may exhibit chaotic dynamics. The importance of chaotic dynamics in dynamical systems is that the eventual state of the system exhibits sensitive dependence on initial conditions, sensitive dependence on system parameters, and a broad-banded frequency response. For these reasons, chaotic dynamics is important in engineering systems, since engineers lose predictability when examining these systems. Although unpredictable, chaos is traditionally believed to be bounded. One aspect of this project has been to investigate

the effect of the chaotic motion versus the periodic motion of the system and to determine if the chaotic motions tend to stabilize or destabilize the ship dynamical system. The effect of chaotic dynamics in increasing or decreasing the amplitude of the response will be evaluated.

An important practical consideration for ship dynamical systems is whether or not a given initial condition will lead to a bounded steady-state motion or will cause unbounded motion and eventual capsizing. In the undamped and unforced system the idea of an escape from a potential well is clear. The potential well is obtained by integrating the spring force with respect to displacement, or by considering the basin of attraction of the stable fixed points. This theoretical idea is a very important practical consideration for a ship dynamical system. In chaotic systems, the possibility of chaos triggering an escape from the potential well (safe region) is an important practical aspect that must be considered (Thompson, (1989)).

In lieu of studying the chaotic escape from a potential well, we will study Lobe dynamics (Wiggins, (1990)); for details, see the chapter on Lobe Dynamics (Chapter VII). Lobe dynamics allows us to study only the dynamics starting with initial conditions inside the lobes created by the intersecting manifolds and to evaluate the possibility of initial conditions being transported from inside the pseudoseparatrix (safe non-capsizing region), to beyond the pseudoseparatrix (safe boundary) to the unsafe capsizing region. Thompson's idea of a chaotic escape from a potential well is based upon Yorke's idea of boundary basin metamorphosis (Grebogi, Yorke and Ott, (1987)). However, practical implementation of these techniques requires studying a fine grid of initial conditions for a number of parameter values and observing the eventual behavior of all these initial data points. Conclusions can only be drawn if a fine enough grid of initial conditions for numerous parameter values is analyzed. However, the manifold intersections and resulting lobes which we study in this work are a necessary first step for the numerous events (e.g., crises) empirically observed

by Thompson and Yorke to occur. The Melnikov criteria and lobe dynamics allows us to predict a priori whether an initial condition in the boundary region (basin) will be safe (eventually achieve a bounded steady-state) or unsafe (capsize).

Since our system is periodically forced (i.e., time varying at a single frequency) due to single a regular wave, we sample the system states once per period at the same phase. Such a sampling is called a Poincaré map. The boundaries between qualitatively different behavior (e.g., attracted to one or another steady-state) are called invariant manifolds. For moderate forcing, these manifolds do not intersect, and it is usually clear where future iterates of an initial condition will eventually settle. These manifolds are calculated for a given system (fixed damping and restoring moment curve) once for all time. However, as the forcing exceeds some threshold value these manifolds intersect. We determine this threshold value, for a given system, using the Melnikov method, (see Chapter VI). The regions bounded by these intersecting manifolds are called lobes. We must carefully study the evolution of initial conditions starting inside the lobes to determine their eventual state.

Overview of various approximations to be used

The various approximate models for degrees of freedom and ship roll restoring moment curve to be considered in the coming chapters are summarized in this section. Although we hope to be clear in the coming chapters about exactly what system we are studying, we summarize these aspects here to avoid future confusion and provide a convenient reference.

degrees of freedom

In order to evaluate both the important effect of the linear coupling of the various degrees of freedom and to practically analyze initial conditions in the plane, we consider both single and multiple degree of freedom models.

1. Multiple degree of freedom model:

$$(\mathbf{M}+\mathbf{A})\ddot{x}+\mathbf{B}\dot{x}+\mathbf{C}x+\underline{G}(x,\dot{x})=\underline{F}(t). \tag{3.29}$$

The elements of the matrices A_{ij}, B_{ij} and C_{ij} are the linear hydrodynamic added mass and damping, and hydrostatic restoring forces in the ith mode of motion due to a unit motion (acceleration, velocity or displacement respectively) in the jth direction of motion. The mass matrix M_{ij} contains the appropriate mass, inertial or coordinate coupling terms. The subscripts refer to the mode of motion and are: 2=sway, 4=roll, and 6=yaw (see Figure 3.1). We note here that the vector G_i contains only the roll nonlinear damping and restoring force, and the vector F_i contains the linear wave exciting force in all three modes of motion.

2. Single degree of freedom model:

$$(I_{44}+A_{44})\ddot{\phi}+B_{44}\dot{\phi}+B_{44q}\dot{\phi}\mid\dot{\phi}\mid+\Delta\, GZ_m(\phi)=F_4\cos(\omega t+\gamma_4) \tag{3.30}$$

Where, I_{44} is the moment of inertia (in air) about the roll axis, A_{44} is the roll hydrodynamic added mass coefficient, B_{44} is the linear roll hydrodynamic and viscous damping coefficient, B_{44q} is the quadratic viscous damping coefficient. The Δ is the vessel displacement, and $GZ_m(\phi)$ is a polynomial approximation to the nonlinear (possibly modified) roll restoring moment curve. The single

frequency external wave exciting moment has amplitude F_4 and phase angle γ_4 (with respect to wave crest amidships).

Various approximations to the hydrostatic curve

In order to completely analyze the important dynamics for the *Patti-B* we consider two types of nonlinear roll restoring moment curves, $GZ(\phi)$ (see Figure 3.6).

1. Righting arm curve as designed

   In our "Bifurcation and Stability Analysis of the Ship Dynamical System" chapter (Chapter III), "The vessel turning problem" and "Simulation of the some aspects of the vessel turning problem" subsections of the "Applications and Results" chapter (Chapter VIII), we consider a standard $GZ(\phi)$ for the *Patti-B* as designed. As designed, this vessel has stability far in excess of that recommended by regulations (Falzarano, (1988)). These studies allow us to evaluate the effect of frequency dependent hydrodynamics and the approximation of uncoupled motion (see Table 3.1).

2. Lolled righting arm curve

   In the remainder of the work, we consider a lolled $GZ(\phi)$ curve as would occur as a result of external damage and flooding or water trapped on deck. In this analysis, we consider four different approximations (see Figure 3.6 and Table 3.1).

   (a) Ninth order approximation

   We use this most accurate ninth order polynomial because it well approximates the shape of the calculated $GZ(\phi)$. We use this approximation in the numerical determination of the invariant manifolds.

(b) Fifth order approximation

We use this fifth order approximation because a fifth order curve is the lowest odd polynomial which can capture both the loll angle and angle of vanishing stability. We use this approximation in the numerical determination of the Melnikov function section in the "Applications and Results" chapter (Chapter VIII).

(c) Third order loll angle approximation

We use this polynomial approximation because our unperturbed trajectories are simple hyperbolic functions and we can analytically integrate the resulting Melnikov integral. This curve well approximates the dynamics around the loll angle.

(d) Third order vanishing angle approximation

We use this polynomial approximation because our unperturbed trajectories are simple hyperbolic functions and we can analytically integrate the resulting Melnikov integral. This curve well approximates the dynamics around the angle of vanishing stability.

Equation	Curve	Chapter Titles (numbers)
3.30	1	Bifurcation and Stability (4) and Applications (8)
3.29	1	Bifurcation and Stability (4) and Applications (8)
3.30	2a	Melnikov (6), Lobes (7) and Applications (8)
3.30	2b	Melnikov (6), Lobes (7) and Applications (8)
3.30	2c	Melnikov (6), Lobes (7) and Applications (8)
3.30	2d	Melnikov (6), Lobes (7) and Applications (8)
3.29	2a	Melnikov (6), Applications (8) and Appendix B
3.29	2c	Melnikov (6), Applications (8) and Appendix B
3.29	2d	Melnikov (6), Applications (8) and Appendix B

Table 3.1: Chapters where various approximations have been considered

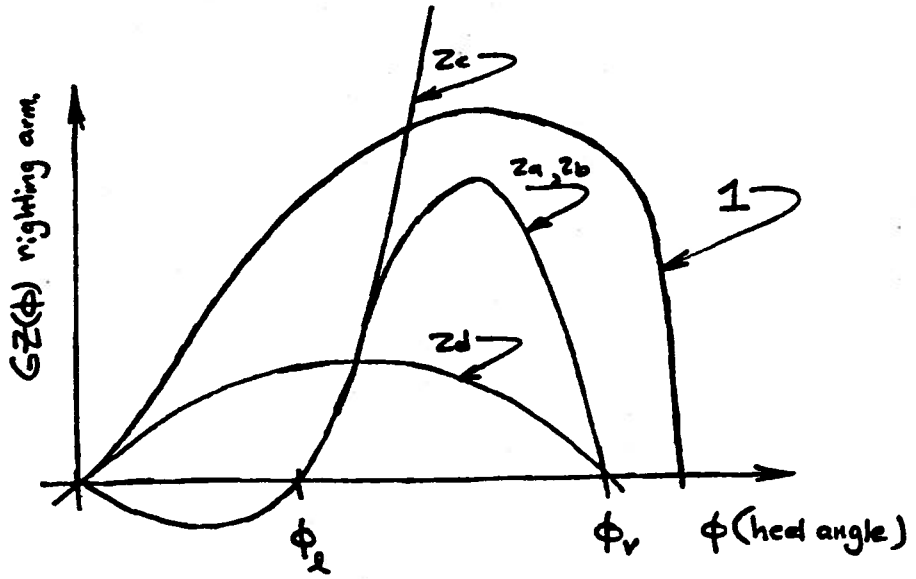

Figure 3.6: Pictorial comparison of various righting arms considered

CHAPTER IV

LOCAL BIFURCATION AND STABILITY ANALYSIS OF THE SHIP DYNAMICAL SYSTEM

As important physical parameters are varied, the shape of the nonlinear roll restoring moment curve leads to very interesting dynamical behavior. To systematically study these changes and analyze the resulting attractiveness or repulsiveness of the new equilibria created or destroyed, local bifurcation theory must be considered. Bifurcation and stability analysis refers to the appearance and disappearance of additional solutions to systems differential equations as parameters are varied and the changes in attractiveness or repulsiveness of these solutions. An example application of bifurcation theory would be the way in which stability of solutions is gained or lost. A detailed description of the mechanisms for gaining or losing stability is contained in Appendix C, "Stability of Periodic Solutions and the Monodromy Matrix".

Nonlinear dynamical systems have the characteristic that they may possess multiple solutions or attracting sets, some of which may be physically realizable (stable) and some of which may not be. Bifurcation analysis is important to the study of ship dynamics because bifurcations may lead to chaos. By this we mean that our generic system may approach a chaotic dynamical system by changing a parameter resulting in a sequence of progressively more complicated regular (periodic) dynamical systems that approach a chaotic dynamical system at a so-called limit point. This is the so-called "period doubling" route to chaos (Schuster, (1984)). Other investigators of

chaotic ship dynamical systems (Nayfeh and Khedir, (1986) and Virgin, (1989)) have analyzed this route to chaos for ship rolling motion. In this work, we instead study chaotic dynamics by considering the invariant manifolds of the associated Poincaré map and determine conditions for these manifolds to intersect. Intersection of these manifolds is a necessary condition for chaotic dynamics to occur. Further discussion of invariant manifolds and Poincaré maps is contained in Chapter VI, while an analytical technique (Melnikov's method) to predict these intersections in terms of the system's parameters is described in Chapter VI.

The bifurcation and stability analysis contained in this chapter concerns the harmonic response of a vessel with a positive roll restoring moment up to the angle of vanishing stability. In other words, the stability analysis in this chapter does not include the initially negative roll restoring moment and loll angle considered in the rest of the work. However, even without the loll angle this work is unique as far as we know in that the coupling of the nonlinear roll motion to the sway and yaw motion, the nonlinear damping, an accurate polynomial approximation to the roll restoring moment (a ninth order polynomial), and the frequency dependence of the hydrodynamics are included. Consideration of all these quantities is accomplished by using numerical path following techniques (e.g., Seydel, (1988), Doedel, (1986)) and numerically integrating the monodromy matrix to determine stability. Therefore, this analysis is not limited to the accuracy and number of terms included in an algebraic perturbation scheme as is the work of other investigators (e.g., Nayfeh and Khedir, (1986)). Instead it is limited to the numerical accuracy and the size and speed of the computer. Furthermore, an assessment of the inaccuracy caused by neglecting the coupling and the frequency dependence of the hydrodynamics is made. The coupling is found to be important.

Numerical path following techniques

For simplicity, we initially consider the single-degree of freedom roll equation of motion. We eventually describe how to extend this to consider the multiple degree of freedom problem. In order to analyze periodic solutions to periodically forced dynamical systems (e.g., our ship dynamical system), we look at the related autonomous systems, by fixing time at various integer multiples of the forcing period. Furthermore, we investigate the bifurcation behavior as the forcing frequency is varied. Therefore, the forcing frequency is our bifurcation parameter.

In setting up the single-degree of freedom roll equation of motion for bifurcation analysis, we follow the formulation for a similar problem used by (Seydel, 1988). In applying numerical path following computer programs such as BIFPACK (Seydel, (1988a)) to investigate harmonic solutions of periodically forced ordinary differential equations, we equate the solution at zero time and after one period of the forcing. In order to investigate how the magnitude and stability properties of steady-state harmonic solutions change as the excitation frequency is varied, we consider the following single degree of freedom roll equation of motion,

$$(I_{44} + A_{44})\ddot{\phi} + B_{44}\dot{\phi} + B_{44q}\dot{\phi} \mid \dot{\phi} \mid + GZ(\phi) = F_4 \cos(\omega t + \gamma_4) \tag{4.1}$$

To begin, we divide through by the sum of the roll inertia and added mass and define $x_1 = \phi$ and $x_2 = \dot{\phi}$. Using these results, we convert our equation into Cauchy standard form as follows,

$$\dot{x_1} = x_2 \tag{4.2}$$

$$\dot{x_2} = -\frac{B_{44}x_2}{(I_{44} + A_{44})} - \frac{B_{44q}x_2 \mid x_2 \mid}{(I_{44} + A_{44})} - \frac{GZ(x_1)}{(I_{44} + A_{44})} + \frac{F_4}{(I_{44} + A_{44})} \cos(\omega t + \gamma_4) \tag{4.3}$$

In order to determine steady-state periodic solutions at the forcing frequency, we impose periodicity i.e., $x_1(0) = x_1(T)$ and $x_2(0) = x_2(T)$. However, since $\omega = 2\pi/T$ and ω is our bifurcation parameter, we need to readjust our time step and discretization each time we change ω. Therefore, we rescale time and as a result our boundary conditions become,

$$T\tilde{t} = t \Rightarrow 0 \leq \tilde{t} \leq 1 \tag{4.4}$$

and therefore,

$$y_1(\tilde{t}) = x_1(t) \text{ and } y_2(\tilde{t}) = x_2(t). \tag{4.5}$$

The time derivatives are defined as follows,

$$\frac{d()}{d\tilde{t}} \cdot = T\frac{d()}{dt} \Rightarrow \frac{d()}{Td\tilde{t}} = \frac{d()}{dt}. \tag{4.6}$$

Therefore, the equations of motion become,

$$\dot{y_1} = Ty_2 \tag{4.7}$$

$$\dot{y_2} = T(-\frac{B_{44}y_2}{(I_{44}+A_{44})} - \frac{B_{44q}y_2 \mid y_2 \mid}{(I_{44}+A_{44})} - \frac{GZ_m(y_1)}{GM(I_{44}+A_{44})} + \frac{F_4}{(I_{44}+A_{44})}\cos(2\pi\tilde{t}+\gamma_4)) \tag{4.8}$$

with boundary conditions $y_1(0) = y_1(1)$ and $y_2(0) = y_2(1)$.

The multiple degree of freedom problem is similar with the multiplication of all terms by the inverted mass plus added mass matrix replacing the operation of simply dividing by the roll inertia and added inertia. The equations become,

$$\dot{y} = -\mathbf{B}^*y - \mathbf{C}^*x + \underline{F}^*(t) + g(x) \tag{4.9}$$

$$\dot{x} = y. \tag{4.10}$$

Here, the matrices $\mathbf{B}^*$ and $\mathbf{C}^*$, and the vectors $\underline{F}^*(t)$ and $g(x)$ have already been multiplied by the inverse of the sum of the mass plus added mass matrix. We note here that the only phase variables of interest are sway velocity, roll velocity, yaw velocity and roll displacement since nowhere in the equations of motion do forces proportional to sway and yaw displacement appear. Therefore, our extra equation is one dimensional and merely defines the derivative of roll displacement as the roll velocity.

Stability of periodic solutions

To study the stability of the steady-state harmonic solutions, we numerically integrate the monodromy matrix following the techniques described in Seydel, (1988). A summary of the relevant characteristics of the monodromy matrix are contained in the appendix on the "Stability of Periodic Solutions and the Monodromy Matrix" (Appendix C). These techniques require that the linearization of the dynamical system be determined. Stability results obtained in this work are in general those expected from classical perturbation analysis of the forced Duffing's equation. Specifically, at the vertical tangents of the magnification curve, (see Figure 4.1) we obtain divergence bifurcations. These bifurcations persist even with the two added degrees of freedom. At these bifurcation points, a pair of stable complex conjugate eigenvalues of the map change to a pair of real eigenvalues. This loss of stability is characterized by one eigenvalue of the map crossing the unit circle at one, so that, at least one eigenvalue becomes greater than one. We note that as stability is gained, by traveling in the reverse direction or leaving the unstable region, the reverse occurs, so that, the eigenvalue greater than one crosses the unit circle at one to become less than one (see Appendix C and Seydel (1988) for details). This bifurcation occurs at the vertical tangents in Figure 4.1.

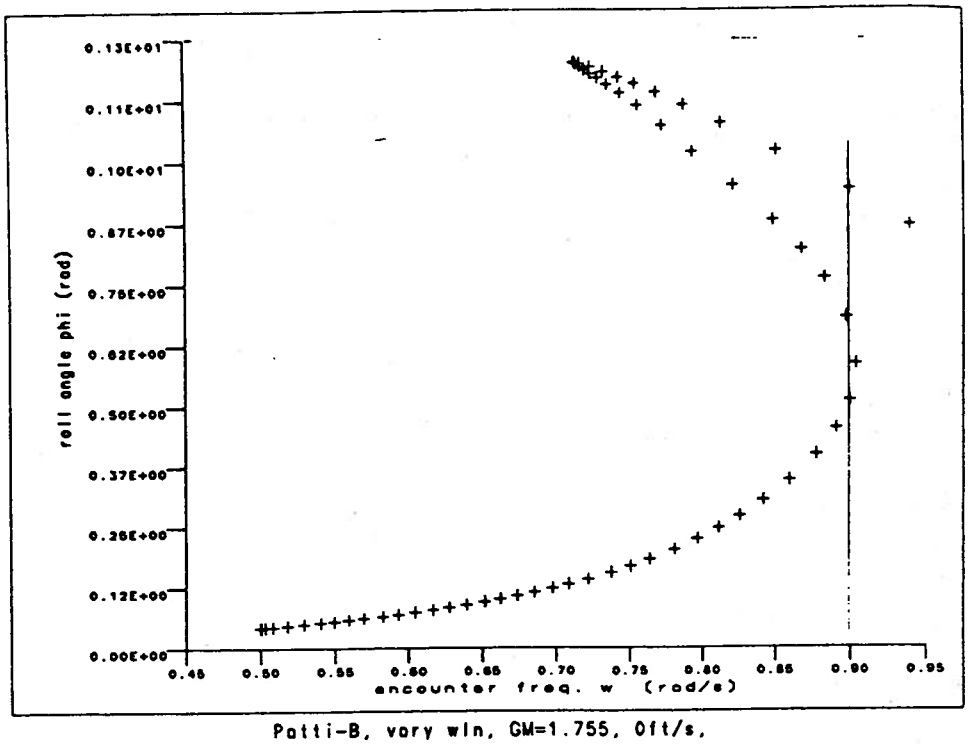

Figure 4.1: Magnification diagram, bifurcations occur at vertical tangent

Local bifurcation theory is discussed in (Guckenheimer and Holmes, (1986), Troger and Stiendl, (1990) and Thompson and Stewart, (1986)) with differing emphasis and varying amounts of detail. Although these texts stress transforming a given set of equations suspected of possessing such bifurcations into standard or generic form for classical bifurcation analysis, the use of computer programs such as BIFPACK (Seydel, (1988a)) eliminate this requirement. Programs such as BIFPACK allow the analysis of more general systems and eliminate the requirement to algebraically reduce general systems to standard form.

Practical application of BIFPACK

To practically apply BIFPACK to the ship multiple degree of freedom dynamical system, a good guess at the starting or initial value of the phase variables must be known. For the single-degree of freedom problem, analytical estimates of starting

values worked well, but for the multiple degree of freedom system vessel turning problem a more reliable guessing procedure was required. This was accomplished by integrating reasonable initial conditions until an approximately steady-state was obtained. By reasonable, we mean within the basin of attraction of the desired steady-state harmonic solution. Steady-state was obtained by integrating for as many as 100 to 1000 periods of the forcing, visually observing (Poincaré sections) and numerically comparing Poincaré points until no changes occurred as a result of further integration. This technique allowed only the stable solutions (nodes or foci) to be obtained. We note here that using this procedure, unstable solutions could be obtained by simple reverse time integration.

However, we had to rely on BIFPACK to path-follow to the non-stable[1] (saddle) type solutions (Parker and Chua, 1989)). These non-stable or saddle solutions could not be obtained by integrating the equation in reverse time, as can be done with unstable (foci or node) solutions, since, in the plane, the stable and unstable manifolds (in the Poincaré section) are one dimensional and very difficult to find for a periodically time-varying multiple degree of freedom system. Furthermore, even if these manifolds were found, since it takes infinite time to move away from (i.e., you *never* move off the saddle) or toward the saddle fixed point, special consideration is required. Analysis of these manifolds (in the Poincaré map) for the time-varying system is the subject of the next chapter (Chapter V). However, BIFPACK results were sometimes used in determining the fixed points in the Poincaré map to be used in these further studies. In addition, relating the BIFPACK results to those obtained in the Poincaré map analysis greatly increased the practical value and our understanding of both techniques (e.g., see Figure 4.2)

---

1 The saddle is neither stable, where in positive time it will achieve an ω equilibrium state nor unstable where in reverse time it will achieve an α equilibrium state, instead it simultaneously has both stable and unstable manifolds.

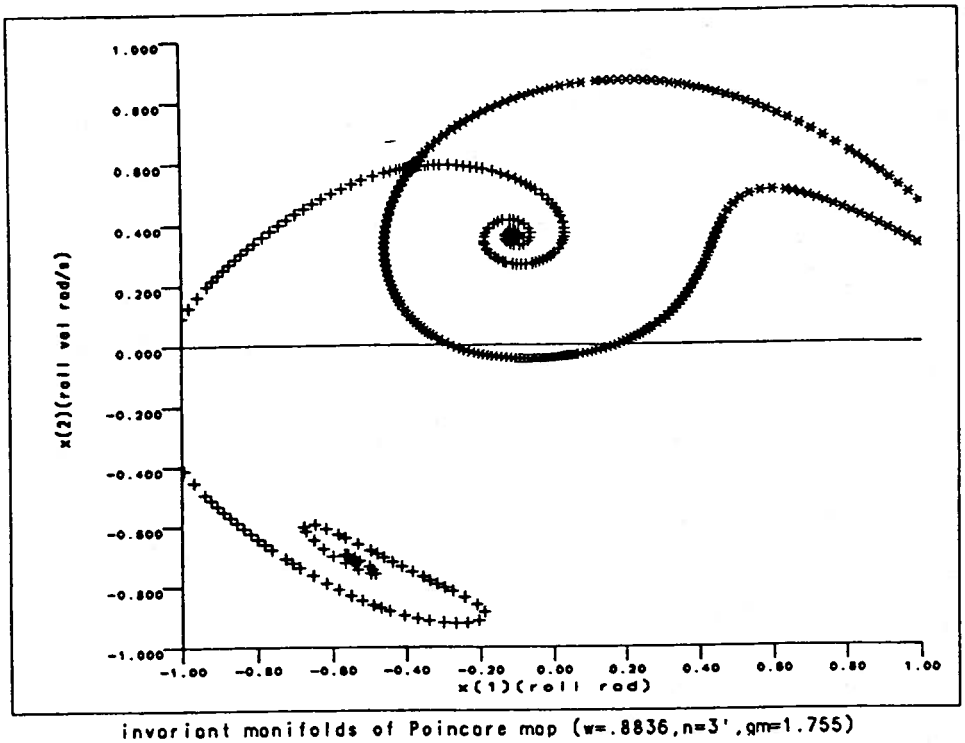

Figure 4.2: Invariant manifolds in the Poincaré map

Bifurcation theory and the slowly turning vessel

The bifurcation analysis of a vessel slowly turning in waves will form our systematic procedure for evaluating the importance of frequency dependent hydrodynamics and multiple degrees of freedom upon nonlinear roll motion.

Vessel operators are frequently forced to change vessel heading to reduce undesirable extreme rolling motion. Experienced operators are well aware that one should often turn into a sea to reduce motion amplitude. The consequent desirable effect is to increase encounter frequency and often decrease the dynamic magnification and the resulting response. However, the practical question that may be asked is what else can unexpectedly occur during this and similar maneuvers?

To answer this practical operational question, we treat the idealized problem of a vessel slowly turning in waves as a nonlinear bifurcation problem (see the "Applications and Results" chapter, Chapter VIII). Concentrating on the seaway effects

on rolling, we will consider only wave (external) excitation and in one case the wave induced parametric (internal) excitation. We will neglect all unsteady turning forces especially those due to the rudder and propeller. We analyze the nonlinear roll problem in increasing levels of accuracy and complexity as follows:

1) Uncoupled single degree of freedom nonlinear roll motion with fixed hydrodynamics.

2) Linearly coupled asymmetric modes; e.g., sway, yaw and nonlinear roll, with frequency dependent hydrodynamics.

We will consider a vessel traveling in regular waves slowly turning through various headings from stern, to beam, to head seas (see the "Applications and Results" chapter, Chapter VIII). We also include the effect of a small vessel forward speed ($U << C_{wave}$) on the encounter frequency $\omega_e = \omega_0 - U\kappa\cos(\beta)$[2]. For the various headings, the wave exciting force and wave induced parametric excitation will change as the heading and encounter frequency vary. The bifurcation approach will provide a framework in which to systematically consider the importance of frequency dependent hydrodynamics ($A_{ij}(\omega), B_{ij}(\omega)$ and $F_i(\omega), i,j = 2,4,6$) [3] and coupling between the nonlinear and possibly multi-valued steady-state roll motion and the other degrees of freedom. The frequency dependence of the hydrodynamics and the coupling have been neglected by previous investigators of nonlinear rolling in beam seas

---

[2] As the vessel turns with constant forward speed (vary beta), the frequency of encounter is changed due to the doppler effect of $\omega_e = \omega_o - U\kappa\cos(\beta)$, where ω_e is the encounter frequency, ω_o is the wave frequency, U is the vessel speed, κ is the wave number ($= 2\pi/\lambda$, λ is the wave length), and β is the heading angle. Zero heading is when the ship is traveling with the waves and π is when the ship is traveling into the waves.

[3] The elements of the matrices A_{ij}, and B_{ij} are the added mass and damping forces in the ith mode of motion due to a unit motion (acceleration, or velocity) in the jth direction of motion. The subscripts refer to the mode of motion and are: 2=sway, 4=roll, and 6=yaw We note here that the vector F_i contains the linear wave exciting force.

(e.g., Nayfeh and Kehdir, (1986)). We seek to determine the the accuracy of these approximations for nonlinear rolling in beam seas and other headings.

CHAPTER V

POINCARÉ MAPS AND INVARIANT MANIFOLDS OF MARINE DYNAMICAL SYSTEMS

As described previously, the intersection of the invariant manifolds in the Poincaré map is the mechanism for chaos in the ship dynamical system. In this chapter, we will describe the background needed to obtain and analyze the invariant manifolds that we obtain for our periodically forced ship dynamical system. These are invariant manifolds of the Poincaré map obtained by discretely sampling our periodically time-varying nonlinear system at the same fixed time lag (constant phase) relative to the external periodic forcing.

Poincaré maps

The study of two-dimensional autonomous systems in the plane is well developed (Andronov, Vitt, and Khaikin, (1966)); this is probably because of the limited types of behavior that are possible. It is common when analyzing a nonautonomous system to define time as an additional phase variable and to study the dynamics in the resulting extended phase space. Furthermore, if the time-dependence in the differential system is periodic, then the resulting dynamics may also be periodic. Therefore, it is reasonable to convert this extended phase space dynamical system to a Poincaré map which samples states of the extended phase space once per period of the forcing.

Two important questions immediately arise. First, how do we select the phase at which we sample the dynamical system? Second, what if the behavior is not harmonic or even periodic? The first question is easily reconciled by considering Proposition 1.6.2 in Wiggins, (1988). This proposition states that for a periodically time-varying differential system any two Poincaré maps sampled at different phases are C^r conjugate. This means that there exists a C^r r times continuously differentiable diffeomorphism that relates any two Poincaré maps at different phases. Practically speaking, what this means is that Poincaré maps at different phases are qualitatively similar although they may have been rotated and deformed (c.f., Figures 8.30 and 8.31). The proof of this proposition is also given by Wiggins. The answer to the second question is exactly why we use the Poincaré mapping technique for periodically forced differential systems. The Poincaré mapping technique allows us to assess the presence and type of periodicity and possible lack of periodicity (e.g., the presence of aperiodic or chaotic response) in the dynamics.

Determining the Poincaré map

We now describe the procedure for converting a nonautonomous differential equation into a Poincaré map following (Wiggins and Shaw, (1988)). To begin, consider an n-dimensional (i.e., $\mathbf{R}^n$) nonautonmous differential equation,

$$\dot{\mathbf{x}} = \mathbf{f}(\mathbf{x}, t), \tag{5.1}$$

where the equation is n-dimensional. Therefore, both the phase variables, $\mathbf{x}$ and the right hand side $\mathbf{f}$ are n-dimensional (i.e., $\mathbf{x} \in \mathbf{R}^n$ and $\mathbf{f} \in \mathbf{R}^n$) and the forcing is periodic with period T (i.e., $\mathbf{f}(\mathbf{x}, t_0) = \mathbf{f}(\mathbf{x}, t_0 + T)$).

We now explicitly convert this nonautonomous equation to an extended autonomous equation by adding time as an additional autonomous variable. We note

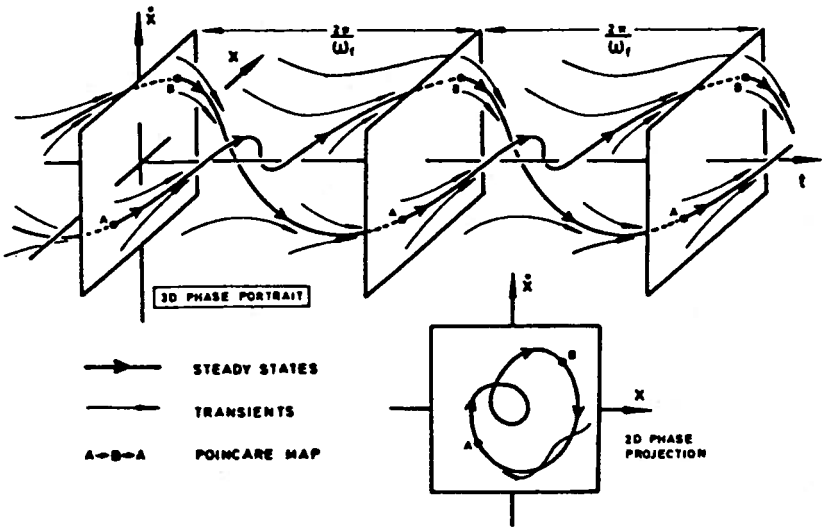

Figure 5.1: The Poincaré section in the extended phase space (Thompson and Stewart, (1986))

that the time dependence is periodic and that for every period of the forcing the equation repeats itself, so we can write the system as follows,

$$\dot{\mathbf{x}} = \mathbf{f}(\mathbf{x}, \theta) \text{ with } \mathbf{x} \in \mathbf{R}^n \tag{5.2}$$

$$\dot{\theta} = 1 \text{ with } \theta \in \mathbf{S}^1 \tag{5.3}$$

Therefore, we say the phase space is in the product space of the n-dimensional euclidian space (i.e., $\mathbf{R}^n$) and the periodic time lives on a one torous (i.e., $\mathbf{S}^1$, $\mathbf{R}^n \times \mathbf{S}^1$).

We now define the fixed time (i.e., $t = t_0$) cross-section $\sum$ on which t is restricted to the fixed phase t_0, which is contained in the open interval from zero to T,

$$\sum = \{(\mathbf{x}, t) | t = t_0 \in (0, T]\} \tag{5.4}$$

Here, $t = t_0$ is the fixed phase of the Poincaré section.

We continue by defining a map P of the cross-section $\sum$ onto itself (i.e., $\sum$) as follows,

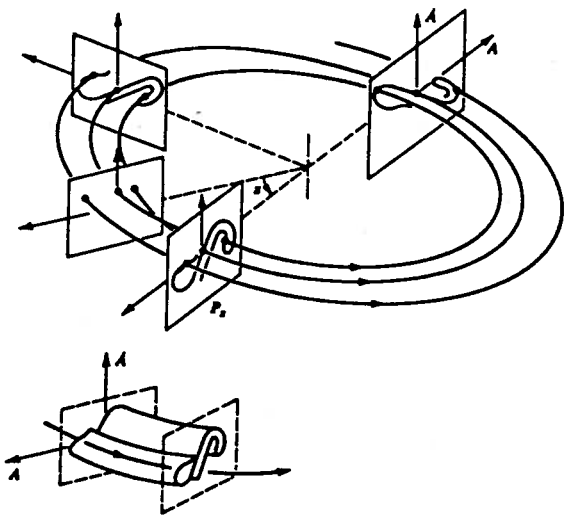

Figure 5.2: The Poincaré section in the cylindrical phase space (Moon, (1989))

$$P : \sum \rightarrow \sum, \tag{5.5}$$

This is equivalent to a point $\mathbf{x}$ with time t_0 mapped to another point $\mathbf{x}$ with time $t_0 + T$,

$$(\mathbf{x}(t_0)) \rightarrow (\mathbf{x}(t_0 + T)) \tag{5.6}$$

The map so defined is called a Poincaré map or a stroboscopic sampling. We can consider the extended phase space $(\mathbf{x}, t) \in \mathbf{R}^{n+1}$ (see Figure 5.1) or in order to visualize the periodicity we may consider the phase space to wrap around on itself $(\mathbf{x}, \theta) \in \mathbf{R}^n \times \mathbf{S}^1$(see Figure 5.2).

In this work, we do not ever explicitly solve for the map. We instead integrate the differential equation for integer periods of the forcing $T = 2\pi/\omega$ (i.e., T, 2T, 3T...) to obtain successive iterates of the map. This procedure is general, and by using it we are able to study harmonic, subharmonic and even chaotic solutions to our differential equation. We add here that if more than one frequency is present this

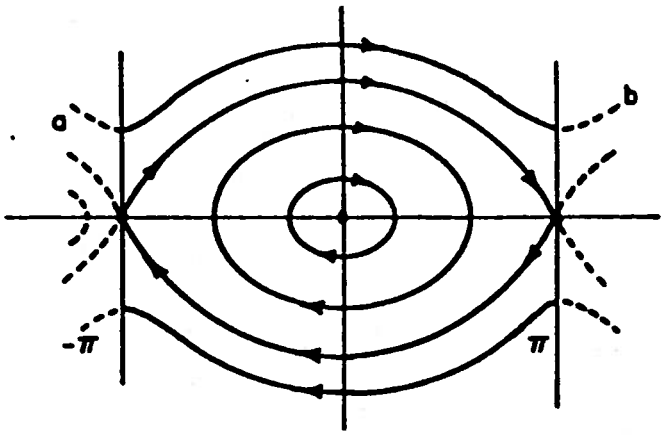

Figure 5.3: Phase portrait of undamped unforced pendulum (Guckenheimer and Holmes, (1986))

technique can be extended. If we have two frequencies and they are incommensurate[1], the motion occurs on a two torous which is the product of two periodic spaces (i.e., $S^1 \times S^1$) and we study the associated double Poincaré section (Wiggins, (1987)).

Invariant manifolds

It is well known that the orbits of a two-dimensional conservative autonomous system are easily calculated and expressible in closed form by solving the energy equation for the velocity in terms of the displacement. An example would be the trajectories describing the dynamics of the simple pendulum as illustrated in Figure 5.3. The undamped and unforced ship dynamics are similar except that the saddles at $\pm 180°$ for the pendulum are replaced by saddles at the positive and negative angles of vanishing stability (i.e., $\pm\phi_v$) for the ship.

---

[1] This means that the ratio of the two frequencies is not equal to the ratio of two relatively prime integers (i.e., $\omega_1/\omega_2 \neq p/q$, where $p, q \in \mathbf{Z}$, recall $\mathbf{Z}$ is the set of integers.

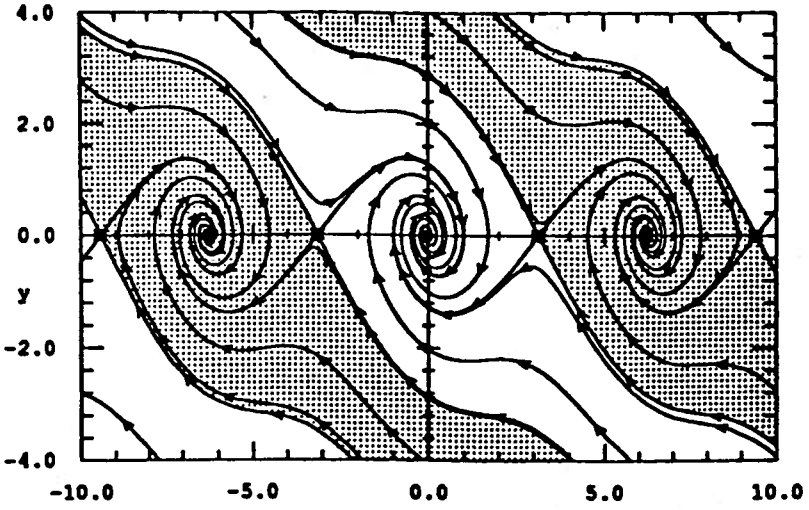

Figure 5.4: Phase portrait of unforced damped pendulum (Parker and Chua, (1989))

Referring to the figure (Figure 5.3), clearly the orbit connecting the two saddles is important since it separates the libation or simple harmonic motion (inside) from the rotational motion (outside). This special curve is called a *separatrix.*

Furthermore, if the system is not conservative, we can still determine trajectories but this must usually be done numerically. However, these trajectories are still invariant with respect to time and need only be calculated once for all time. The separatrix of the undamped system is replaced by invariant manifolds; one set that originates from infinity and approaches the saddle; and another set that originates at the saddle and approaches the stable node. We will call the manifold approaching the saddle its stable manifold and the manifold originating from the saddle its unstable manifold (see Figure 5.4).

When time dependence is added to the differential equations of motion (through forcing), the trajectories are no longer invariant with respect to time. If the time dependence is periodic, we may be able to eliminate the time dependence by averaging the equations (Hale, (1969)) and examining a related averaged set of equations whose behavior is often similar to the Poincaré map of the system. Yet this similarity does

not always persist for infinite time or when global bifurcations occur (Guckenheimer and Holmes, (1986)). Although special circumstances exist where the similarity between the averaged equations and the related Poincaré map is preserved, this is not a general rule. Systems such as our system are exceptions to this rule.

Our system possesses homoclinic and heteroclinic orbits in the unperturbed system (without damping or forcing) and must be considered more carefully. Recall, a homoclinic orbit connects a saddle to itself while a heteroclinic orbit connects two different saddles. In our case, averaging does not detect the subtle global bifurcations that occur because of the possibility of transverse homo(hetero)clinic intersections occurring in our further perturbed system (with damping and forcing). In this case, the invariant manifolds of the Poincaré map must be studied to detect these intersections. Alternatively, we may apply perturbation methods that allow us to detect such intersections. Such a method is the Melnikov method which we describe in the next chapter.

Discussion on determining the invariant manifolds

In order to determine the invariant manifolds associated with a fixed point in the Poincaré map, we should be more precise about what this means. In this description, we follow Parker and Chua, (1989). The reduction of our extended phase space (including time), continuous time system is a map or a discrete time system. Analogous to the unforced conservative (or dissipative) pendulum where the manifolds associated with the saddle fixed points[2] separate the distinct types of behavior of libation and rotation (and convergence to one or another bounded steady-state), we consider the invariant manifolds of the saddles in the Poincaré map. Saddles are called non-

[2] Considering the saddle as a fixed *point* and the manifolds as lines are only completely true in $\mathbf{R}^2$. However, for simplicity, we will limit our discussion to $\mathbf{R}^2$.

stable to distinguish them from stable fixed points and unstable fixed points[3]. We define the stable invariant manifold as the set of points which, when iterated by the map P, (i.e., $x_{i+1} = P(x_i)$), k times (i.e., $x_{i+k} = P^k(x_i)$) will approach the fixed point x^* as $k \to +\infty$. We define the unstable invariant manifold as the set of points which when iterated k times (i.e., $x_{i+k} = P^k(x_i)$) will approach the fixed point x^* as $k \to -\infty$. In our system, we recall that the Poincaré map is obtained by sampling the system after accurately time integrating the continuous time differential system for one period of the time dependent forcing ($T = 2\pi/\omega$). The invariant manifolds of our Poincaré map are not a continuous line if we consider a single solution iterated for many periods. The invariant manifolds are a continuous curve only if we consider the set of all possible starting times. However, neglecting the fact that the invariant manifolds of our Poincaré map is not a continuous curve is imprecise and may lead to errors. Although when using computers, continuous time differential systems are discretely approximated using finite difference schemes, our map is in fact a discrete time system which we obtain by integrating our continuous time system for integer periods of the forcing (i.e., ...-2T,-T,0,T,2T...). We also note here that if the invariant manifolds correspond to a fixed point with negative eigenvalues the concept of a single connected curve is much flawed, since we switch back and forth between the two branches every other iterate. For simplicity, we overcome this shortcoming by considering even iterates of the map (i.e., $x_{i+2n} = P^{2n}(x_i)$) which avoids switching back and forth between the two branches.

In order to further understand the structure of the manifolds and the results included herein, we highlight some of the details of the algorithms used to calculate them. Similar to the continuous time system, our discrete time system also has eigenvalues (m) and eigenvectors (η). However, the eigenvalues are those associated

---

[3] The saddle is neither stable, where in positive time it will achieve an ω equilibrium state nor unstable where in reverse will achieve an α equilibrium state, instead it simultaneously has both stable and unstable manifolds.

with the linearization $\mathbf{A}$ of the nonlinear map P (i.e. For a zero equilibria, $x_{i+1} = P(x_i) \approx \mathbf{A}x_i$)[4]. Since we are no longer talking about a continuous time dynamical system, the eigenvalues of $\mathbf{A}$ are multipliers where $|m| < 1$ is stable and $m > 1$ is unstable[5]. For a saddle type fixed point x^* in the plane, we have one stable eigenvalue and associated stable invariant manifold $W^s(x^*)$ and one unstable eigenvalue and associated unstable invariant manifold $W^u(x^*)$. We consider the unstable manifold starting from the fixed point[6] and iterate away from the fixed point. We consider the unstable half manifold that points in the direction of the unstable eigenvector $W^{u+}(x^*)$. Given a point on the manifold, if we iterate the map P forward (i.e., $x_{i+k} = P^k(x_i)$ for $k > 1$), we move away from the fixed point, and if we iterate the map P backwards (i.e., $x_{i+k} = P^k(x_i)$ for $k < 1$), we move toward the fixed point. In order to find the fixed points of the map (periodic solutions), we set $H(x_i) = P(x_i) - x_i$, determine the Jacobian of $H(x)$, (i.e., $DH(x_i) = DP(x_i) - I$), and solve the resulting nonlinear map using a Newton-Rapson technique (Parker and Chua, (1989)). In order to begin our calculation, we approximate a point on the manifold close to the fixed point (x^*) by its linearization,

$$\overline{x} = x^* + \alpha\eta_u, \text{ for some small } \alpha. \tag{5.7}$$

If $\overline{x}$ is very near x^* (the fixed point) we can approximate the map by its linearization, P_l which is obtained by taking the lowest order term (i.e., the Jacobian matrix D) in the Taylor series expansion of the nonlinear map P,

---

[4] For nonzero equilibria, $\eta_{i+1} = \mathbf{A}\eta_i, \mathbf{A} = DP(\overline{x})$, where $x = \overline{x} + \eta, \overline{x} =$ fixed point

[5] Note here again that for $|m| < 0$ we have a subharmonic (period 2) system for simplicity we might want to consider even iterates of the map (i.e., $x_{i+2n} = P^{2n}(x_i)$) and $m^2 < 0$!

[6] Actually near the fixed point, since if we start exactly on the fixed point it will take infinite time to move away from it.

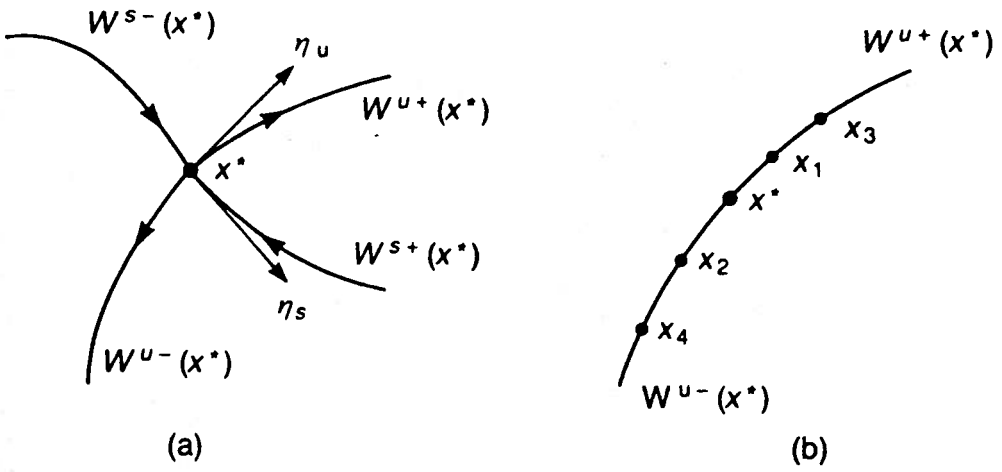

Figure 5.5: Invariant manifold of the Poincaré map (Parker and Chua, (1989))

$$P_l(x) \approx x^* + DP(x^*)(x - x^*) \tag{5.8}$$

$$P(\overline{x}) \approx x^* + \alpha m_u \eta_u. \tag{5.9}$$

We choose α such that $\overline{x}$ is close to x^*, close enough so that $\overline{x}$ is near $W^u(x^*)$ yet not so close that $P(\overline{x})$ does not move away from $\overline{x}$ quickly enough. In order to determine the other branch of the unstable manifold $W^{u-}(x^*)$, integrate along the eigenvector in the direction opposite to that which we just studied (i.e. $-\eta_u$). In order to determine the stable manifolds $W^s(x^*)$, invert the eigenvalue m and use η_s. A typical invariant manifold with the various elements described in this subsection is labeled in Figure 5.5. Also included is a sketch of a manifold for $m < 0$, (a period two subharmonic case).

Invariant manifolds as boundaries of behavior

Invariant manifold analysis as described in this chapter is of practical use. This is because invariant manifolds separate distinct types of behavior. In particular, for the

ship dynamical system, the stable invariant manifolds that originate from the angle of vanishing stability separate safe (non-capsizing) behavior from unsafe (capsizing) behavior (see Figure 5.6). Specifically, the non-intersecting manifolds in the Poincaré map form a crisp basin boundary between the various oscillatory or growing steady-state solutions that can occur. Recall, that an initial condition $(\phi, \dot{\phi}, t = t_p)$ of roll displacement, roll velocity taken at some phase in the Poincaré section (recall time is mod (2π)) will never cross a nonintersecting invariant manifold at that phase for any value of time [7].

However, the emphasis of this work is not on such well behaved and easily understood systems, but on systems where the manifolds do intersect. As stated previously, when these manifolds intersect once, it can be shown that they intersect infinitely many times (Wiggins, (1990)). All order is not lost when these manifolds intersect. However, a more systematic and careful study of the initial conditions that occur within the lobes formed by the intersecting manifolds must be done (see Figure 7.6). Although the details will be discussed in the chapter on lobe dynamics (Chapter VIII), we will preview some of the important practical results here. Manifold intersection and the resulting lobes may allow initial conditions inside lobes in the safe (non-capsizing) region to be transported across the basin boundary by repeated iterates of the map to the unsafe (capsizing) region and visa versa.

---

[7] We know that the invariant manifolds are distorted and rotated as it evolves through one period and we know that from successive iterates the points will, in general, not cross the manifolds.

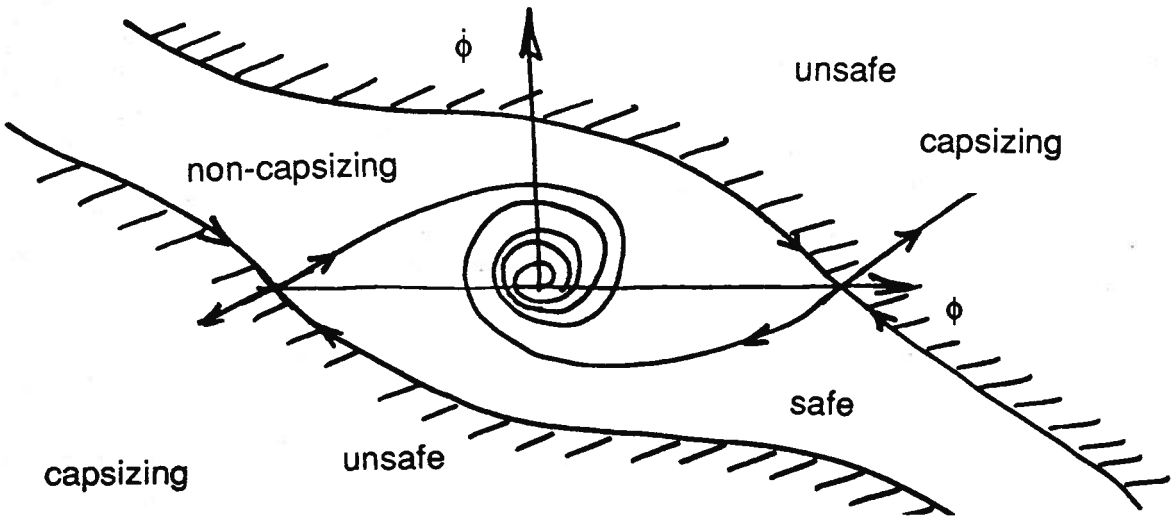

Figure 5.6: Boundary between safe and unsafe region

CHAPTER VI

MELNIKOV'S METHOD APPLIED TO THE SHIP DYNAMICAL SYSTEM

One of the few analytical methods available to predict the occurrence of chaotic dynamics is the Melnikov method (Guckenheimer and Holmes, (1986)). Using the Melnikov method, we start with an unperturbed system where the trajectories are known and use these to determine the characteristics of the perturbed system. The unperturbed system is usually a time-invariant integrable Hamiltonian system; systems for which we know a great deal. The perturbation must be small in some sense but known explicitly. The Melnikov method allows determination of a criterion for transverse homo(hetero)clinic intersections in terms of the parameters of the system. In order to illustrate the basic idea, we start with a description of the homoclinic system. The homoclinic system is more easily understood and consequently has been thoroughly investigated. Later in the chapter we describe the heteroclinic intersections and eventually describe how the two types of orbits may intersect.

The homoclinic case

The undamped, unforced simple dynamical system describing the rolling of the ship with damage or water-on-deck has a homoclinic saddle connection (see Figure

6.1a). A homoclinic saddle connection describes how for the undamped autonomous (i.e., nonforced) system the unstable and stable manifolds are the same trajectory and how this trajectory connects the saddle ($\phi = 0$) to itself. This connection surrounds the periodic orbits about the stable centers ($\phi = \pm\phi_l$). For the ship, this corresponds to oscillation around either the positive or negative loll angle. As described previously, the dynamics of such a system are well understood. It is known that such an undamped system is structurally unstable, which is usually cause for concern. However, Melnikov's method is well suited to analyze such systems. When damping is added to perturb the system, the saddle connection breaks with the flow along the unstable manifold from the saddle ending up at the stable node (without damping, this node was a center). The orbit to the saddle now originates from infinity. The saddle connection is said to have been broken (see Figure 6.1b). Once periodic forcing is added to further perturb the original system, the phase trajectories are no longer constant but evolve with time (see Figure 6.1c). For sufficiently small forcing and damping, it is known (Guckenheimer and Holmes, (1986)) that the fixed points (they evolve with time or are in a Poincaré section) of the perturbed system are in some sense close to those of the unperturbed system.

In addition, we can express the perturbed periodic orbits in terms of the unperturbed orbits (Appendix A). This means, that there exists an invariant manifold in the Poincaré section of the perturbed system that originates close to the unstable manifold of the saddle and another perturbed manifold that terminates close to the stable manifold of the saddle in the phase plane of the unperturbed system.

The Melnikov method is used to calculate the distance between the stable and unstable manifolds and to detect transverse homoclinic intersections. It will be shown how the existence of transverse homoclinic intersections is a necessary (but not sufficient) condition for complicated dynamics. For further details about the relationship between transverse intersections and chaos, see the final section in this

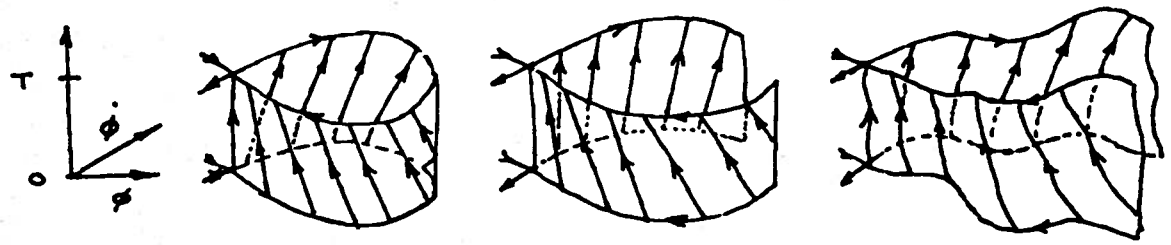

Figure 6.1: Homoclinic orbits, a) unperturbed b) damped c)periodically forced

chapter. The Melnikov method determines the distance between these two manifolds by beginning with a dynamical system where the homoclinic solutions are known, and perturbing this system slightly to determine what happens to these manifolds as a result of the perturbation. The mathematical development of the Melnikov method is described in Appendix A. This procedure results in a formula or criteria for the distance between the stable and unstable manifolds in terms of the system parameters and the phase. In order to apply the Melnikov method, we need to be able to express our periodically time-varying dynamical system in the form,

$$\dot{\mathbf{x}} = \mathbf{f}(\mathbf{x}) + \epsilon \mathbf{g}(\mathbf{x}, t);$$

$$\mathbf{x} = (u, v) \in \mathbf{R}^2 \ .$$

where, $\mathbf{f}(\mathbf{x})$ is a known autonomous vector field (usually but not always a Hamiltonian vector field) and $\mathbf{g}(\mathbf{x}, t)$ is a periodically time varying perturbation of fixed period, $\mathbf{f}(\mathbf{x}) = (f_1(\mathbf{x}), f_2(\mathbf{x}))$ and $\mathbf{g}(\mathbf{x}, t) = (g_1(\mathbf{x}, t), g_2(\mathbf{x}, t))$.

The resulting formula is called the Melnikov function and is determined by calculating an improper integral over all time $(-\infty < t < +\infty)$ which is called the Melnikov integral, $M(t_0)$. The Melnikov integral is,

$$M(t_0) = \int_{-\infty}^{+\infty} \mathbf{f}(q^0(t)) \wedge \mathbf{g}(q^0(t), t + t_0)dt, \tag{6.1}$$

or is equivalently,

$$M(t_0) = \int_{-\infty}^{+\infty} \mathbf{f}^{\perp}(q^0(t)) \cdot \mathbf{g}(q^0(t), t + t_0)dt. \tag{6.2}$$

This integral[1] is expressed in terms of the unperturbed, $\mathbf{f}(\mathbf{x})$ and perturbed terms, $\mathbf{g}(\mathbf{x}, t)$ of the governing equation evaluated along the unperturbed trajectories, $q^0(t)$. Therefore, we never need to calculate the solutions to the perturbed equations. This results in a formula in terms of the system parameters and time. The system parameters considered in our case are the height of the vessel center of gravity, which is related to the amount of damage or water-on-deck (see Appendix E), and the presence and size of fitted bilge keels. The bilge keels are important for the nonlinear damping. For more details, see Himeno, (1981) or the chapter on "The Formulation of the Ship Dynamics Problem" (Chapter III). Simple zeros, as t_o is varied, of the Melnikov function correspond to transverse homoclinic intersections.

The Melnikov integral has been calculated for a single degree of freedom roll equation of motion with a linear and quadratic damping coefficients and nonunity linear and cubic roll resstoring coefficients. In our study of the homoclinic dynamics, we intially use a locally valid (around the loll angle) cubic approximation. We use a cubic approximation because the unperturbed trajectories are simple hyperbolic functions and the Melnikov function can be analytically evaluated. We use a different locally valid cubic approximation to study the heteroclinic trajectories. In the "Applications and Results" chapter (Chapter VIII), we evaluate the effect of this approximation by numerically evaluating the Melnikov function using a quintic approximation to the roll restoring curve. The non-dimensionalized homoclinic equation for analysis

---

[1] The symbol, $\wedge$ is the vector cross-product in $\mathbf{R}^2$. The $\mathbf{f}^{\perp}$ is the normal to $\mathbf{f}$. The symbol, $\cdot$ is the vector dot-product in $\mathbf{R}^2$.

is as follows,

$$\ddot{x} + \alpha\dot{x} + \alpha_q\dot{x} \mid \dot{x} \mid -x + kx^3 = f\cos(\omega\tau). \tag{6.3}$$

Expressing the perturbation as an $O(\epsilon)$ quantity is required for the Melnikov method. For our analysis, since α, α_q and f are assumed small (i.e., $\sim O(\epsilon)$), we define $\epsilon\delta = \alpha, \epsilon\delta_q = \alpha_q$ and $\epsilon\gamma = f$.

The homoclinic Melnikov function we obtained is just a generalization of the one obtained by Holmes (Guckenheimer and Holmes, (1986)). Comparison to Holmes' result was used to check our result. The resulting curves display wave frequency versus required wave amplitude for homoclinic intersections for various quadratic dampings corresponding to the size of possible bilge keels (*Patti-B* had no bilge keels) and a linear restoring force corresponding to various metacentric heights. For specific results, see the "Applications and Results" chapter (Chapter X). The homoclinic Melnikov function calculated for a cubic approximation to the lolled $GZ(\phi)$ is as follows,

$$M(\tau_0) = +\gamma\pi\omega\sqrt{\frac{2}{k}}\text{sech}(\frac{\omega\pi}{2})\sin(\omega\tau_0) - \frac{4}{3k}\delta - \frac{2}{k}\sqrt{\frac{2}{k}}\delta_q\frac{4}{15}. \tag{6.4}$$

The parameters considered describe the twice capsized *Patti-B*. Numerical experiments have been performed and the trends of these versus predictions are similar to those obtained by other investigators for mathematically similar simple mechanical systems (Moon, (1988)),(i.e., regions of periodic and chaotic motion are mixed, e.g. see Figure 6.2). Further, we also obtain regions of chaos and no chaos above our Melnikov boundary, as we expect would occur since the intersections of the manifolds predicted by the Melnikov method are a necessary but not a sufficient condition for observed chaos (i.e., it is a lower bound).

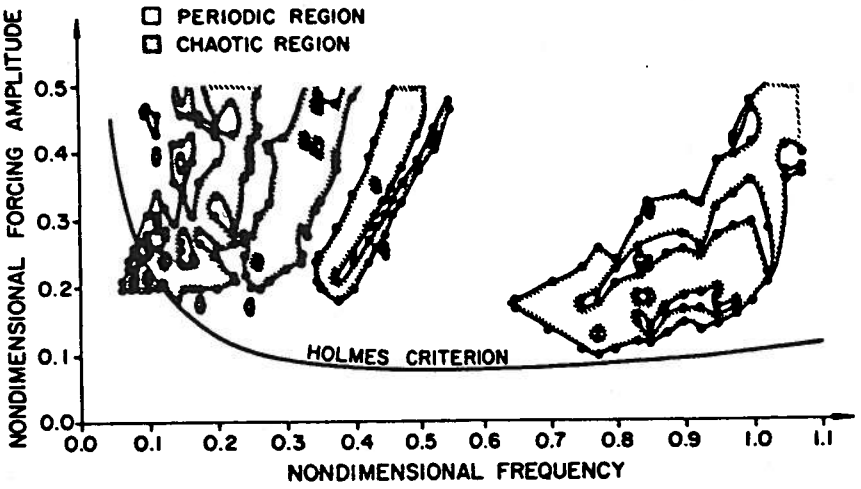

Figure 6.2: Regions of periodic and chaotic motion mixed (Moon, (1988))

Subharmonic Melnikov function

As previously discussed, other investigators have considered the period doubling route to chaos. By this we mean a sequence of period doubling bifurcations resulting in an accumulation point where chaos occurs. Bifurcations to higher and higher order subharmonics are known to occur in the neighborhood of the stable node ($\phi = \pm\phi_l$) and the region encircled by the homoclinic orbit. In numerically analyzing the Poincaré map we noticed a sequence of flip bifurcations (period doubling) at the stable node as the forcing was increased beyond a certain value.

Consideration of heteroclinic orbits

One important practical goal of this work is to investigate the question: does chaos lead to capsizing? In order to answer this question, we must consider the heteroclinic manifolds originating and terminating at the saddles in the Poincaré map that correspond to the positive and negative angles of vanishing stability (i.e.,

$\phi = \pm\phi_v$). Although the occurrence of transverse homoclinic intersections is well understood, not as much is known about heteroclinic intersections. It is well known that the phase portrait of an undamped, unforced pendulum has a homoclinic saddle connection. The saddle point are at +180 degrees and -180 degrees; since the phase space is periodic ($\theta \in \mathbf{S}^1$) +180 degrees and -180 degrees are the same point, the saddle connection is homoclinic. The phase space for a ship with an angle of vanishing stability (saddle point) at some angle less than 180 degrees appears qualitatively similar to that of the pendulum. Moreover, since the point $+180/\beta$ degrees is not the same point as the point $-180/\beta$ degrees for $\beta > 1$, these saddles are not at the same point (although they are symmetric for the unforced system) so the saddle connection is heteroclinic. Much of the theory developed for homoclinic intersections applies to heteroclinic intersections with subtle limitations (Wiggins, (1988)).

The Melnikov function for the heteroclinic intersections has been analytically determined and compared to a similar one calculated by (Morosov, (1976)). The scaled differential equation and heteroclinic Melnikov function for a cubic approximation to the righting arm curve near the angle of vanishing stability are as follows,

$$\ddot{x} + \alpha\dot{x} + \alpha_q\dot{x} \mid \dot{x} \mid + x - kx^3 = f\cos(\omega\tau) \tag{6.5}$$

$$M(\tau_0) = -\frac{\gamma\pi\omega\sqrt{2}}{\sqrt{k}}\operatorname{csch}(\frac{\omega\pi}{\sqrt{2}})\cos(\omega\tau_0) + \frac{2\sqrt{2}\delta}{3k} + \frac{8\delta_q}{15k^{3/2}}. \tag{6.6}$$

Recall, zeroes of the Melnikov function correspond to transverse intersections of the stable and unstable manifolds.

Heteroclinic versus homoclinic intersections

Although homoclinic intersections have been extensively studied by other investigators in other fields (e.g., Guckenhiemer and Holmes, (1986)), they are not as

important in ship dynamics as are heteroclinic intersections. Although homoclinic connections have been shown to exist for ship dynamical systems (Falzarano, (1988)) due to the presence of a water-on-deck induced loll angle; the loll angle dynamics occur at a roll angle often much less than the angle of vanishing stability. The angle of vanishing stability corresponds to a static loss of stability, or the angle at which the roll restoring moment ceases to be positive.[2] In the damped and forced dynamical system, there is a saddle in the Poincaré map corresponding to the angle of vanishing stability. The invariant manifolds that originate (unstable) and terminate (stable) at this saddle separate safe (non-capsizing) from unsafe (capsizing) eventual behavior of the vessel. When the manifolds do not intersect, averaging and classical methods of analyzing nonlinear systems work well and capture the system's dynamics. However when these manifolds intersect, averaging may fail especially near the separatrix (Guckenheimer and Holmes, (1986)).

In order to predict vessel capsizing, the intersections of the heteroclinic manifolds are most important but it is also possible that the homoclinic manifolds may intersect the heteroclinic. The dynamics of the system with a loll angle and an angle of vanishing stability are similar to the system studied by (Shaw and Wiggins, (1988))[3]. They have Duffing-like homoclinic connections similar to ours and pendulum-like homoclinic connections, while we have heteroclinic pendulum-like dynamics corresponding to the saddle at the angle of vanishing stability $\pm\phi_v$.

---

[2] Although bounded steady-state solutions may mathematically exist beyond the angle of vanishing stability, they are practically unsafe since downflooding and eventual vessel floundering may occur.

[3] This paper is filled with analysis and results and is well worth reading in order to gain additional understanding of a similar problem

Evaluation of approximations and more realistic systems

As mentioned previously, the analysis of the complete six-degree of freedom dynamically exact (Euler's equation of motion and Euler angle kinematics) and exact expressions for the general externally applied hydrodynamic forces has not yet been done. Although simulating the dynamically exact equations is quite straight forward, analyzing these equations is algebraically intense and practically impossible (even when using a symbolic manipulation program such as MACSYMA (Mathlab, (1983)). In this section we describe various approximations and eventually seek justification for decoupling the roll equation from the linearly coupled asymmetric (roll, sway and yaw) equations.

Coupling

We note a complication to the single degree of freedom dynamics is the coupling of the ship rolling motion to the other modes of motion. Various higher levels of approximation are commonly used in ship dynamics. Some of these are:

1) Neglecting damping, the roll motion may be approximately decoupled from sway and yaw (Webster, (1989)). After decoupling, the coupled linear sway and yaw equations are solved. Using the known sway and yaw motion, the nonlinear roll equation is solved using numerical integration.

2) Because of the port/starboard symmetry of most ships, the *linear* symmetric and asymmetric modes decouple dynamically (with respect to inertia and coordinates), hydrodynamically (with respect to added mass and damping) and hydrostatically. These approximations are similar to the approach used in linear ship motion theory, except for the inclusion of nonlinear quadratic damping and consideration of a nonlinear roll restoring moment curve. At this level of approximation, the non-

linear coupled roll, sway and yaw equations, and separately surge, heave, and pitch equations must be simultaneously solved using numerical integration.

3) The dynamically exact solution involves using Euler's equations of motion for a body fixed system and finite rotations, Euler angles (Chapter III). The complete set of six first-order velocity equations must be solved using numerical integration. Simultaneously, the three supplementary angular differential equations and another three algebraic relations relating to the Euler angle kinematics must be solved.

All these levels of approximation are straightforward to carry out numerically in simulations, and have been (Chapter VIII). However, in this work, we choose to concentrate on analytical methods and to use simulations only to verify analytical approximations. The algebraic complexity and interpretation of the results for the higher degrees of freedom have proven difficult. For various levels of approximation, the simulation results to date are qualitatively similar; although, as expected, quantitatively different. Specifically, the single degree of freedom (no decoupling) and the six-degree of freedom models are most similar. In addition, the previous linear dynamic stability analysis of the roll, sway and yaw equations shows that, although the degree of stability is affected by the size of the damping, the sign of the roll spring determines stability (Falzarano, (1988)).

Coordinate systems

Because it is much easier to visualize and analyze motion in the plane (either a two dimensional phase plane or a two-dimensional Poincaré map), we wish to determine how to obtain an equivalent two-dimensional (roll, roll velocity) system from our four dimensional system (sway velocity, roll velocity, yaw velocity, roll). It is common practice in the ship dynamics field to assume that single degree of freedom roll motion occurs about a roll center (Webster, (1989)). However a roll center exists

only if we have no damping and forcing. In an attempt to approximately determine the elusive roll center for our damped and forced system, we have examined the behavior of only two of the four eigenvalues and their corresponding eigenvectors of our three degree of freedom system [4]. The phase variables are the sway velocity, the roll velocity, the yaw velocity and the roll displacement. Recall, the multiple degree of freedom equation of motion [5] is,

$$(\mathbf{M}+\mathbf{A})\ddot{x}+\mathbf{B}\dot{x}+\mathbf{C}x+\underline{G}(x,\dot{x})=\underline{F}(t). \tag{6.7}$$

The elements of the matrices A_{ij}, B_{ij} and C_{ij} are the forces in the ith mode of motion due to a unit motion (acceleration, velocity or displacement)in the jth direction of motion. The mass matrix M_{ij} contains the appropriate mass, inertial or coordinate coupling terms. The subscripts refer to the mode of motion and are: 2=sway, 4=roll, and 6=yaw (see Figure 3.1). We note here that the vector G_i contains only the nonlinear roll damping and restoring force and the vector F_i contains the linear wave exciting force in all three modes of motion.

The eigenvalues/eigenvectors at the fixed points of the Poincaré map of the damped and periodically forced system correspond to local behavior of the map near the fixed points. The fixed points are the saddles corresponding to the zero heel angle and the angle of vanishing stability and zero roll velocities. In each case, the two eigenvalues/eigenvectors examined correspond to the least stable mode ($m \gg 1$) and most stable mode ($m \ll 1$) eigenvalues of the multiple degree of freedom system. These eigenvalues/eigenvectors are analogous to those of the single degree of freedom system, but are not always similar.

---

[4] We recall that because of the presence of a static restoring force in only the roll mode of motion and the absence of such forces in the sway and yaw modes, we need not consider the sway and yaw displacements. Therefore, we have four and not six phase variables with our three degree of freedom physical system.

[5] In order to analyze this equation we must convert this equation to Cauchy form (Chapter IV)

Various alternative coordinate systems have been considered. These coordinate systems include:

1) *The traditional ship motion coordinate system* with its origin at amidships and the waterline.

2) *A center of gravity coordinate system* with its origin at the center of gravity.

3) *A so-called principal normal modes coordinate system* with a) the origin of this system translated in such a way that the sway-roll and sway-yaw inertial and hydrodynamic added mass coupling is eliminated and b) the axes rotated to a principal axis so that the roll-yaw inertial and hydrodynamic added mass coupling are eliminated.

4) *A family of coordinate systems* where the height of the origin is systematically varied but the longitudinal location is always at the center of gravity.

For the family of coordinate systems, the requirements of minimization of the sway velocity coupling and alignment of the least and most stable eigenvalues/eigenvectors often conflicted.

Reduction to an equivalent system

In order to reduce the more exact multiple degree of freedom system to an equivalent single degree of freedom system certain conditions must be satisfied. Here, we investigate the existence of a translated coordinate system for which we have only roll displacement and roll velocity intersections. To accomplish this, we try to *minimize the sway velocity component* of the least and most stable eigenvalues while we maintain the direction of their corresponding *eigenvectors to lie in a plane.* It turns out that, these two conflicting requirements cannot simultaneously be met in most cases.

Another consideration is the correspondence between the local behavior as de-

Figure 6.3: Wire-frame plot of invariant manifolds in three-dimensions

scribed by the eigenvalues and their corresponding eigenvectors at the fixed points to the global behavior as determined by integrating the invariant manifolds along these directions [6]. The answer to this question is that the global behavior (with respect to lying in a plane) is well described by the local behavior in most cases (see Figure 6.3).

More exact polynomial fit to the GZ curve

Another extension to more realistic systems includes consideration of the exact polynomial curve fit of the roll spring (i.e., up to a twentieth-order polynomial) in the analytic Melnikov method. In the analysis so far, a cubic approximation to the roll spring has been used in the Melnikov analysis. However, a globally accurate representation has been used in the numerical determination of the invariant manifolds and in the simulations. It is obvious, that at least a fifth-order polynomial is required to accurately represent the $GZ(\phi)$ curve around the loll angle and to the angle of

[6] We know that the global stable and unstable manifolds (nonlinear) are locally tangent to the eigenvectors at the fixed point (Wiggins, (1988)).

vanishing stability. A cubic roll spring (Duffing's equation) is attractive since the resulting unperturbed (Hamiltonian) trajectories are simple hyperbolic functions. However, when a fifth-order polynomial is considered, the unperturbed trajectories can only be expressed in terms of special functions (elliptic integrals and hypergeometric functions) or alternatively, they must be numerically determined. This runs contrary to the purpose of using the Melnikov method, the practical strength of which is to start with a simple form known for all time and perturb it. Using greater than a cubic, the trajectories are still known for all time, but are no longer simple.

In order to consider these higher-order terms, we have to evaluate the improper Melnikov integral numerically (Shaw, (1990), Ling, (1987), and Li and Moon, (1990)). According to Shaw, the procedure to determine the Melnikov function numerically is to numerically integrate along the unperturbed trajectory and then to approximate the improper (doubly infinite) Melnikov integral over some large but obviously finite time interval, such that convergence is achieved. In addition, it is often possible to factor out parameters to make the results more general. The details of determining the Melnikov integral numerically for our dynamical system can be found in the "Applications and Results" chapter, (Chapter VIII).

Alternative criteria for complicated dynamics

The Melnikov criteria is a necessary, yet not sufficient condition for observable chaotic dynamics and represents a lower bound in most cases. Noting the less than satisfying agreement between theoretical Melnikov calculations and experimental and numerical results, Szemplinska-Stupnika, (1987) has determined an alternative criteria. In a series of papers (e.g., Szemplinska-Stupnika, (1989) and (1987) and Rudowski and Szemplinska-Stupnicka, (1987)), she and her collegues use the method of harmonic balance and analyze the small and large amplitude oscillations of the buckled beam. In lieu of analyzing the oscillatory part of the small amplitude

solution in isolation, she instead chooses to combine the minimum and maximum displacement and determines under what conditions no stable small amplitude harmonic solutions can exist. She reasons that this instability may lead to complicated dynamics. She notes that comparison between her analytical results and numerical results is promising.

In her analysis of the maximum amplitude of the response, she determines the frequency of the horizontal tangent ν_D and the frequency of the vertical tangent ν_C (see Figure 6.4). We know from our experience with nonlinear oscillators that the vertical tangent is a stability limit. She expresses the small amplitude solution as

$$x(t) = A_0 + A_1 \cos(\nu t + \theta)$$

Further she defines the maximum and minimum amplitudes as follows,

$$A_{max} = A_0 + A_1 \text{ and } A_{min} = A_0 - A_1.$$

She states, "Although one cannot prove that the point with horizontal tangent is also a stability limit, a physical intuition says that the resonant branch of maximum displacement $A_{max}(\nu)$ where $dA_{max}/d\nu > 0$, should not be realized in physical systems." Therefore, she concludes that if $\nu_D < \nu_C$, the system will be well behaved, however, if $\nu_D > \nu_C$ chaos may occur.

Since ν_D and ν_C are functions of both amplitude of the external forcing and the damping, she continues by determining the value of external forcing required for a given damping in order to get chaotic motion. Therefore, her results can be compared directly to those obtained using the Melnikov technique. It turns out that the Melnikov technique is a lower bound for the occurence of chaos, and that her criteria are slightly higher than those determined using the Melnikov technique.

Relationship between transverse intersections and chaos

We know that when two manifolds intersect transversely at a point q, they intersect along a curve in the extended phase space, (see Figure 6.1c). Further, since

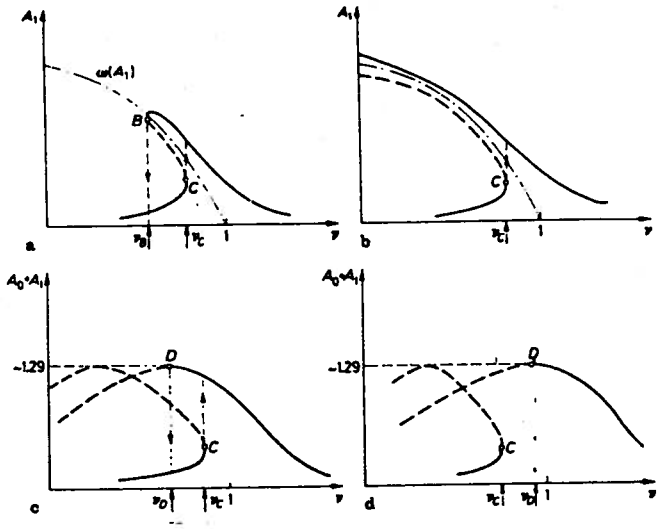

Figure 6.4: Various cases for maximum amplitude (Rudowski and Szemplinska-Stupnika, (1989)

the point q must simultaneously be on the stable and unstable manifolds we must have infinitely many forward and reverse iterates of q (Wiggins, (1990)). These intersections result in an infinity of lobes as we approach the saddle. These lobes rapidly become compressed along the orbit and expanded normal to the orbit. This distortion of phase space and their eventual re-intersection results in complicated homo(hetero)clinic tangles and greatly complicates the resulting dynamics (see Figure 6.5).

Having rapid expansion and contraction of phase area in complementry directions and eventual re-intersection is the physical mechanism for horseshoe dynamics (see Figure 6.6). The existence of a Smale horseshoe given transverse intersections can be mathematically proven using either Moser's theorem or the Smale-Birkhoff theorem (Wiggins, (1990)). For our purposes, these theorems are very similar yet differ in the recurrence times they predict. These theorems essentially state that a dynamical system which possesses a transverse homoclinic point has Smale horseshoe dynamics and thus has: 1) a countable infinity of periodic orbits of arbitrarily high periods (these are saddle type orbits), 2) an uncountable infinity of aperiodic orbits, and 3)

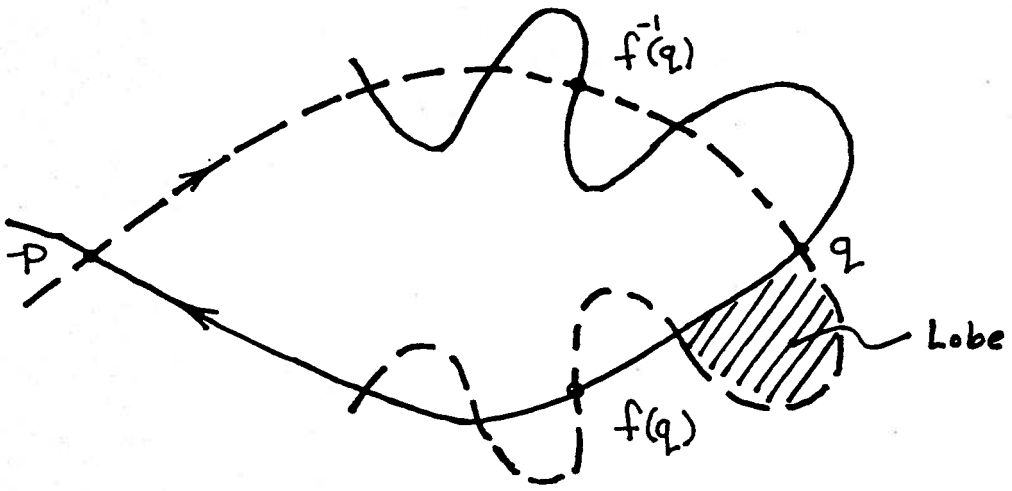

Figure 6.5: Poincaré maps of intersected manifolds

a dense orbit. Therefore as a result of these two theorems, we have the necessary (but not sufficient) condition for chaotic dynamics to occur. Nowhere is it stated that we will have chaotic dynamics given transverse intersections. However, for this route to chaos[7], transverse intersections are required. This explains why even after we have manifold intersections we do not necessarily get chaotic dynamics but may instead get some kind of periodic solution. Moreover, horseshoes have chaos but they are not necessarily attractive. This is so because although aperiodic motions exist they may not be attractive (i.e., a strange attractor) and the chaos we describe is a steady-state phenomena (i.e., not transient chaos). Throughout this work we study steady-state harmonic, subharmonic and chaotic solutions and investigate the transient motions that lead to them.

---

[7] Other routes to chaos or stochasticity have been observed, predicted and analyzed by various investigators. These include period doubling, crises, and KAM theory (Schuster, (1984)). All these types of chaos are based upon horseshoes which arise from similar global bifurcations (Shaw, (1990)). However, we concentrate on predicting the transverse homo(hetero)clinic intersections using Melnikov's method because of its application to periodically forced dissipative systems, representative of our ship dynamical system.

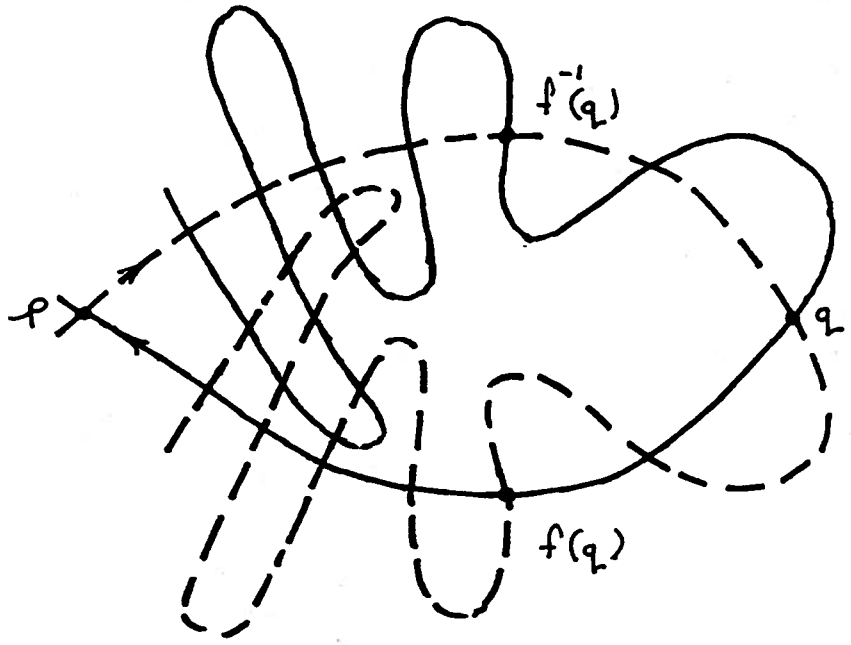

Figure 6.6: Poincaré maps of re-intersected manifolds and tangles

CHAPTER VII

LOBE DYNAMICS FOR THE SHIP DYNAMICAL SYSTEM

In order to study the eventual state of vessel motion originating in a given region of the Poincaré section, when the invariant manifolds intersect, we must consider lobe dynamics. This study is especially important in ship dynamics since movement to some regions in the phase plane[1] may result in eventual undesirable motion; that is capsizing! This technique uses numerically calculated invariant manifolds or the Melnikov function to separate regions in the phase space which iterate to safe or unsafe regions in the phase space. Thus, using this technique, we can predict the evolution of all regions in the phase space or Poincaré map, even when the manifolds have intersected. The details of using the Melnikov function to study lobe and size is contained in the appendix on the Melnikov function (Appendix A).

We know for an unforced nonlinear equation with multiple equilibria there is often a smooth curve separating the basins of attraction of each of the equilibria. This is easy to visualize in the phase plane. An example would be the unforced Duffing's equation with a negative linear restoring force coefficient. The stable and unstable trajectory beginning and ending at the saddle form a boundary between initial conditions that will eventually settle at the right $(+\phi_l)$ or the left $(-\phi_l)$ equilibria

[1] To be more exact, it is actually the Poincaré section.

(see Figure 7.1). Once small forcing is added we may consider either the manifolds of the averaged equations or the invariant manifolds in the Poincaré section. The analysis of the forced (averaged) system would then be analogous to the unforced equation. As previously discussed, caution must be exercised in situations where unperturbed homo(hetero)clinic connections exist. This is so because the possibility of the perturbed stable and unstable invariant manifolds intersecting will complicate the dynamics and make the simple averaging analysis invalid (Holmes and Holmes, (1981)).

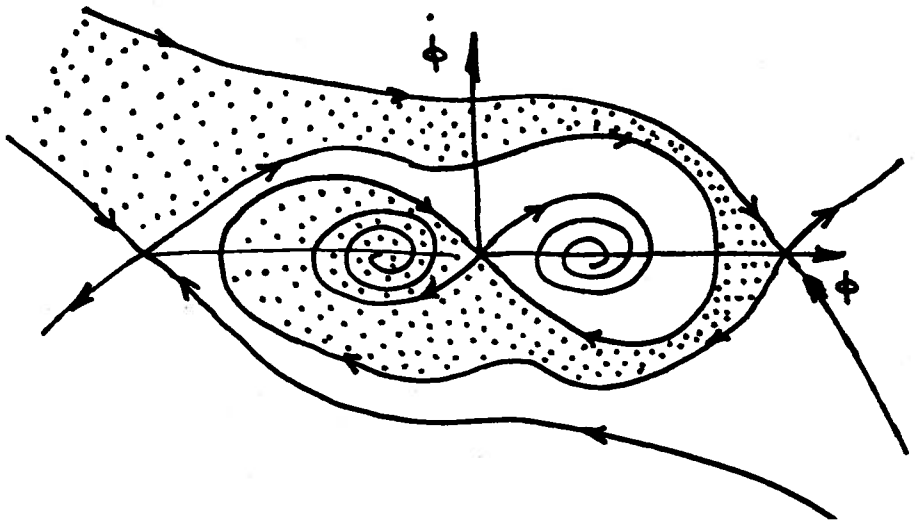

Figure 7.1: Multiple attractors and basins of attraction

However, all hope is not lost when these manifolds intersect. We need not consider all possible initial conditions throughout the phase space at all possible phases (t_o) of Poincaré sections; we need only consider the so-called tangle dynamics or the dynamics inside the lobes (Rom-Kedar and Wiggins, (1990)). These lobes may be calculated numerically (Parker and Chua, (1989)) by integrating for positive time along the unstable manifold of the saddle and for negative or reverse time along the stable manifold of the saddle. For the details of calculating the invariant manifolds associated with the saddles, see the chapter on "Poincaré Maps and Invariant

Manifolds" (Chapter V). Starting exactly on the saddle, since we know it takes an infinitely long time to approach or leave the saddle, without using specialized techniques, we might naively integrate forever and never move away from the saddle. However, since we do not know exactly where these manifolds are a priori we initially linearly approximate their location in order to move away from the fixed point. We know the the global nonlinear manifolds are tangent to the eigenvectors at the fixed point. For optimum accuracy, a compromise must be made between 1) not being too close to the saddle point so that it takes a long time to move away from the saddle and accumulate error and 2) not being too far from the fixed point so that our linear approximation to the nonlinear manifold is no longer valid must be made. Alternatively, we may approximate the size and location of the lobes using the Melnikov function (Rom-Kedar, Leonard and Wiggins, (1990)). The details of using the Melnikov function to study lobe size are contained in the appendix on the Melnikov function (Appendix A).

The relationship between vessel capsizing and lobe dynamics

When the invariant manifolds of the Poincaré map do not intersect, the manifolds form simple boundaries between the basins of attraction of the various equilibrium solutions. These steady-state solutions may be bounded periodic motions or unbounded divergent motions. The bounded motions would be periodic motions which may be either at the frequency of the external forcing (harmonic) or at some fraction of this frequency (subharmonic)[2]. The invariant manifolds form the boundary curves between the regions of initial conditions that result in bounded motion from the regions of initial conditions that may result in unbounded motion (see Figure 5.6). The unbounded motion would physically be capsizing and the bounded motion

[2] Also there may be additional response components at some multiple of the forcing frequency (super or ultra harmonic).

would physically be non-capsizing. We might consider the unbounded motion to be attracted to infinity but for the ship all motion attracted to beyond the angle of vanishing stability would be practically unbounded[3]. Therefore, whenever the invariant manifolds do not cross, we can clearly predict whether the vessel will eventually achieve a steady-state periodic motion or if its motion will steadily grow and eventually become unbounded (capsize). We do not get simple boundaries when the manifolds intersect and such simple conclusions are no longer valid.

When either the homoclinic or heteroclinic manifolds intersect themselves or one another, the dynamics will not be simple and the boundaries no longer crisp. We note here that it can be shown that only stable manifolds can intersect unstable manifolds and visa versa. The intersecting manifolds may be associated with the same fixed point (homoclinic) or different fixed points (heteroclinic). However, stable and stable and unstable and unstable manifolds cannot intersect themselves or one another. This would violate uniqueness of initial conditions. In general, same stability type manifolds (Rom-Kedar and Wiggins, (1990)) from the same or different fixed points can not intersect; otherwise, the intersection point would simultaneously be on two different manifolds of the same stability type. When the manifolds intersect, all order is not lost. To analyze the dynamics following manifold intersections, we must carefully analyze initial conditions inside the intersected regions. All the interesting dynamics occur inside these regions, called lobes, outlined by the tangled manifolds. To do this, we use the systematic procedure described by Wiggins and his colleagues in a series of papers and his new book (Rom-Kedar and Wiggins, (1990), Rom-Kedar, Lenoard and Wiggins, (1990), and Wiggins, (1990)).

Practically speaking, this phenomena is important in that initial conditions starting inside the region of previously bounded solutions may no longer be safe. The

---

[3] Although bounded steady-state solutions may mathematically exist beyond the angle of vanishing stability they are practically unsafe since downflooding and eventual vessel floundering may occur.

boundary between safety and capsizing is the so-called *pseudoseparatrix.* When the heteroclinic stable and unstable manifolds intersect, the initial conditions inside the lobe boundaries may on future iterates of the Poincaré map move to outside of the safe region. This mechanism of capsizing may be described as an *unexpected capsizing.*

However, if the vessel is damaged or water-on-deck is present, our system's phase plane may possess two types of intersecting invariant manifolds. Our dynamics are similar to that studied by Shaw and Wiggins, (1988) where they had small amplitude Duffing's type homoclinic intersections and large amplitude pendulum type homoclinic intersections. Our dynamics are similar with their large amplitude pendulum type homoclinic intersections replaced by our heteroclinic intersections due to the manifolds originating at the saddles in the Poincaré map corresponding to the positive and negative angles of vanishing stability. As a result of these two sets of manifolds, another less likely but even more unexpected mechanism for escape from the safe region may occur. This event occurs when the unstable homoclinic manifolds intersect the stable heteroclinic manifolds. This event will cause initial conditions lying close to the loll angle to be transported (along the unstable homoclinic manifold) to the safe boundary. We refer to the possible capsizing caused by this event as *totally unexpected capsizing.*

Although possible, it is extremely difficult and time consuming to completely analyze dissipative dynamical systems using the systematic procedure described in (Rom-Kedar and Wiggins, (1990)). Because of dissipation, all lobes at all phases (t_0's) of Poincaré sections need to be analyzed. Without dissipation, phase area is conserved and forward and backward iterates of the Poincaré map are equivalent. Moreover, as a result of equation symmetries and because phase area being conserved, different phase Poincaré maps satisfy additional symmetry conditions. The example of an undamped Duffing's equation described in (Rom-Kedar and Wiggins, (1990))

makes extensive use of symmetries so that a single lobe analyzed for eight iterates of the map accurately determines the systems lobe dynamics.

Practical aspects of lobe dynamics

We recall that lobe dynamics is a possible mechanism to transport phase areas of initial conditions (lobes) which are inside the pseudoseparatrix (safe region) to outside the pseudoseparatrix (unsafe region). The pseudoseparatrix is the curve which connects the homoclinic point p to the intersection point q via the unstable manifold of the saddle and connects q to p via the stable manifold of the saddle (see Figure 7.2). Without transverse intersection of the manifolds, it was clear where initial conditions might travel upon successive iterates of the map. One may fairly accurately guess a possible route from the current location to the eventual steady-state by simply not allowing the successive iterates to cross the invariant manifolds. For this case, the manifolds are definite and smooth boundaries and the safety or vulnerability of the vessel with given initial conditions can be assessed at a glance. However, such is not the case with a dynamical system where the invariant manifolds have intersected. Recall, that it can be shown that when a set of invariant manifolds intersects once, they intersect an infinite number of times. This is so because the single intersection point is simultaneously on both the stable and unstable manifolds and therefore, must have an infinite number of forward and backward iterates which asymptote to the saddle. These iterates are also intersection points and so from this single intersection point we obtain an infinite number of intersection points.

For simplicity, we assume that the intersection preserves orientation, therefore, we must have at least one primary intersection point between the intersection point and its forward and backward iterates (see Figure 7.2). Primary intersection points result in non-reintersecting lobes, the type of lobes which we will concentrate on in our application of lobe dynamics.

This infinite number of intersections results in an infinite number of lobes. Although the lobes might be geometrically quite simple and distinct (separated) near the intersection points, far from the saddles they eventually grow normally and are compressed tangentially to the unperturbed orbit as they approach the saddle. Moreover, it can be shown (Wiggins, (1990)) that forward and reverse iterates of the outer lobes will eventually intersect each other (see Figure 6.6) and this coupled with lobe distortion may result in very complicated long-term dynamics and possible eventual re-entrainment of phase area. Although consideration of all these aspects would be required for a complete study of the long-term tangle dynamics, we choose to concentrate on simple cases to demonstrate the practical use of lobe dynamics.

Considering only the most fundamental aspect of lobe dynamics, we know that we may assume that only one lobe will transport phase area from inside to outside the pseudoseparatrix and another will transport phase area from outside to inside. This exchange of area will occur near the so-called turnstile. For a simple example, refer to Figure 7.3. In this example, the inside lobe a will iterate to outside $f(a)$, while the outside lobe b will iterate to inside $f(b)$. Therefore, the point q is the turnstile for this example; that is the point where inside lobes iterate to outside and outside lobes iterate to inside. We stated earlier that if the manifolds do not intersect, then initial conditions starting in a basin of attraction corresponding to one equilibria will iterate with time toward that equilibria. During this evolution, it will not cross, at that phase of the Poincaré map, an invariant manifold boundary. Recall, that for a continuous time system the invariant manifolds at the various phases will be different but C^r conjugate and, therefore, we must refer to iterates of the point's evolution and not the actual motion that occurs between Poincaré samplings. At first glance, intersecting manifolds and lobe dynamics seem to violate this rule and, therefore, requires further explanation. We know that although all Poincaré maps are similar (C^r conjugate), they are different because the manifolds oscillate as the dynamics

evolve in time. They may be rotated and slightly distorted from one another (c.f., Figures 8.30 and 8.31).

Figure 7.4 borrowed from Rom-Kedar and Wiggins, (1990) shows rather clearly, using a series of Poincaré sections, exactly how a lobe boundary might evolve with time as it passes through the turnstile during one period. For this case, we see that the initial conditions do not actually cross the invariant manifold; the lobe evolves and distorts with time and its area simply transports across the seemingly arbitrary pseudoseparatrix as the manifold deforms outward. Studying the lobes in the neighborhood of the turnstile is quite straightforward and yields useful information quite rapidly. However, due to the distortion of the lobes as they approach the saddle their intersections get rather complicated very quickly. To demonstrate this point, I again borrow from (Rom-Kedar and Wiggins, (1990)) to illustrate how a stretched and deformed lobe may intersect another lobe in a rather complicated fashion (see Figure 7.5).

Referring to the figure, we can see how the initially safe inside initial conditions (black) are transported in one iterate of the map to outside the pseudoseparatrix into the unsafe region. By the second iterate, we can see that some initially unsafe (white) area eventually becomes re-entrained due to secondary intersections of the manifolds. In order to completely analyze a dynamical system, one must consider all similar possible special cases. As you can see from our numerical invariant manifold calculations (see Figure 7.6), we are not able to calculate more than a few lobes. This is because, as mentioned before, the lobes quickly become tangentially compressed and normally amplified and are, thus, hard to distinguish from other nearby trajectories. This may be especially true in our system due to the dissipation. For a practical application of the lobe dynamics to our ship dynamical system see the "Application and Results" chapter (Chapter VIII).

Basin boundary metamorphasis

Yorke and his colleagues at the University of Maryland (e.g., Grebogi, Ott and Yorke, (1983), and (1987)) describe a series of changes that occur in the basin boundaries of which the intersection of the period one stable and unstable manifolds (the case we study) is just the first of many. The manifold intersections described in the previous sections are the events that cause the basin boundaries to initially become fractal. They also discuss manifold intersections of period four saddles which results in dramatic changes in the basin boundaries. Also in this work they discuss the mechanism of crisis. Crisis is the collision of a strange attractor and the basin boundary and result in the destruction of the attractor. Although the phenomena described by Yorke are interesting and give further understanding to the phenomena described in previous chapters, they are sparse on analytical prediction. These techniques rely heavily upon extensive simulation results which are time consuming to implement. Yet these techniques do produce a practical description of the size of the various basin boundaries.

This work has found engineering application by Thompson and his colleagues at University College London, (e.g., Thompson, (1989a) and (1989b), and Thompson and Ueda, (1989)) in which they describe the so-called engineering integrity diagram. The engineering integrity diagrams demarcates the period one saddle intersections (predicted by Melnikov), the intermediate period four saddle collisions, (the event that substantially reduces the area of the safe basin), and the final crises where the chaotic attractor collides with the boundary and for all practical purposes eliminates the safe basin.

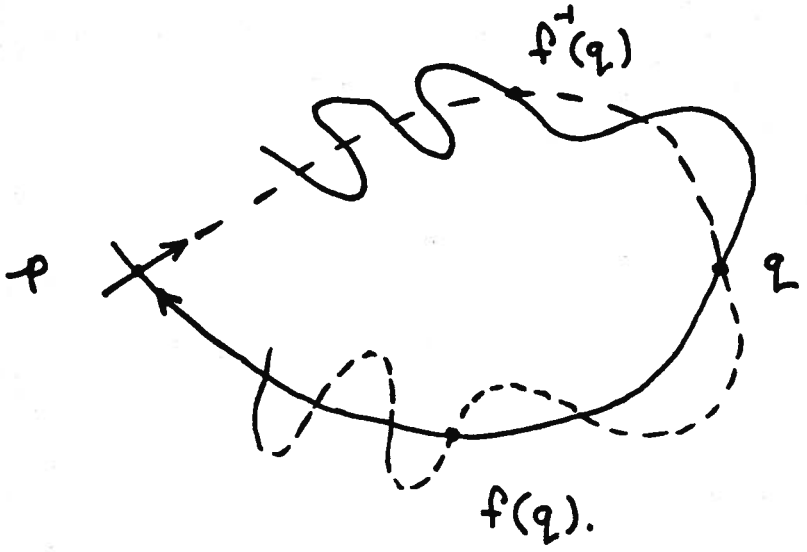

Figure 7.2: Forward and backward iterates of intersection point

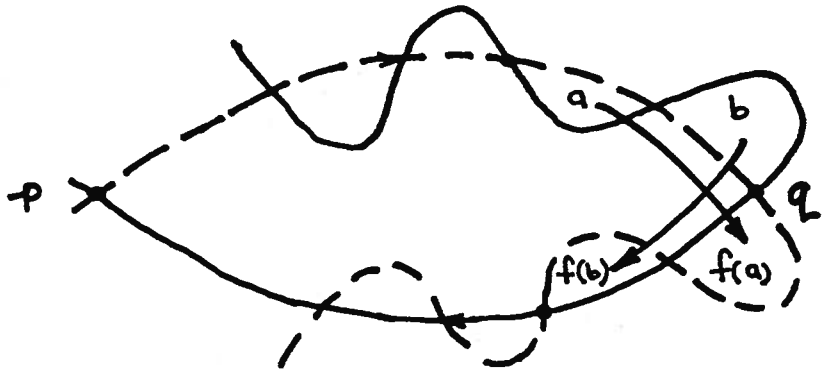

Figure 7.3: Lobe iteration through the turnstile

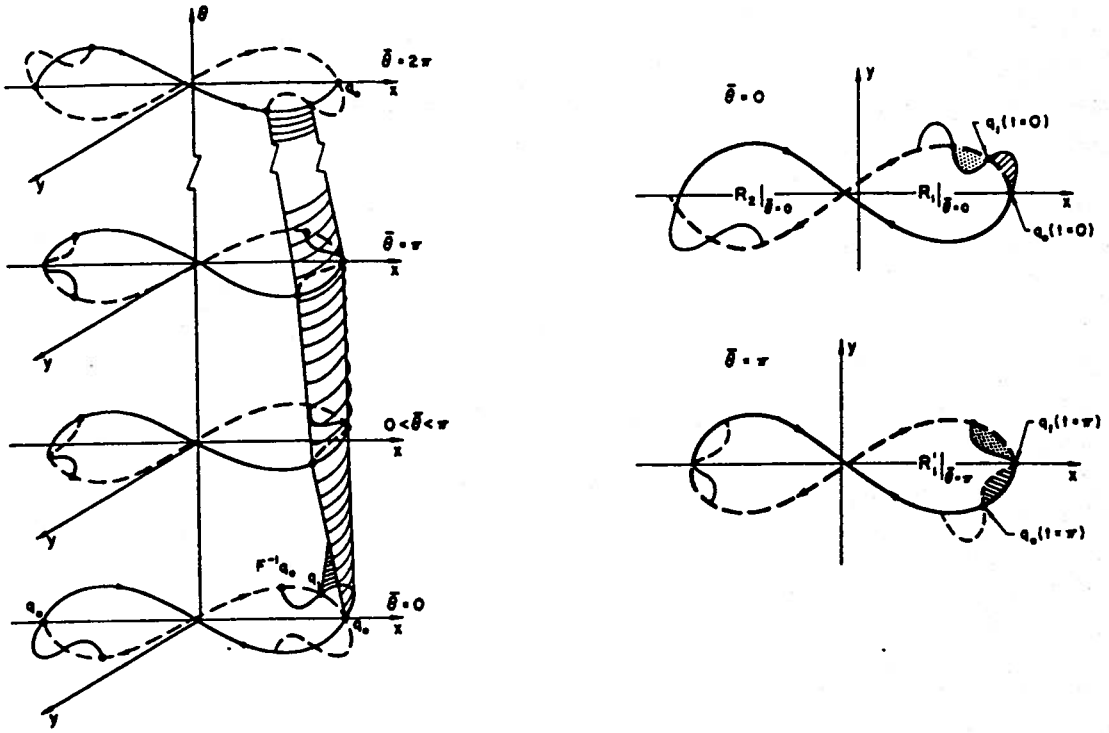

Figure 7.4: Lobe evolution with time (Rom-Kedar and Wiggins, (1990))

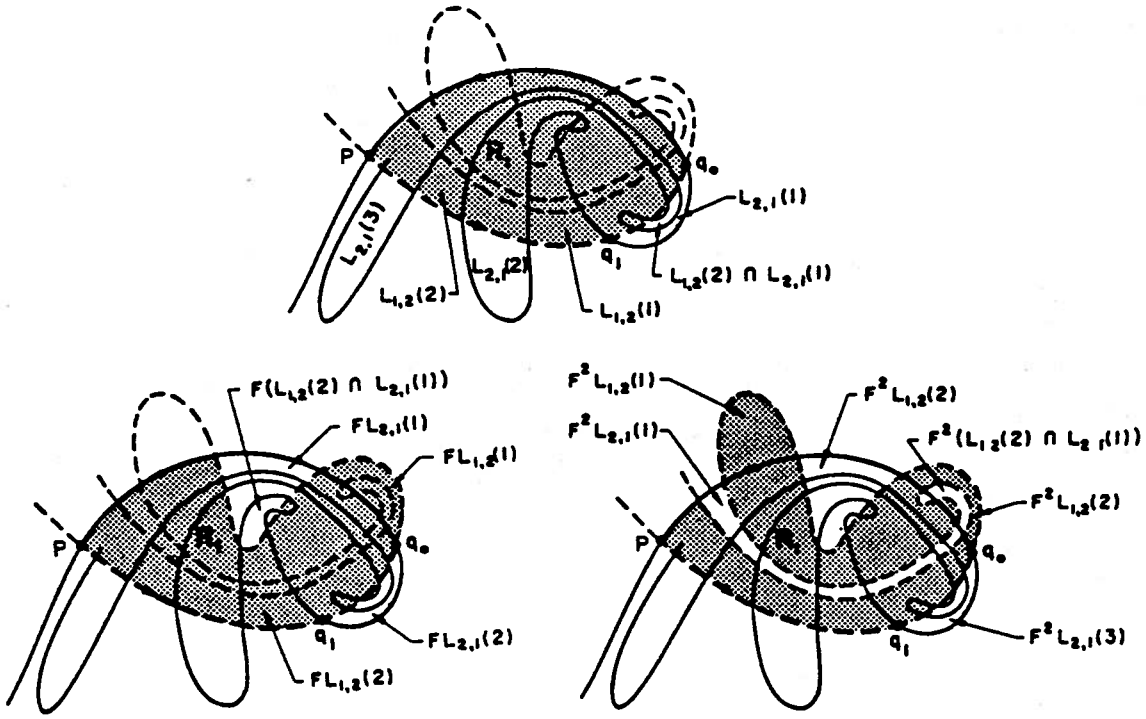

Figure 7.5: Lobe evolution with iterates (Rom-Kedar and Wiggins, (1990))

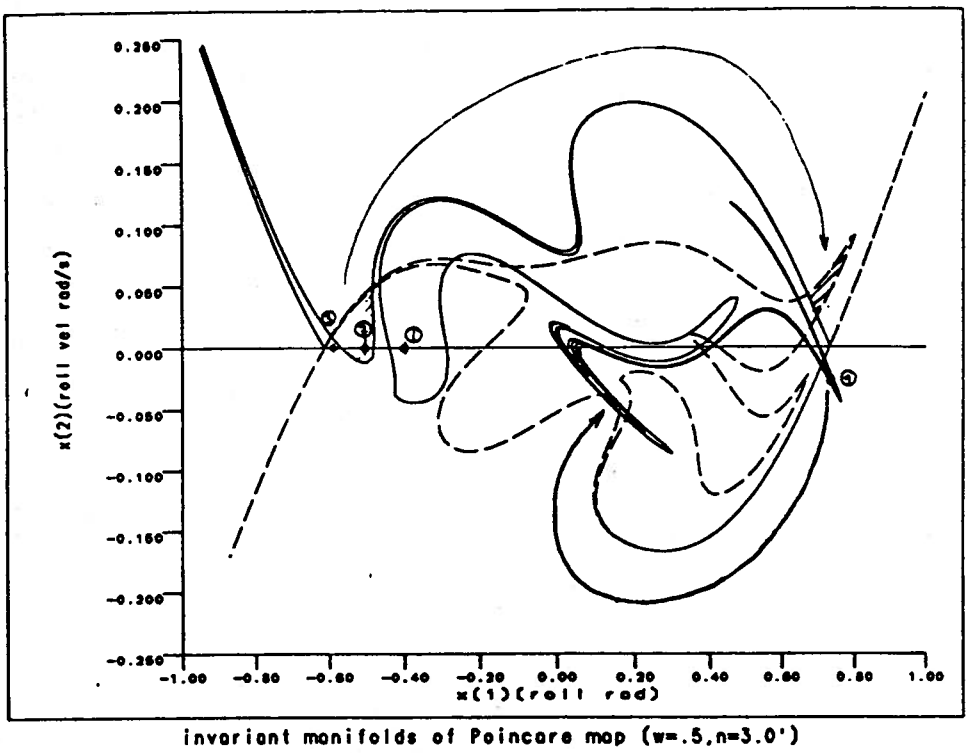

Figure 7.6: Lobes for clam dredge boat Patti-B

CHAPTER VIII

APPLICATIONS AND RESULTS

In order to gain a clearer understanding of methods described in the previous chapters, we apply these techniques to the twice capsized clam dredge *Patti-B*. The *Patti-B* was previously analyzed and vessel characteristics can be found in an eariler project report (Falzarano, (1988)).

We begin our analysis by using a numerical path following computer program to study bifurcation and stability of a vessel slowly turning in waves. We use this problem to evaluate the importance of the frequency dependence of the linear hydrodynamic coefficients and coupling between the modes of motion. Next, we apply the geometric methods to analyze the *Patti-B*. We begin by comparing the numerically observed intersection of the invariant manifolds to the Melnikov prediction. We note here the importance of choosing the correct axis system in order to reduce the multiple degree of freedom system to an equivalent single degree of freedom system. Next, we describe the details of determining the Melnikov function analytically and numerically. Motivated by the importance of reducing the degrees of freedom, we describe the conditions that must be satisfied in order to approximately reduce the degrees of freedom. Next, we describe the importance of each of the homoclinic and heteroclinic manifold intersections and the special case of the intersection of the unstable homoclinic and stable heteroclinic manifolds and show some typical results.

Next, we describe how we can use the powerful tool of lobe dynamics (Wiggins, (1990)) to predict whether or not an initial condition upon future iterates of the map will be safe or not. We show some surprising results to demonstrate a practical application of this method. Next, we show a series of results where we have tried to find an intersection of the unstable homoclinic and stable heteroclinic manifolds. Although Wiggins (1990) has rigorously shown the equivalence of different phase Poincaré maps, we show some results to demonstrate how two different phases of the Poincaré map look, in order to heuristically justify our only looking at a single phase of the Poincaré map. We return to the vessel turning problem at this point and demonstrate, using numerical integration, some aspects of the magnification curves; these include the non-stable saddle, and traveling through resonance. We return to the lolled righting arm curve to show three qualitatively different types of behavior that the Duffing equation may have; they are harmonic, subharmonic and aperiodic. We use this opportunity to demonstrate the usefulness of the three common methods of presenting integration results; these are a time history, a projected phase plane and a Poincaré map. The final result we show in this section is a so-called strange attractor which is the distinctive figure that bounded chaotic motions form in the Poincaré map. In the next section, we continue to analyze and describe chaotic motion in more detail. In this section, we calculate the Lyapunov exponents and dimension for another chaotic response. Finally, we give a variety ofresults for combined parametric and external excitation.

Vessel turning problem

Because this section does not include the lolled $GZ(\phi)$ curve as is included elsewhere, the section may at first glance appear to be unrelated to the rest of the work; however, this is not the case. In addition, this section may initially appear to be something that can be easily solved using classical perturbation methods. Although

one could readily solve the single degree of freedom constant hydrodynamics problem analytically using perturbation methods (e.g., Nayfeh and Sanchez, (1989)), one would be hard pressed to solve the multiple degree of freedom frequency dependent problem. However, using a numerical path following computer programs such as BIFPACK (Seydel, (1988a)), solving the multiple degree of freedom frequency dependent hydrodynamics problem is only slightly more difficult and computationally intense than the single degree of freedom fixed hydrodynamics problem. In addition, with path following computer programs there is no limit on the degree of nonlinearity or coupling as is the case with a perturbation scheme. For all these reasons, the practical results included herein were produced using BIFPACK (Seydel, (1988a)).

In this section, we study the clam dredge *Patti-B* with a constant forward speed turning in waves. We use this problem to evaluate the importance of nonlinearity, multiple degrees of freedom and frequency dependent hydrodynamics for the *Patti-B*. Throughout this section, unless otherwise stated, we analyze the *Patti-B* with the static righting arm curve with which she was believed (NTSB, (1979) and Falzarano, (1988)) to have capsized (i.e., GM=1.755 feet), with a forward speed of 10 feet/second, in 300 foot long deep water waves. We consider the multiple degree of freedom equations of motion. The frequency dependent hydrodynamics were calculated using the linear ship motions computer program SHIPMO (Beck and Troesch, (1989)). The frequency dependence of the hydrodynamic coefficients is due to the variation of the frequency of encounter as the vessel turns (Chapter III)[1].

We note that using a linear ship motions computer program the response is quantitatively similar to the nonlinear results, but important qualitative features are

---

[1] As the vessel turns with constant forward speed (vary β), the frequency of encounter is changed due to the doppler effect of $\omega_e = \omega_o - U\kappa\cos(\beta)$, where ω_e is the encounter frequency, ω_o is the wave frequency, U is the vessel speed, κ is the wave number ($= 2\pi/\lambda$, λ is the wave length), and β is the heading angle, zero heading is when the ship is traveling with the waves and π is when the ship is traveling into the waves.

ignored (Figure 8.1). Although the magnitude, away from the peak, is relatively well predicted using an equivalent linearization of the roll damping (Chapter III). Since, the linear ship motion program must use a linear roll restoring moment curve, it misses the important features such as the bending back of the peak of the magnification curve. This bending back results in a multivalued solution which must be reconciled by considering the stability of the solution. The next plot shows that slightly changing the magnitude of the metacentric height (Appendix E), which is the initial slope of the $GZ(\phi)$ curve, dramatically changes the character of the resulting response curve (see Figure 8.2). We see as the magnitude of this term is increased slightly, from around 1.755 feet, how the magnification curve eventually *pinches off* the bent back peak. These systematic changes explain the relationship between the two seemingly unrelated types of curves, first, the relatively uninteresting single-valued curves for high GM and second, the interesting multivalued magnification curves for the lower GM's. It should be noted here that after the peak is pinched off from the main branch, it does not disappear, it just becomes unstable and difficult to find.

Finally, we demonstrate the importance of multiple degrees of freedom and frequency dependent hydrodynamics. In Figure 8.3, we compare the vessel's response while executing a very slow turn (vary β) in a five foot and seven and a half foot wave amplitude seaway. We compare the more complete multiple degree of freedom solution with the commonly used approximate single degree of freedom roll equation. We note here that the single degree response in a seven and a half foot seaway is roughly equal to the multiple degree of freedom response in a five foot seaway. The single degree of freedom approximation can cause substantial error. Although it is conservative in this case, it need not always be and in any event it can be misleading. In addition, we include a curve where the heading was kept constant ($\beta = 135$degrees) and the wave length is varied (Figure 8.4). Although keeping the hydrodynamics

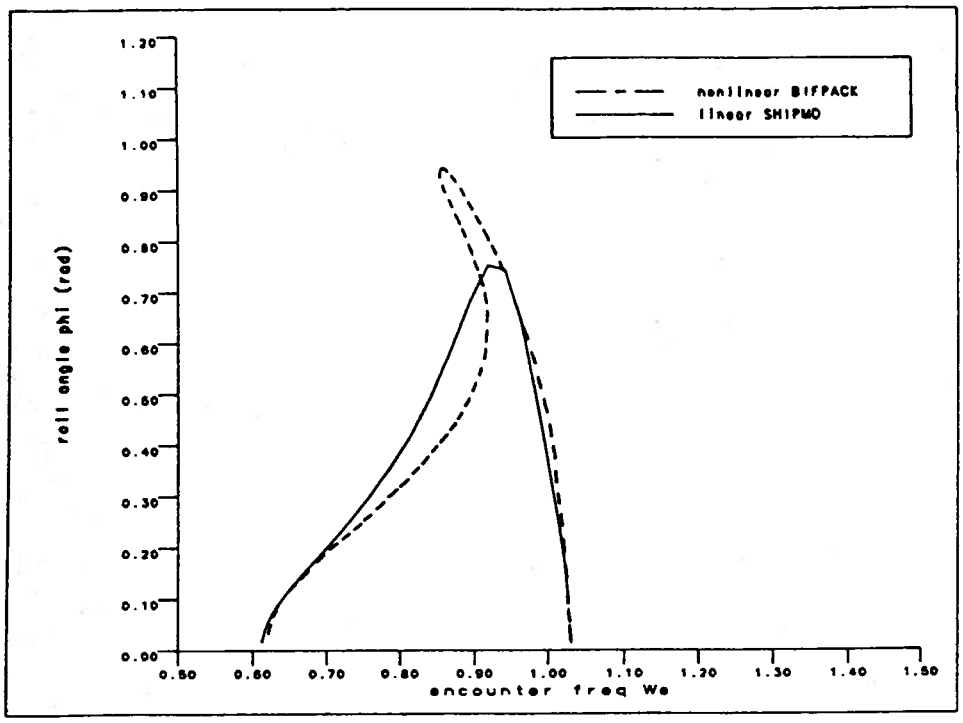

Figure 8.1: Comparison of linear and nonlinear solution

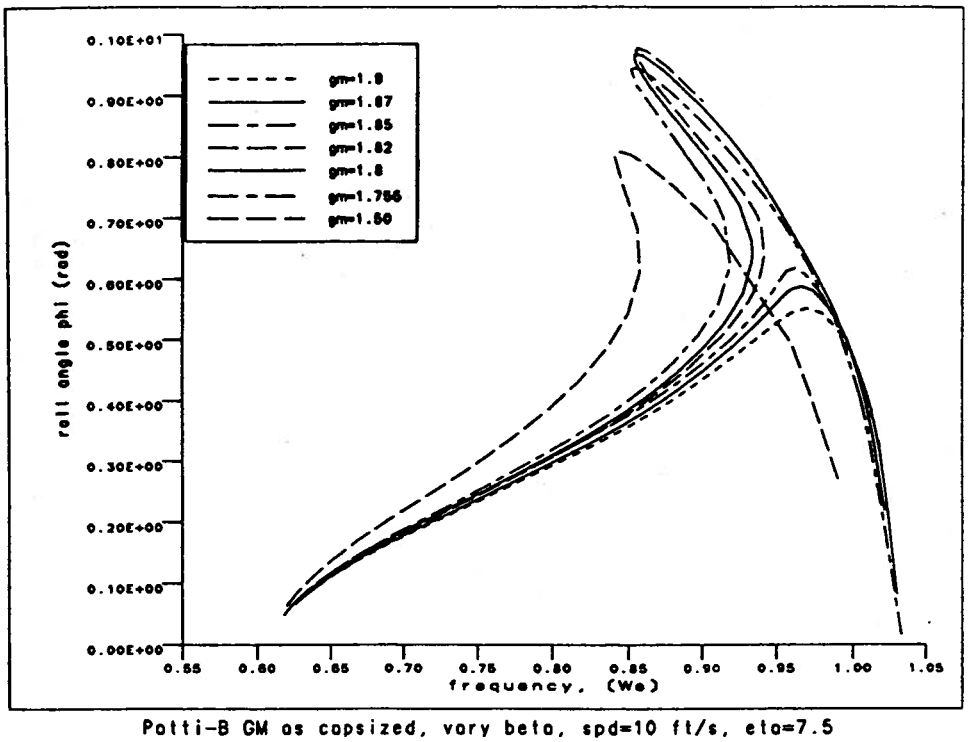

Figure 8.2: Nonlinear solution, note pinching off of the solution

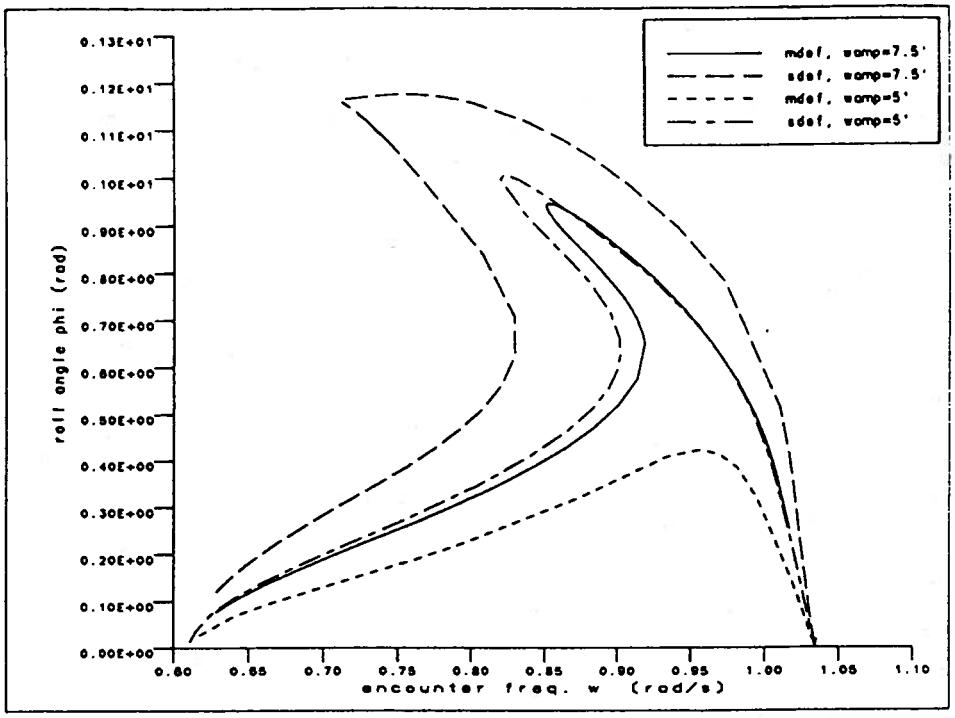

Figure 8.3: Single vs. multiple degree of freedom (vary β)

constant at the vessel natural frequency as the wave length is varied may be a reasonable approximation for a constant heading, as the vessel executes a turn, this approximation may no longer be reasonable. Therefore, we compare the constant coefficients approximation to the more accurate frequency dependent coefficients for only the varying wave length problem (Figure 8.5). The frequency dependence is not found to be as important quantitatively as the number of degrees of freedom, but we note the under and over prediction caused by this constant hydrodynamics approximation.

In addition to finding solutions, we also evaluate the stability of given solutions and the way in which stability is gained or lost. We evaluate these changes in stability by observing how the eigenvalues of the map change with frequency, which is the bifurcation parameter (see Figure 8.6). In addition, we can locate the fixed points of the Poincaré map and establish their stability properties. Then using other techniques, we can demarcate the basins of attraction of the various steady-

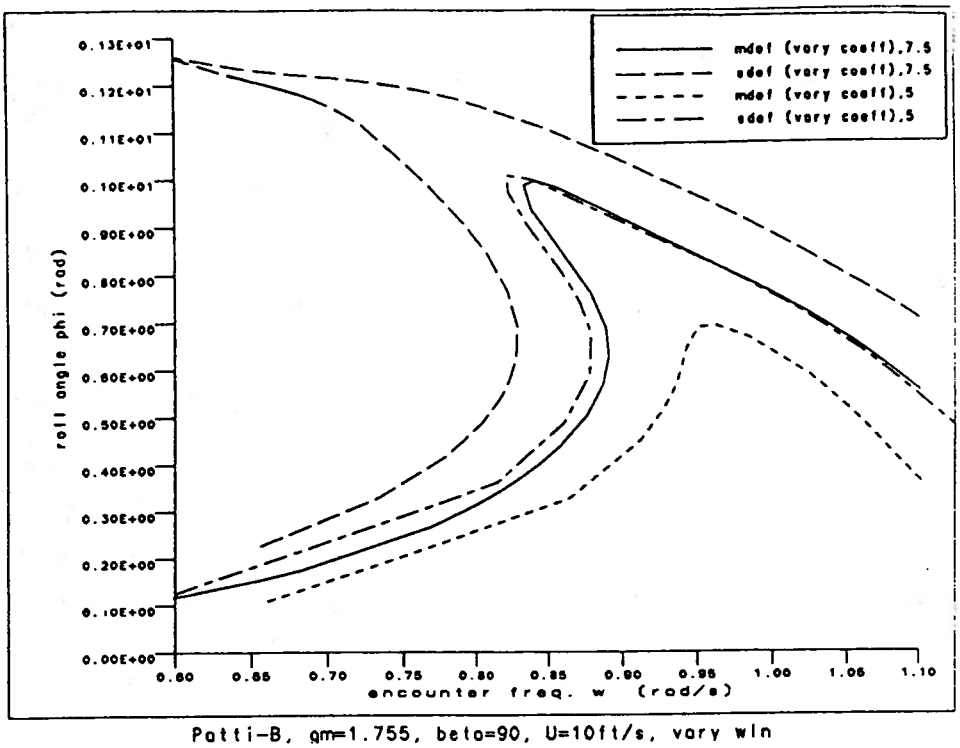

Figure 8.4: Single vs. multiple degree of freedom (vary λ)

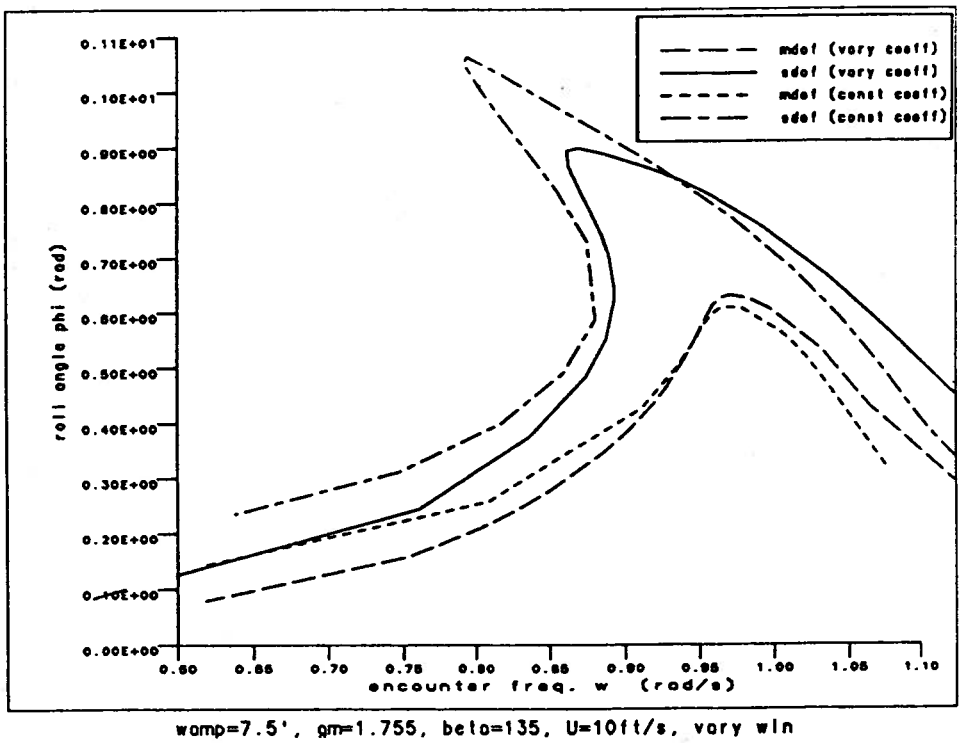

Figure 8.5: Fixed vs. frequency dependent hydrodynamics (vary λ)

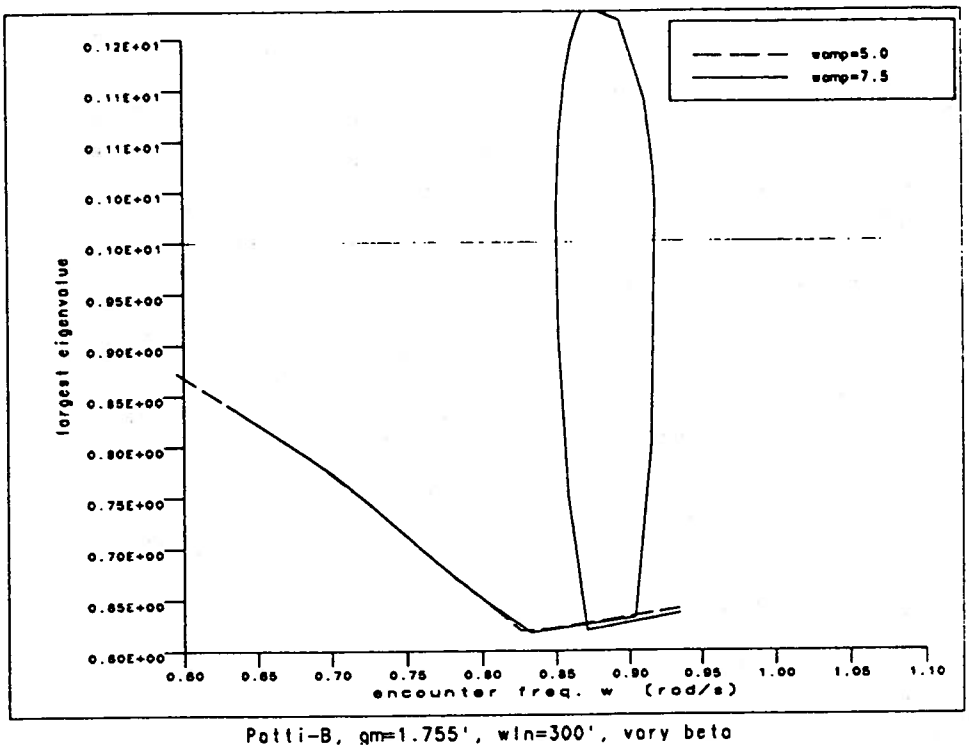

Figure 8.6: Typical result of a stability calculation

state solutions (Chapter III). For the cases considered here, we found the stability to be lost at the vertical tangent and regained as the peak was passed. The only unexpected behavior we found was when the curve pinched off the unstable branch. However, in the section on parametric excitation, the final section in this chapter, we observe additional mechanisms for losing stability related to combined external and parametric excitation.

Applications of geometric methods

In this section, we apply the modern geometric methods for analyzing dynamical systems, previously described, to the problem of vessel capsizing with damage or water-on-deck. Recall, we approximate water-on-deck or damage by modifying the the hydrostatic curve which for our example includes a loll angle. The modern methods in contrast to the more traditional perturbation techniques are not limited to small nonlinearity (weakly nonlinear systems) or small regions near equilibria (local analysis). The modern methods, instead, are general and are able to consider large nonlinearity and large regions in phase space which may include multiple equilibria and the orbits or manifolds that connect or surround them. We specifically apply these methods to analyze the clam dredge *Patti-B's* capsizing mechanisms. We analyze the *Patti-B* because it has the dubious distinction of having capsized *twice*! Her first capsizing (NTSB, (1979)) occurred in shallow water off of Ocean City, Maryland and she was salvaged. About two years later, *Patti-B* was at sea, far offshore (USCG, (1979)) when she capsized again. The two *Patti-B* capsizings are especially disturbing because she is typical of a large number of similar sized and designed fishing vessels, and apparently met all the then existing recommendations (Falzarano, (1988)). However, the fact that she had a proportionately large after deck prone to trapping water may have adversely contributed to her unfortunate safety record.

Comparison of analytical and numerical Melnikov calculations

In this subsection, we intend to answer two questions. First, can we get transverse homoclinic and heteroclinic intersections for a typical ship dynamical system? Second, how well do the analytical approximations made compare to the more exact numerical integrations of the manifolds (Parker and Chua, (1988))? In order to answer these questions, we consider the single degree of freedom Melnikov function

for a variety of coordinate systems. We desire a single degree of freedom system at this point because the transverse intersections are much easier to detect. We will investigate multiple degree of freedom systems in the coming sections. In all cases, we consider a modified righting arm curve which has an initial loll angle (Appendix E).

Specifically, we present results for the homoclinic and heteroclinic Melnikov function for a variety of coordinate systems (Figures 8.7 and 8.8). These coordinate systems are: 1) the standard ship motions axis system with its origin at the waterline (SHIPMO, $zgo = -1.88'$), 2) a center of gravity coordinate with its origin at the center of gravity (CG, $zgo = 0.0'$), and 3) a principal normal modes coordinate system with its origin translated to a location eliminating all coordinate coupling including added mass (pna, $zgo = 1.0'$). We note, for the principal normal modes coordinate system and higher frequencies, the required wave amplitude for the heteroclinic intersections are actually less than those for homoclinic intersections. Although this seems counter-intuitive, it may be due to the relative importance of the various terms in the two Melnikov integrals. We avoid these higher frequencies in our analysis. The large differences between the various curves shows the importance of transforming to the correct axis system in order to obtain an equivalent single degree of freedom system[2]. Choosing the correct, or at least a best approximation to uncoupling the roll from the sway and yaw prior to extracting the roll equation from the multiple degree of freedom system will be discussed more fully in a later subsection on "Reduction of degrees of freedom to an equivalent system".

However, once we have decided upon a coordinate system and extracted the roll equation from the multiple degree of freedom system, the comparison between the

---

[2] We note here that the Melnikov result for the multiple degree of freedom problem would be independent of coordinates; However, our goal in selecting an equivilent single degree of freedom system is to approximately decouple the roll equation of motion from the other degrees of freedom. The differences reflect the importance of coupling.

analytical Melnikov predictions and those determined by numerically determining the manifolds is reassuringly close. We see a typical result (Figure 8.9) for wave encounter frequency of $\omega_e = 0.45$ radians/second and amplitude of $\eta_o = 0.1625$ feet where the manifolds are just beginning to intersect. We refer to the analytically predicted homoclinic Melnikov results (Figure 8.7), specifically the solid line (i.e., SHIPMO), and notice the value of the curve is about 0.15 feet.

Consideration of the previous results suggests the importance of extracting the correct equivalent single degree of freedom system from the multiple degree of freedom system. Along with the coming subsection on "Reduction of degrees of freedom to equivalent system", we discuss this problem more fully in Appendix B. For the purposes of the Melnikov vector, we require the unperturbed system to be uncoupled with no damping and no forcing. We include everything else in the perturbation. Since we are able to do this, we are able to express the additional degrees of freedom (i.e., sway and yaw) as slowly varying oscillators (Wiggins and Shaw (1988)).

For the purposes of a closed form Melnikov estimate, we initially approximate each the homoclinic and the heteroclinic righting arm curve with a different locally valid cubic approximation. As stated previously, this is done because the unperturbed homo(hetero)clinic orbits are simple hyperbolic functions. Due to the limitations of a cubic approximation to the righting arm curve, it is not difficult to see that each of these two approximations are only locally valid at their respective saddles and are very different globally. Specifically, the homoclinic approximation is valid only up to the loll angle and neglects the angle of vanishing stability while the heteroclinic approximation is only valid about the angle of vanishing stability and totally neglects the loll angle. However, the numerically determined Melnikov analysis uses a more accurate quintic polynomial approximation to the righting moment curve. The numerically determined manifolds use a still more accurate ninth order polynomial approximation. At this point, we digress in order to compare the approximate ana-

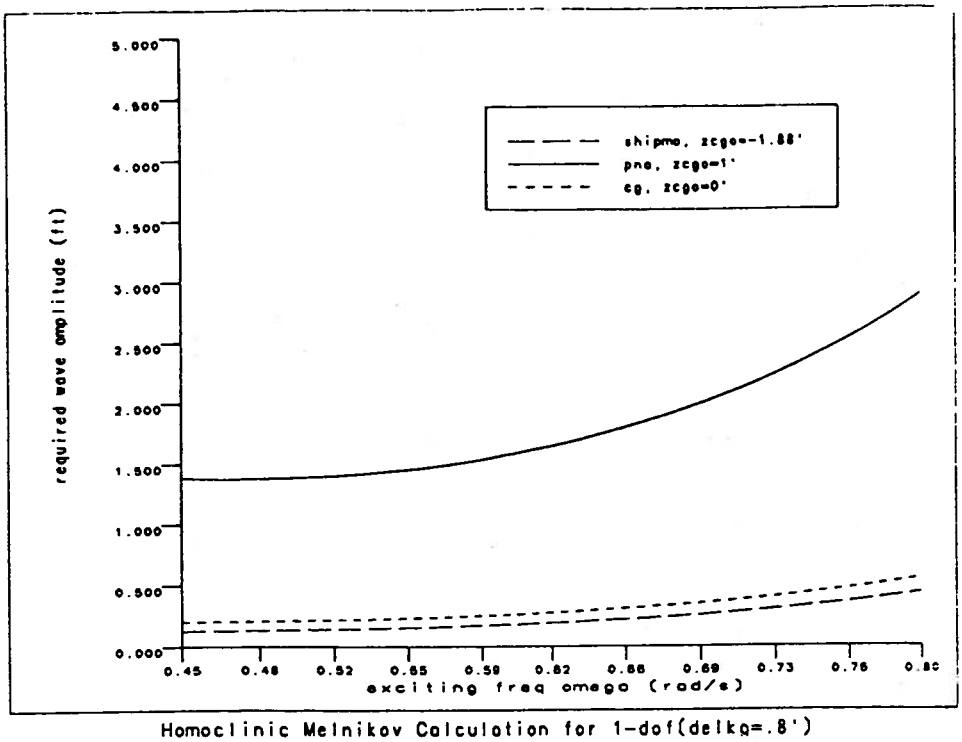

Figure 8.7: Homoclinic Melnikov function

lytic results to the more accurate numerical approximation of the Melnikov integrals in the next section.

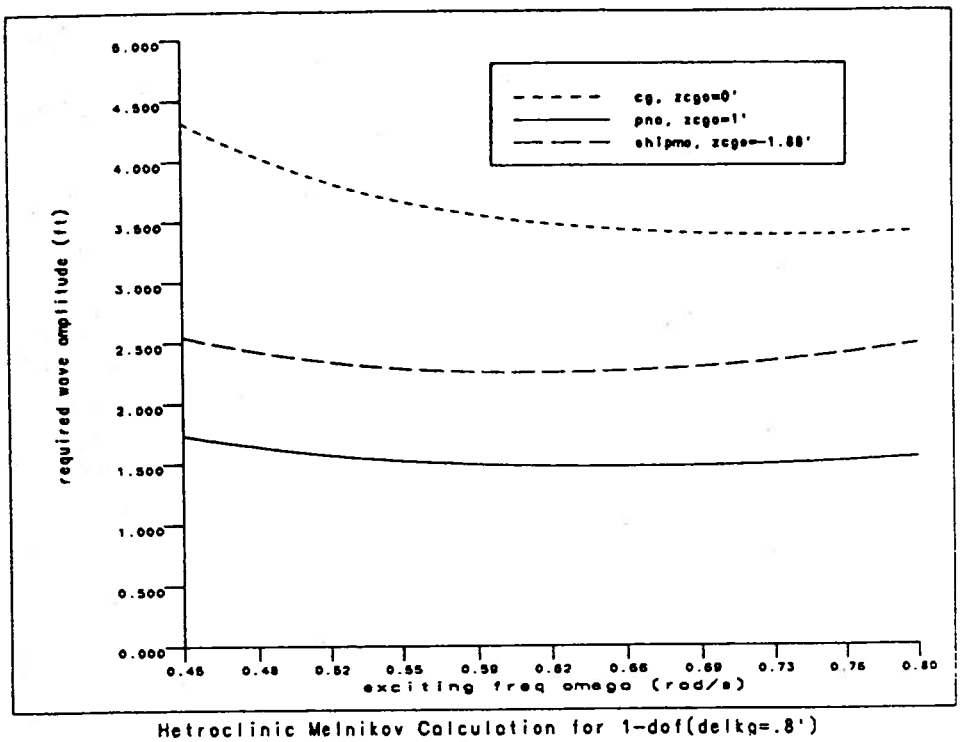

Figure 8.8: Heteroclinic Melnikov function

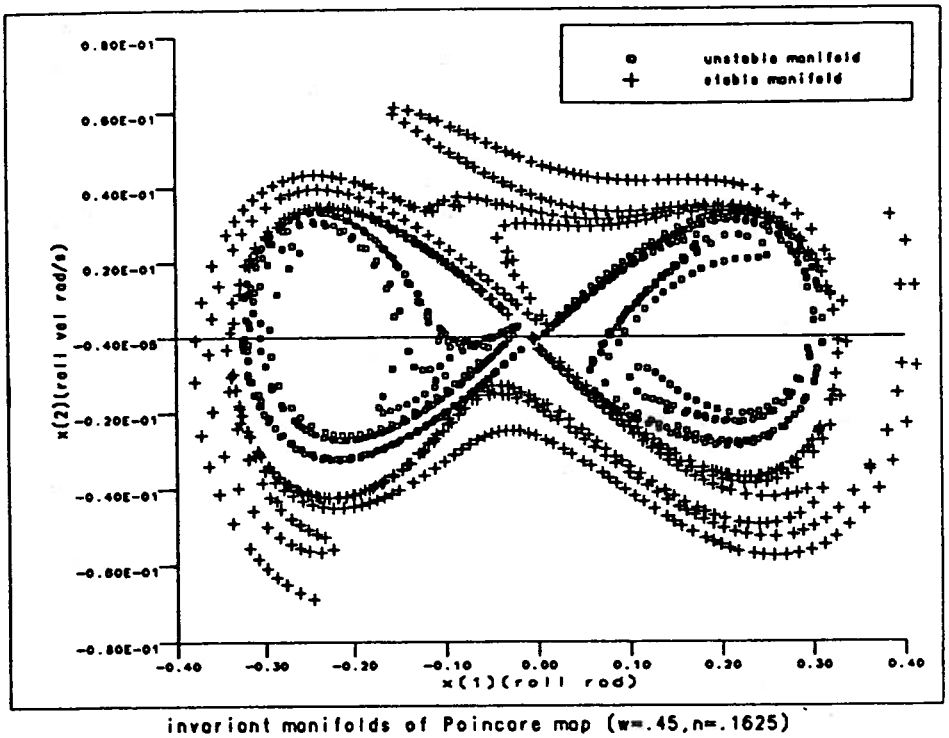

Figure 8.9: Sample manifold intersection

Determination of the Melnikov function

In this section we discuss the details of determining the homoclinic and heteroclinic Melnikov integrals analytically and numerically.

Recall, the Melnikov function is as follows

$$M(t_0) = \int_{-\infty}^{+\infty} f(q^0(t)) \wedge g(q^0(t), t + t_0)dt, \tag{8.1}$$

or is equivalently,

$$M(t_0) = \int_{-\infty}^{+\infty} f^{\perp}(q^0(t)) \cdot g(q^0(t), t + t_0)dt. \tag{8.2}$$

In the previous chapters, we have already given the analytical results for both the homoclinic and heteroclinic Melnikov function. Each was determined using a different locally valid cubic approximation to the roll restoring moment curve. In Figure 8.10, we compare the two scaled (rescale time so that $\omega_n = 1$) cubic approximations to the righting arm curve to a scaled quintic approximation.

In order to evaluate the accuracy of these approximations it seems reasonable to formulate a numerical Melnikov integration procedure. The numerical results could then be compared to the analytical estimates to assess the accuracy of the two locally valid cubic approximations. Recall, the benefit of approximating the roll restoring moment curve as a cubic is that the homoclinic and heteroclinic trajectories can be expressed analytically in terms of hyperbolic functions.

The homoclinic Melnikov analysis

Recall, our scaled homoclinic differential equation is,

$$\ddot{x} + \alpha\dot{x} + \alpha_q\dot{x} \mid \dot{x} \mid -x + kx^3 = f\cos(\omega\tau). \tag{8.3}$$

In order to get this equation into the form for the Melnikov method (see Appendix A), α, α_q and f are required to be small (i.e., $\sim O(\epsilon)$). We define $\epsilon\delta = \alpha, \epsilon\delta_q = \alpha_q$ and $\epsilon\gamma = f$. The unperturbed homoclinic trajectories corresponding to this equation with $(x, \dot{x}) = (x_1, x_2)$ defined are,

$$(x_1, x_2) = \sqrt{\frac{2}{k}}(\text{sech}(t), -\text{sech}(t)\tanh(t)) \tag{8.4}$$

In Figure 8.11, we start at time zero and observe how an initial condition travels toward the saddle. By reversing time we could trace out the unstable manifold of the saddle (reflected about the roll axis), or alternatively, we could multiply the whole expression by minus one and obtain the other stable manifold (reflected about both axes). From the figure, since the points all have the same time step ($dt = .1$ seconds) you can see that it takes finite time to get arbitrarily close to the saddle point but it takes an infinite time to actually land on the saddle. Alternatively, if one starts on the saddle it takes infinite time to leave the saddle. Therefore, in our numerical work, we either start away from the saddle and approach it or we linearly approximate the unstable manifold of the saddle in order to start away from the saddle. Finally, in Figure 8.12, you can see the justification for truncating the numerical Melnikov improper (infinite upper and lower limits) integral after a very short finite time. This is so because the roll velocity quickly asymptotes to zero.

Using the specified homoclinic trajectories, the analytic Melnikov integral is,

$$\begin{aligned} M(t_0) = \quad & \sqrt{\tfrac{2}{k}}\sin(\omega t_0)\gamma\int_{-\infty}^{+\infty}\sin(\omega t)\text{sech}(t)\tanh(t)dt \\ & -\delta\tfrac{2}{k}\int_{-\infty}^{+\infty}\text{sech}^2(t)\tanh^2(t)dt \\ & -\delta_q(\tfrac{2}{k})^{3/2}\int_{-\infty}^{+\infty}\text{sech}^2(t)\tanh^2(t)|\text{sech}(t)\tanh(t)|dt. \end{aligned} \tag{8.5}$$

Evaluating these integrals we obtain the following Melnikov function,

$$M(\tau_0) = +\gamma\pi\omega\sqrt{\frac{2}{k}}\text{sech}(\frac{\omega\pi}{2})\sin(\omega\tau_0) - \frac{4}{3k}\delta - \frac{2}{k}\sqrt{\frac{2}{k}}\delta_q\frac{4}{15}. \tag{8.6}$$

Alternatively, for a more general form of the roll restoring moment curve, we may numerically determine the homoclinic trajectory (x_1, x_2) and numerically evaluate the following integral,

$$M(t_0) = 2\sqrt{\frac{2}{k}}\sin(\omega t_0)\gamma\int_0^{+\infty}\sin(\omega t)x_2 dt - 2\delta\frac{2}{k}\int_0^{+\infty}x_2^2 dt - 2\delta_q(\frac{2}{k})^{3/2}\int_0^{+\infty}x_2^2|x_2|dt \tag{8.7}$$

The heteroclinic Melnikov analysis

Recall, our scaled heteroclinic differential equation is as follows,

$$\ddot{x} + \alpha\dot{x} + \alpha_q\dot{x} \mid \dot{x} \mid + x - kx^3 = f\cos(\omega\tau). \tag{8.8}$$

The unperturbed heteroclinic trajectories corresponding to this equation with variables redefined as above are,

$$(x_1, x_2) = -\frac{1}{\sqrt{k}}(\tanh(t), \frac{1}{\sqrt{2}}\text{sech}^2(t)). \tag{8.9}$$

In Figure 8.13, we start at time zero and observe how an initial condition travels toward the saddle. Again, from the figure, you can see that it takes finite time to get arbitrarily close to the saddle point but it takes an infinite time to actually land on the saddle. Finally, in Figure 8.14, you can again see the justification for truncating the improper (infinite upper and lower limits) Melnikov integral after a very short finite time because the roll velocity quickly asymptotes to zero.

Using the specified heteroclinic trajectories, the analytic Melnikov integral is,

$$\begin{aligned} M(t_0) = \; & -\sqrt{\tfrac{1}{2k}}\cos(\omega t_0)\gamma\int_{-\infty}^{+\infty}\cos(\omega t)\mathrm{sech}^2(\tfrac{t}{\sqrt{2}})dt \\ & +\delta\tfrac{1}{2k}\int_{-\infty}^{+\infty}\mathrm{sech}^4(\tfrac{t}{\sqrt{2}})dt \\ & +\delta_q(\tfrac{1}{2k})^{3/2}\int_{-\infty}^{+\infty}\mathrm{sech}^4(\tfrac{t}{\sqrt{2}})|\mathrm{sech}^2(\tfrac{t}{\sqrt{2}})|dt \end{aligned} \tag{8.10}$$

Evaluating the various improper integrals we obtain the following Melnikov function,

$$M(\tau_0) = -\frac{\gamma\pi\omega\sqrt{2}}{\sqrt{k}}\mathrm{csch}(\frac{\omega\pi}{\sqrt{2}})\cos(\omega\tau_0) + \frac{2\sqrt{2}\delta}{3k} + \frac{8\delta_q}{15k^{3/2}}. \tag{8.11}$$

Alternatively, for a more general form of the roll restoring moment curve, we may numerically determine the heteroclinic trajectory (x_1, x_2) and numerically evaluate the following integral,

$$M(t_0) = -2\sqrt{\frac{1}{2k}}\cos(\omega t_0)\gamma\int_0^{+\infty}\cos(\omega t)x_2dt + \frac{\delta}{k}\int_0^{+\infty}x_2^2dt + 2\delta_q(\frac{1}{2k})^{3/2}\int_0^{+\infty}x_2^2|x_2|dt \tag{8.12}$$

Numerical evaluation of the Melnikov integral

In both cases, use was made of the oddness or evenness of the various integrals in eliminating trivial integrals and in setting up the remaining integrals for numerical integration. Having an analytic solution of the Melnikov function will allow us to evaluate the accuracy of the algorithm we develop. Our numerical scheme must satisfy the following,

$$2\int_0^{+\infty}F(t,\omega)dt \approx 2\sum_{i=1}^{N}F_N(t,\omega)\Delta t. \tag{8.13}$$

We know from the definition of the integral that these two will be exactly equal in

the limit as N goes to infinity ($\lim N \rightarrow \infty$), and Δt goes to zero ($\lim \Delta t \rightarrow 0$)[3]. We found that our Δt was some function of ω (e.g., $G(\omega)$) since the oscillatory nature of the integral ultimately determined the size of our Δt.

We note here that although the numerical evaluation of the Melnikov integral does not lead to a simple formula in terms of integer constants and simple functions as the analytic formulation did, we are able to factor out most of the system parameters. For a given righting moment curve, we need only evaluate the Melnikov integral at each frequency. The numerically determined Melnikov function will then allow us to evaluate the required wave amplitude for intersections given a fixed linear and quadratic damping coefficient. This procedure is more general and does not require the unperturbed homoclinic and heteroclinic trajectories to be expressible in terms of simple functions; nor does it require the resulting improper Melnikov integrals to be readily available (e.g., Gradshteyn and Ryzhik, (1980)).

For our numerical evaluation of the Melnikov integral, we choose a fifth-order polynomial that approximates the exact $GZ(\phi)$ curve, with the same loll angle ϕ_l and angle of vanishing stability ϕ_v (see figure 8.14). Although the conservative trajectories can be expressed in terms of elliptic integrals and hypergeometric functions. these special functions would also need to be evaluated numerically along with the resulting Melnikov integrals. Therefore, phase plane analysis of the conservative system was used in order to find the integration starting point in the phase plane. From these starting points, a fourth order Runga-Kutta and losoda, a NAAS (CCMemo 407, (1979)) self-correcting integration code was used and compared to the phase plane analysis results (see figures 8.15 and 8.16). These results (t, x_1, x_2) were then inserted into the improper Melnikov integral and numerically evaluated using a trapezoidal rule. Convergence studies were undertaken to determine how small a Δt was

---

[3] Note here that for our numerical approximation of this integral t_{max} is fixed at some large number and as Δt changes the number of interval N changes accordingly. So that for fixed t_{max}, we have the $\lim N \rightarrow \infty$ and $\lim \Delta t \rightarrow 0$

required to be and what was the required maximum time (i.e., t_{max}) in order to approximate the infinite upper limit.

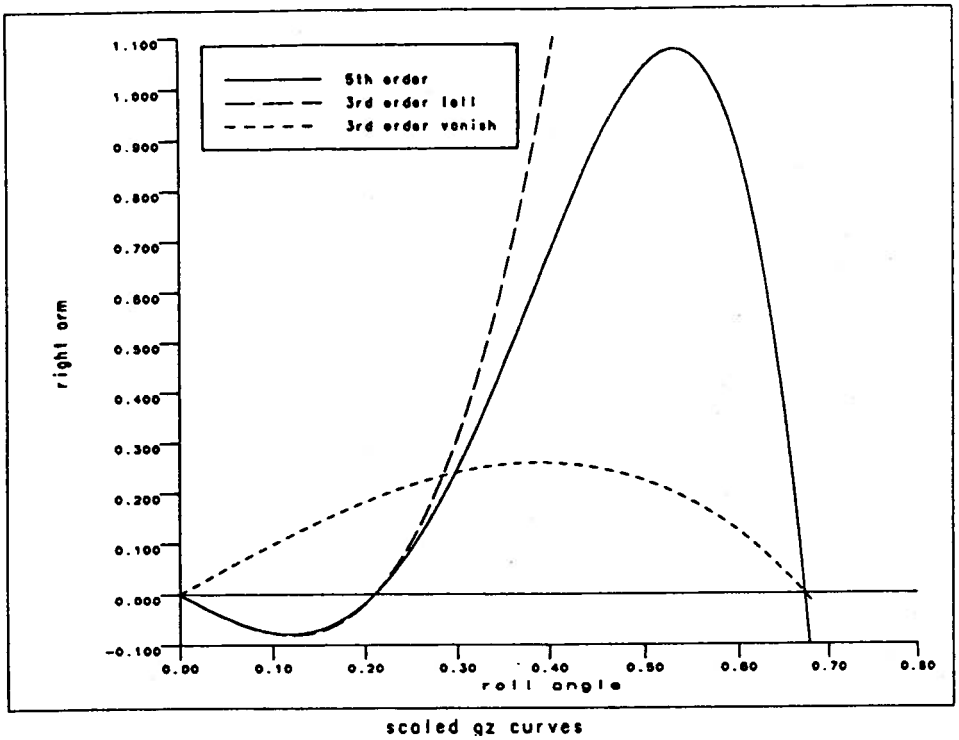

Figure 8.10: Cubic vs. quinitic ship restoring moment

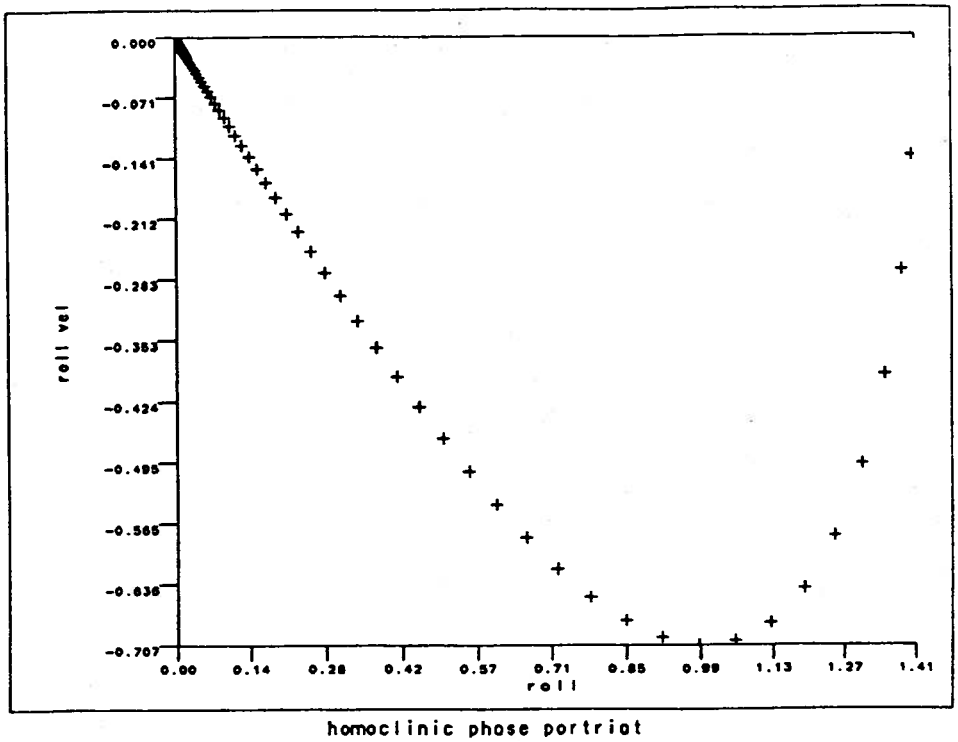

Figure 8.11: Homoclinic phase plane (k=1)

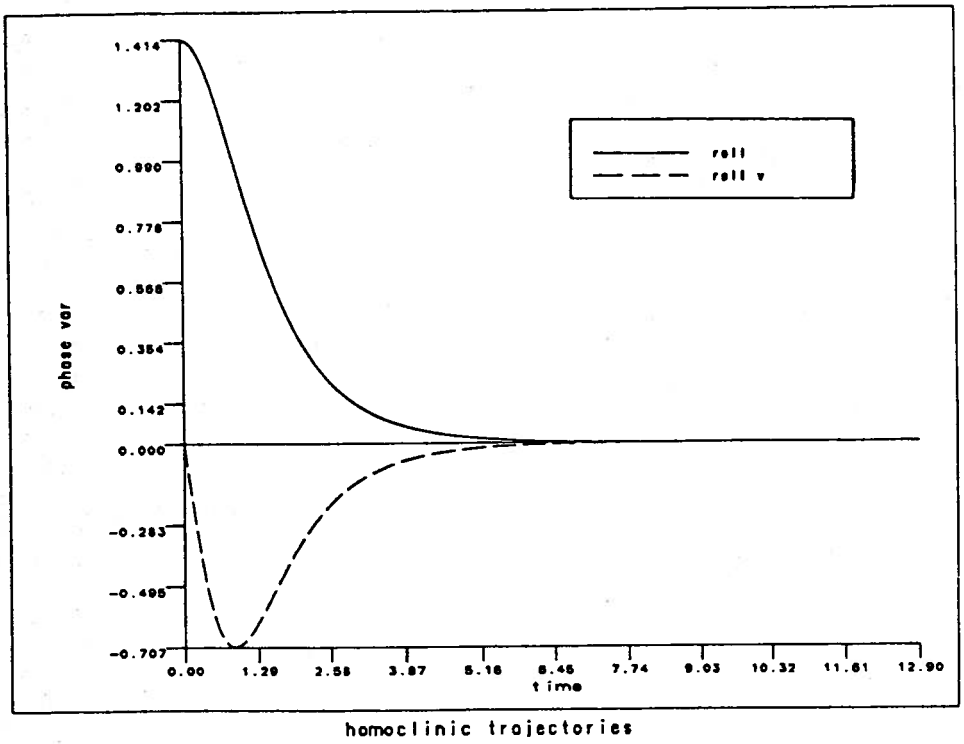

Figure 8.12: Homoclinic phase variables vs. time (k=1)

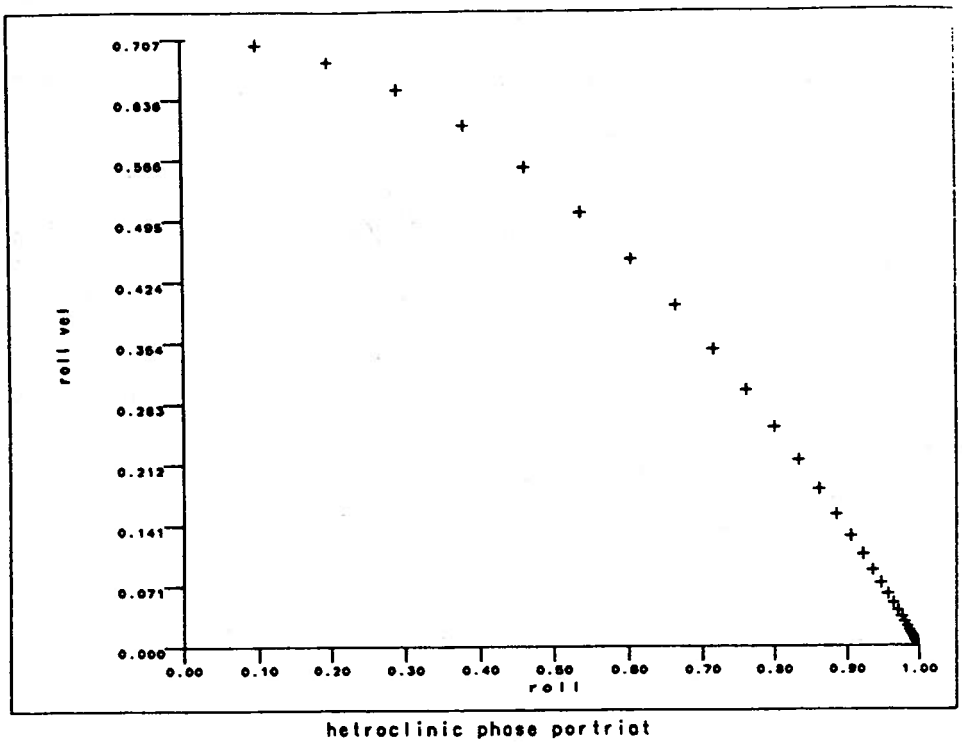

Figure 8.13: Heteroclinic phase plane (k=1)

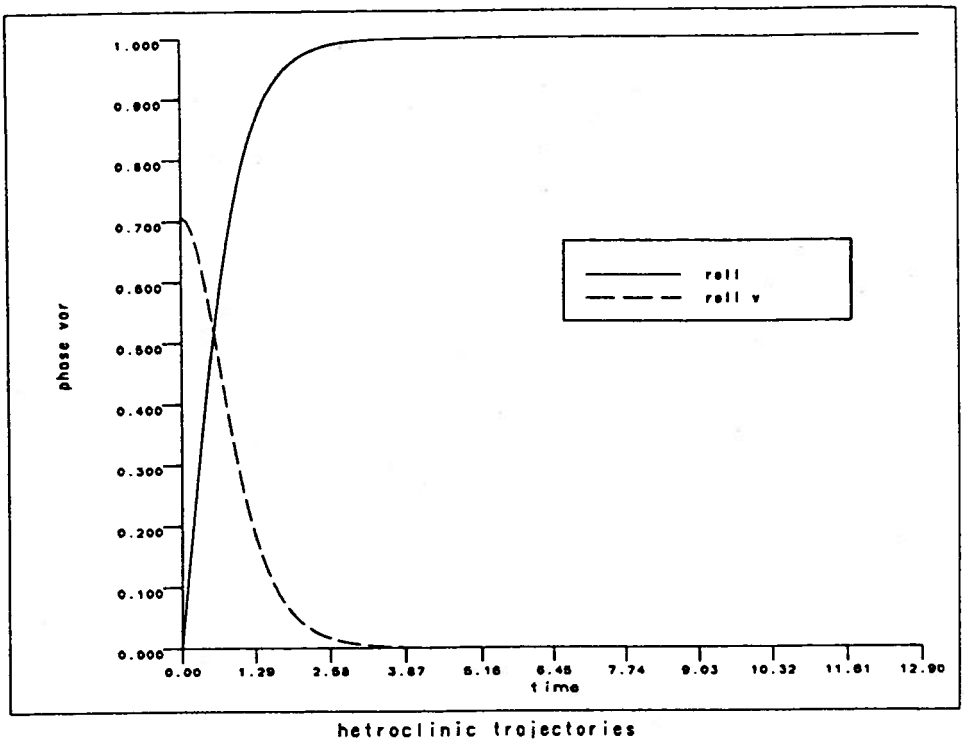

Figure 8.14: Heteroclinic phase variables vs. time (k=1)

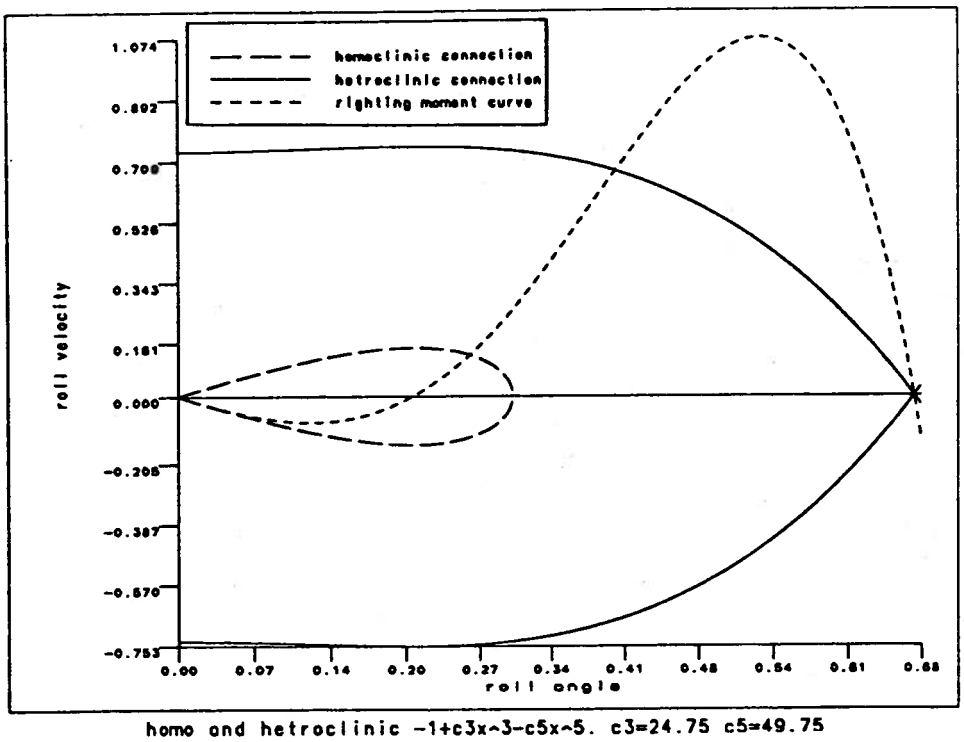

Figure 8.15: 5th order approximation to GZ curve and unperturbed orbits

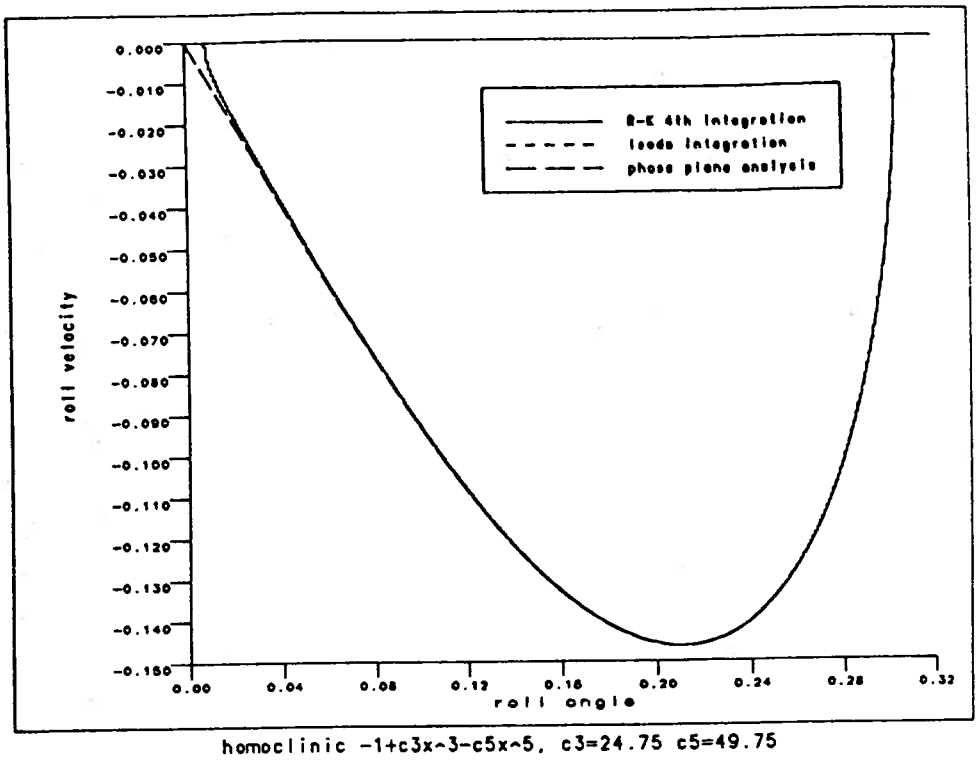

Figure 8.16: Numerical integration of 5th order homoclinic trajectory

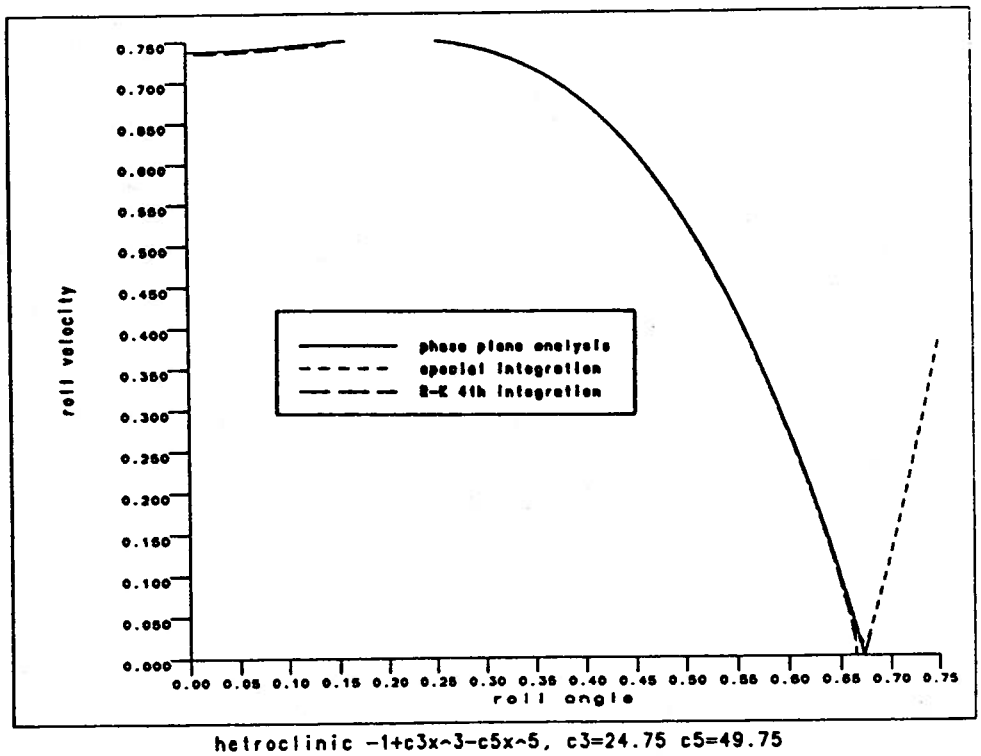

Figure 8.17: Numerical integration of 5th order heteroclinic trajectory

Reduction of degrees of freedom to an equivalent system

As discussed in the coordinate systems section of the chapter on the Melnikov method (Chapter VII), in order to be able to analyze (using lobe dynamics for example) a simplier system, we desire to know if it is possible to reduce the multiple degree of freedom system to an equivalent single degree of freedom system. We conjecture that this may be done by considering the eigenvalues of the Poincaré map and numerically integrating along the most dominate eigen-directions. We know that for an unforced and undamped linear system this is possible using simple techniques (i.e., principal axes). However, our system is nonlinear and it has damping and forcing, and we know it is not possible to exactly decouple even the linear system (Schuarz and Ma, (1988)). As stated previously (Chapter IV), in order to carry out this approximate reduction, we begin by observing that the most stable and least stable eigenvalues often mimic the single degree of freedom eigenvalues. In evaluating if the single degree of freedom and multiple degrees of freedom eigenvalues and eigenvectors are similar, there are two often conflicting requirements on these quantities. First, the eigenvalues should have minimum sway and yaw velocity relative to the roll displacement and roll velocity. The yaw velocity is often very small, but the value of the sway velocity varies. Second, the two corresponding eigenvectors should lie in a plane.

Tables 8.1 and 8.2 show for vertical variations in the location of the origin of the coordinate system for a fixed wave amplitude and wave frequency. In these tables, z_{go} is the distance between the ship center of gravity and the origin, ζ_{2v} is the sway velocity, ζ_{4v} is the roll velocity, e.v. is the eigenvalue. We note that zero sway velocity occurs between z_{go}=.5 feet and .625 feet for the least stable eigenvalues but occurs between z_{go}=.625 feet and .75 feet for the most stable eigenvalues. As you can see, only in very few cases are the two previously mentioned requirements simultaneously

z_{go}	ζ_{2v}	ζ_{4v}	e.v.
-1.88	-.290649	-.231528	25.3142
0	.0723217	.226169	23.541
.5	-.0135644	-.22268	22.4019
.625	-.000800453	.221714	22.0954
.75	.0149986	-.220717	21.7829

Table 8.1: Least stable eigenvalues for $\omega = .45$ and $\eta = .5'$

z_{go}	ζ_{2v}	ζ_{4v}	e.v.
-1.88	-.300466	-.227303	.0418515
0	.0819356	.231118	.0396976
.5	-.0247267	-.227296	.041807
.625	-.0106784	-.226057	.0425171
.75	-.00324916	.224709	.0433037

Table 8.2: Most stable eigenvalues for $\omega = .45$ and $\eta = .5'$

satisfied. Figures 8.18 and 8.19 show two sets of wire frame plots which graphically illustrate that satisfaction of the two requirements is often conflicting. The first figure (Figure 8.18) shows the two eigenvectors to lie in a plane both locally and globally, but the size of the (translational) sway velocity (x in the figure) is as important as the (rotational) roll velocity (y in the figure). The second figure (Figure 8.19) demonstrates that, although we may be able to substantially reduce the size of the sway velocity relative to the roll velocity. The eigenvectors may no longer lie in a plane. In both cases, we are looking down the roll axis.

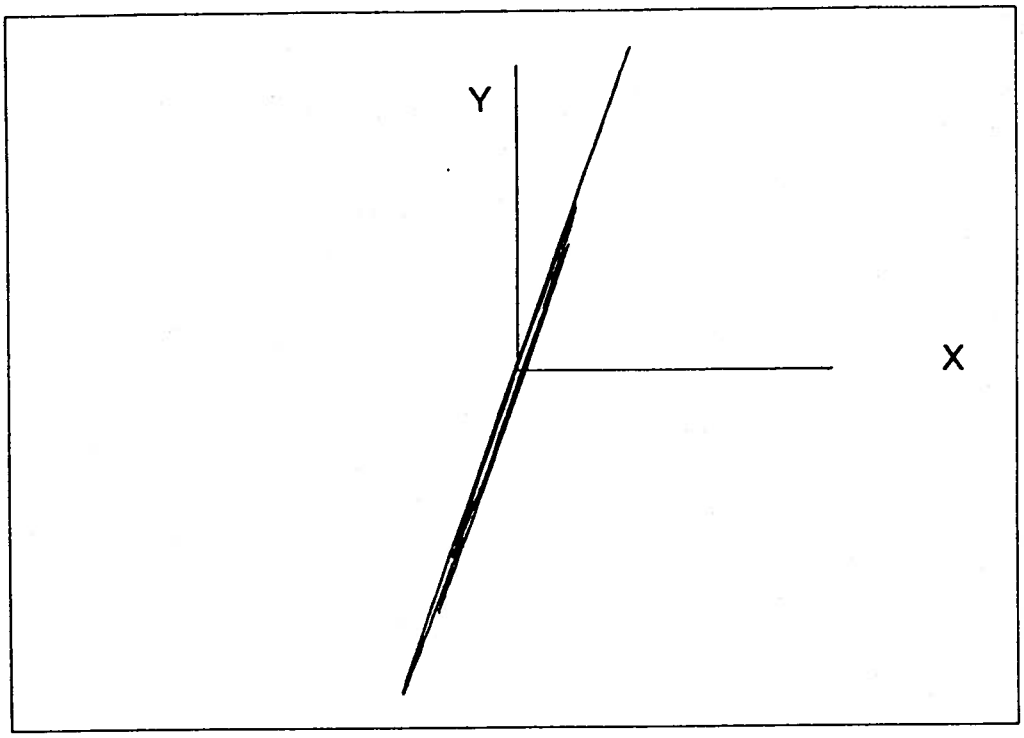

Figure 8.18: Wire-frame showing vectors in a plane yet large sway

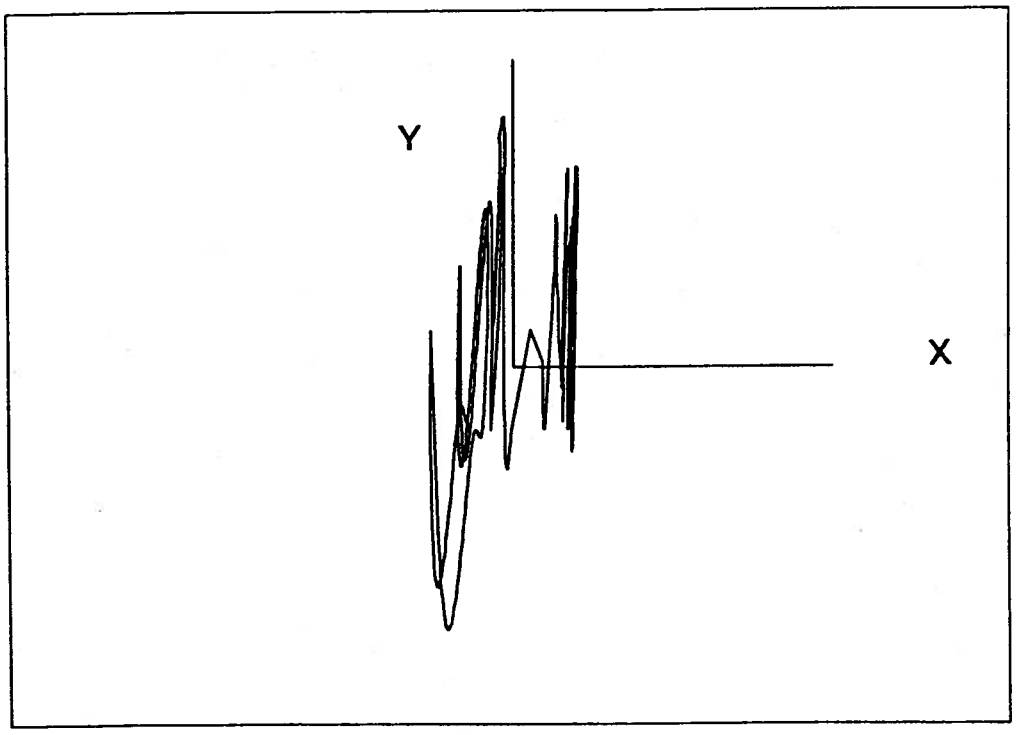

Figure 8.19: Wire-frame showing small sway yet vectors not in a plane

Intersection of the manifolds

In this section, we study the intersection of the invariant manifolds of Poincaré maps for the vessel *Patti-B*. We note here that for the vessel with a lolled $GZ(\phi)$ curve (see Chapter III and Appendix E) there are two sets of invariant manifolds. First, are a set of homoclinic invariant manifolds which originate at the saddle in the Poincaré map corresponding to the zero roll angle of the unforced system. The unstable manifold starts from this saddle and eventually encircles the stable focus corresponding to the loll angle. The stable manifold begins at infinity and eventually ends up at the saddle. Second, are a set of heteroclinic manifolds that originate from the saddles in the Poincaré map corresponding to the plus and minus angles of vanishing stability in the unforced system.

We digress here for a moment to recall that only stable manifolds can intersect unstable manifolds and visa versa. This is due to uniqueness of initial conditions, that stable manifolds cannot intersect other stable manifolds nor can unstable manifolds intersect other unstable manifolds otherwise the intersection point would simultaneously have to be on two manifolds of the same stability type, which is not possible. Moreover, such a point would be asymptotic to two different points as $t \rightarrow \infty$ or $t \rightarrow -\infty$.

We begin by repeating the results of the section on the comparison of the analytical and numerical results. We can see in Figure 8.20 that for the delta kg of .80 feet the manifolds intersect at very small wave amplitudes. We note here that the homoclinic intersections alone result in interesting dynamics but probably not capsizing. Since these motions are often bounded, they are not as important if considered in isolation, but we will return to the importance of the homoclinic unstable manifolds later.

The next result we show is the intersection of the heteroclinic invariant manifolds.

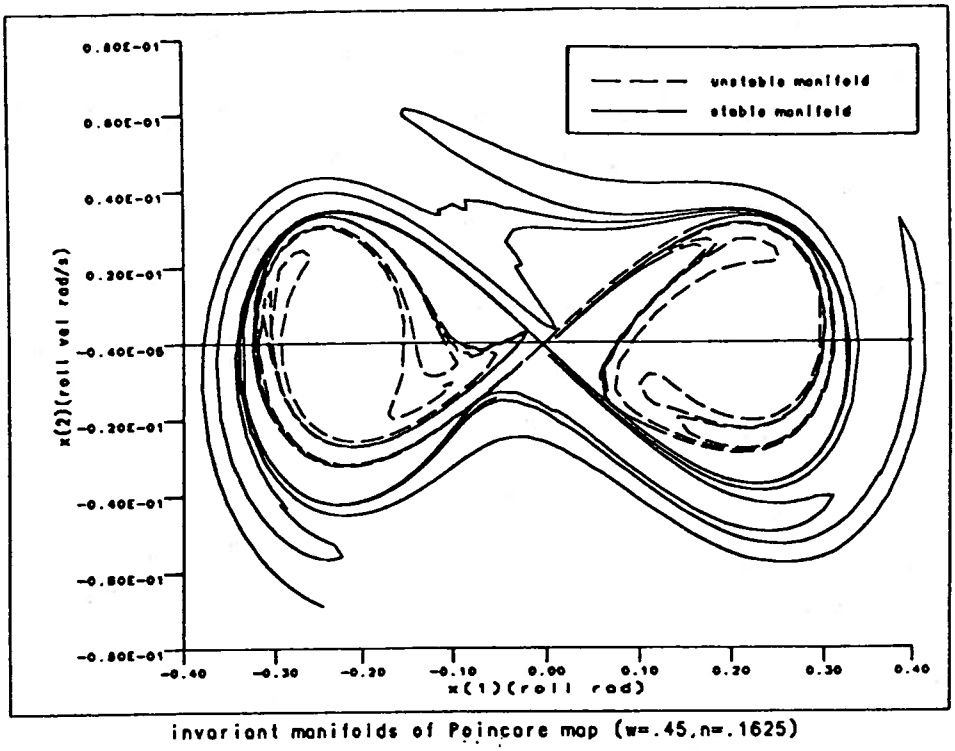

Figure 8.20: Homoclinic intersection

Before these manifolds intersect the boundary between safety (non-capsizing) and danger (capsizing) is crisp although it may be very contorted. We show here (Figure 8.20) that for a wave frequency of .5 radians/second a wave amplitude of 2.5 feet will result in heteroclinic manifold intersections. As a result of this intersection, the initial conditions beginning inside this apparently safe region may diverge beyond the pseudoseparatrix to the unsafe region upon future iterates of the map. We refer to this event as an *unexpected capsizing.*

The final intersection related event that we describe in this section is the intersection of the unstable homoclinic manifold with a stable heteroclinic manifold. Initial conditions near origin and along the unstable homoclinic manifold will be dragged beside the unstable manifolds to the stable heteroclinic boundary and into a lobe. Again a whole region of initial conditions inside this lobe will be transferred from the seemingly safe region to unsafe region outside. We refer to this event as a *totally unexpected capsizing.*

Since we were not able to locate an intersection of an unstable homoclinic and stable heteroclinic manifold, we only show pictorially in Figure 8.22 what could occur. Studying the arrangement of the manifolds, it seems as though the required wave amplitude for unstable homoclinic and stable heteroclinic manifold intersections must be greater than that for unstable heteroclinic and stable heteroclinic manifold intersections. Although, we cannot prove this conjecture we state it as a hypothesis as follows:

Conjecture *By graphically considering the various possibilities, it seems reasonable that for unstable homoclinic and stable heteroclinic manifold intersections the required wave amplitude (external forcing) must be greater than that for unstable heteroclinic and stable heteroclinic manifold intersections.*

Although we can determine the Melnikov function for each the separate homoclinic and the heteroclinic intersections, since we do not have any $\epsilon = 0$ structure to perturb for the unstable homoclinic and stable heteroclinic manifold intersection, we do not yet see a way to determine the corresponding Melnikov function. Otherwise, this conjecture could be easily shown.

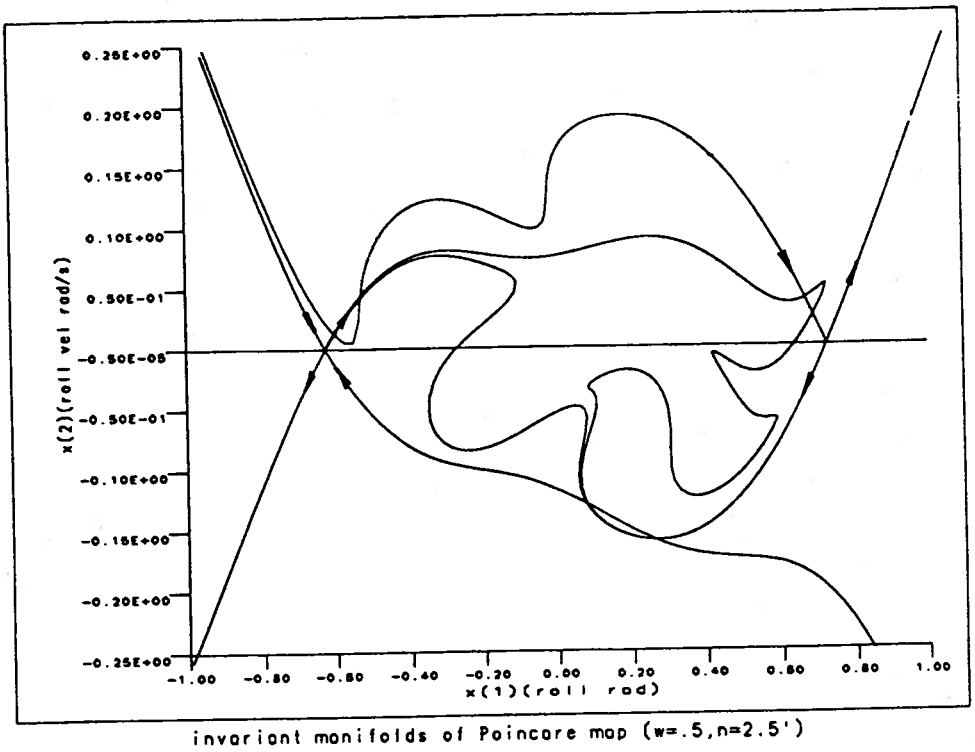

Figure 8.21: Heteroclinic intersection

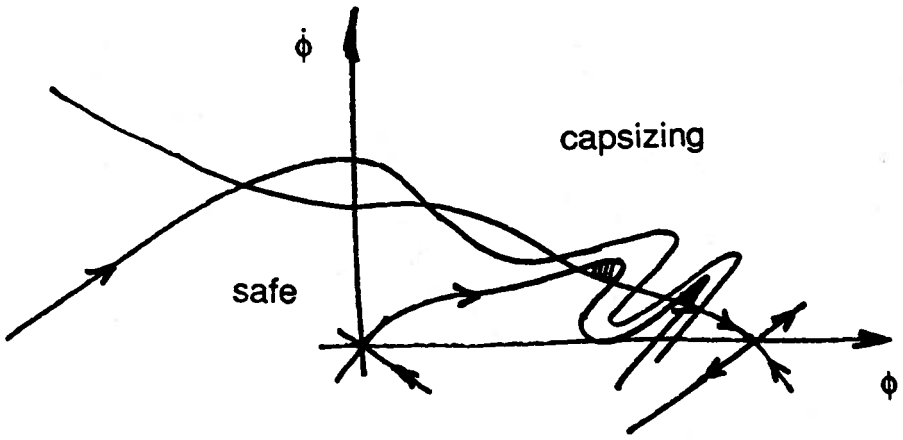

Figure 8.22: Homoclinic unstable and heteroclinic stable manifold intersection

Practical application of lobe dynamics

In order to demonstrate the surprising ship dynamics which can occur when the manifolds intersect, we study the motion of the clam dredge *Patti-B* excited by a wave of frequency ω_e =.5 radians/second and amplitude $\eta_o = 3$ feet. Since the vessel speed is zero, the encounter frequency is equal to the wave frequency ($\omega_e = \omega_o$)

First, we consider the three initial conditions (see Figure 8.23): a) one within the shaded lobe (2), $(\phi_o, \dot{\phi}_o)$ = (-.50,0.0); b) one outside the lobe at a lesser initial roll angle (1), $(\phi_o, \dot{\phi}_o)$ = (-.40,0.0); and c) one outside the lobe but at a greater initial roll angle (3), $(\phi_o, \dot{\phi}_o)$ = (-.59,0.0). Considering the most fundamental aspects of lobe dynamics as described in the chapter on lobe dynamics (Chapter VII), we know that one lobe will transport phase area from inside (safe) the pseudosepartrix to outside the pseudosepartrix (unsafe) through the turnstile.

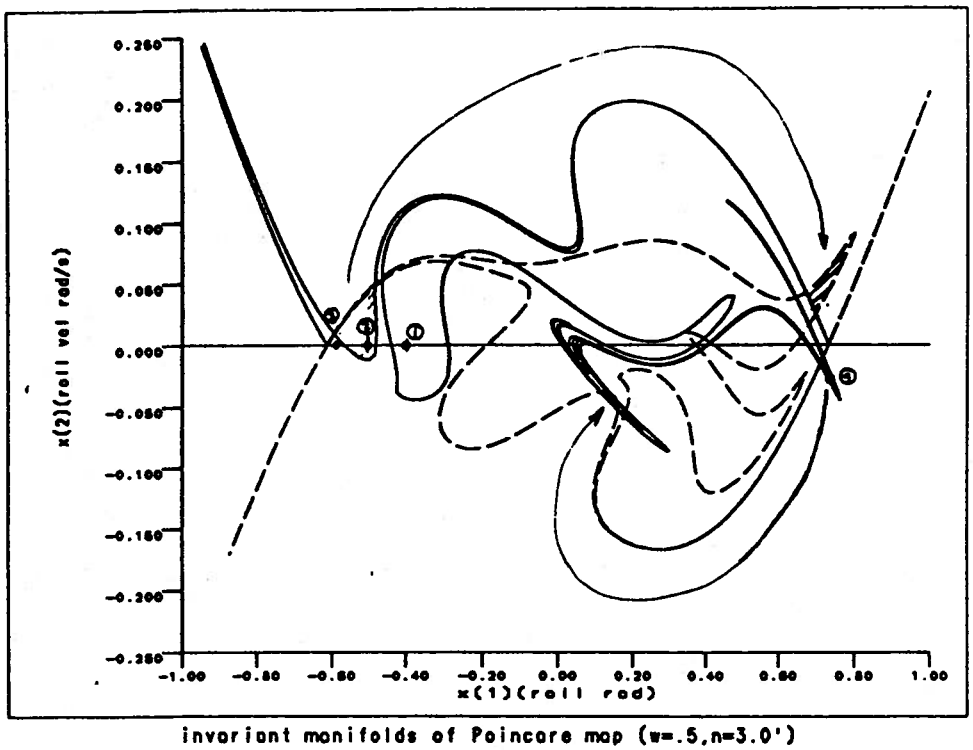

Figure 8.23: Lobes for Patti-B

Considering lobe dynamics, we predict that initial condition (2) will iterate from

its current location inside the pseudosepartrix (safe) lobe to outside the pseudosepartrix into the possibly unsafe region. When initial condition (2) (see Figure 8.23) is cast into the unsafe region, it has a negative roll restoring moment and may be vulnerable to capsizing. Upon simulating the system, we observe initial condition (2)(Figure 8.24) iterates outward and capsizes soon afterward.

Using statics as a guide, we might be tempted to just decrease the initial roll angle. For a small enough initial roll angle, we would hope the vessel does not iterate outward and eventually settle to a bounded steady-state motion. Decreasing the initial roll angle and keeping the same zero roll velocity, we obtain initial condition (1). Considering lobe dynamics, we do not expect this initial condition to iterate outside. As expected, upon simulating the system, we see (see Figure 8.24) initial condition (1) does not iterate to outside but stays within the bounded region. The vessel eventually settles to a bounded steady-state subharmonic oscillation. The Poincaré sections are indicated by arrows in Figure 8.24.

Using this limited amount of empirical evidence, and ignoring lobe dynamics, one might propose a safety criterion demanding a roll angle less than the vulnerable initial roll angle. However, this does not always work as we shall show. To disprove the proposed criteria, we consider an initial condition (3) (see Figure 8.23) with an initial roll angle greater than (2) and the same zero roll velocity, but outside the lobe. Considering lobe dynamics, we do not expect this initial condition (3) to iterate outward. Upon simulating the system, we see this initial condition (3) does not iterate outward and eventually settles to a bounded steady-state subharmonic solution (see Figure 8.24).

The usefulness of lobe dynamics is thus clearly demonstrated using these simple examples. Here an initial condition with larger roll angle (3) is eventually more safe than an initial condition with smaller roll angle (2). However, the smaller roll angle was inside a lobe (see Figure 8.23) and we correctly predicted it would iterate

outward.

Considering lobe dynamics, all initial conditions inside lobes are not vulnerable. To demonstrate this, we consider an initial condition outside the pseudoseparatrix but inside a lobe. Considering lobe dynamics, we predict the initial condition (4) (see Figure 8.23) $(\phi_o, \dot{\phi}_o) = (+.729, 0.021)$ will iterate from outside (unsafe) to inside (safe). Upon simulating the system, this does occur (see Figure 8.25).

Finally, we reverse time integrate from the given locations in the Poincaré maps to demonstrate the extreme sensitivity to initial conditions which this system has. Note how close the three trajectories are for negative times and how rapidly they diverege for positive times.

Extreme sensitivity to initial conditions is a characteristic of dynamical systems with complicated dynamics (see Figures 8.24 and 8.25). For a further description of Lyapunov exponents, a technique which can be used to quantify extreme sensitivity to initial conditions, see Appendix D.

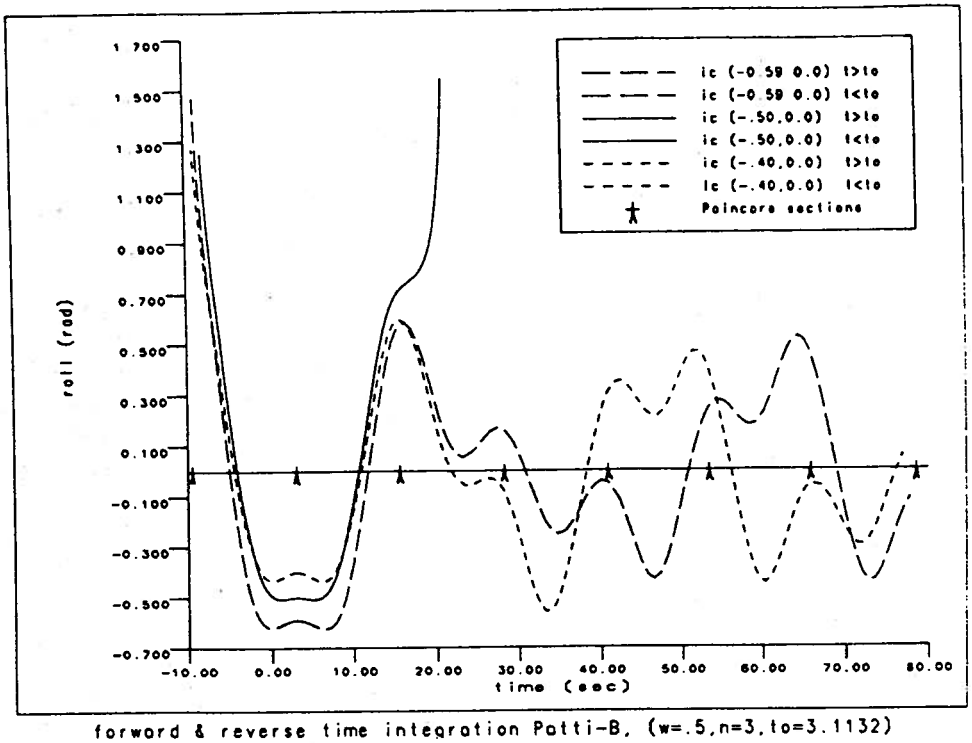

Figure 8.24: Time history for Patti-B

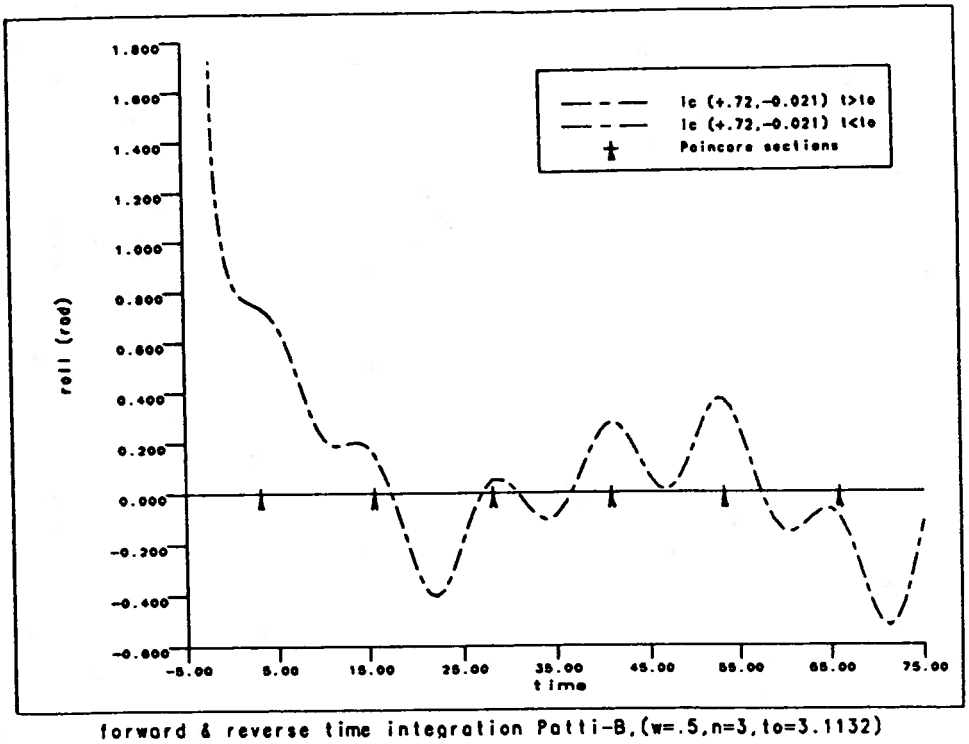

Figure 8.25: Time history for Patti-B

The search for a totally unexpected capsizing

We discussed in the subsection on the intersection of the manifolds that it may be possible that an initial condition near the origin (in the phase plane) may become unbounded. We call this event *totally unexpected capsizing.* This is possible if the unstable homoclinic manifold intersects the stable heteroclinic manifold (Figure 8.22). Recall, the conjecture that the required wave amplitude for this intersection (unstable homoclinic and stable heteroclinic) must be greater than that required for the purely heteroclinic intersection. For the case considered in the "Practical applications of lobe dynamics" subsection (ω_e =.5 radians/second, and η_o =3.0 feet), when we increased the wave amplitude in order to find a totally unexpected capsizing, the unstable homoclinic manifold grew more compact. It, therefore, appears as though no such intersection can occur at this frequency (i.e., ω_e =.5 radians/second). We, therefore, investigated lower and higher frequencies (i.e., ω_e =.45 and ω_e =.55 radians/second). We were also unsuccessful in finding the unstable homoclinic and stable heteroclinic intersections at these frequencies (see Figure 8.26, 8.27, 8.28, and 8.29). Please note the very compressed unstable homoclinic manifolds near the origin for the ω_e =.55 radians/second, and η_o =2.5 feet case (Figure 8.29). According to Shaw (1990), finding the unstable homoclinic and stable heteroclinic intersection may be possible with a different wave exciting force which is periodic but not sinusoidal (e.g., consider a Fourier series).

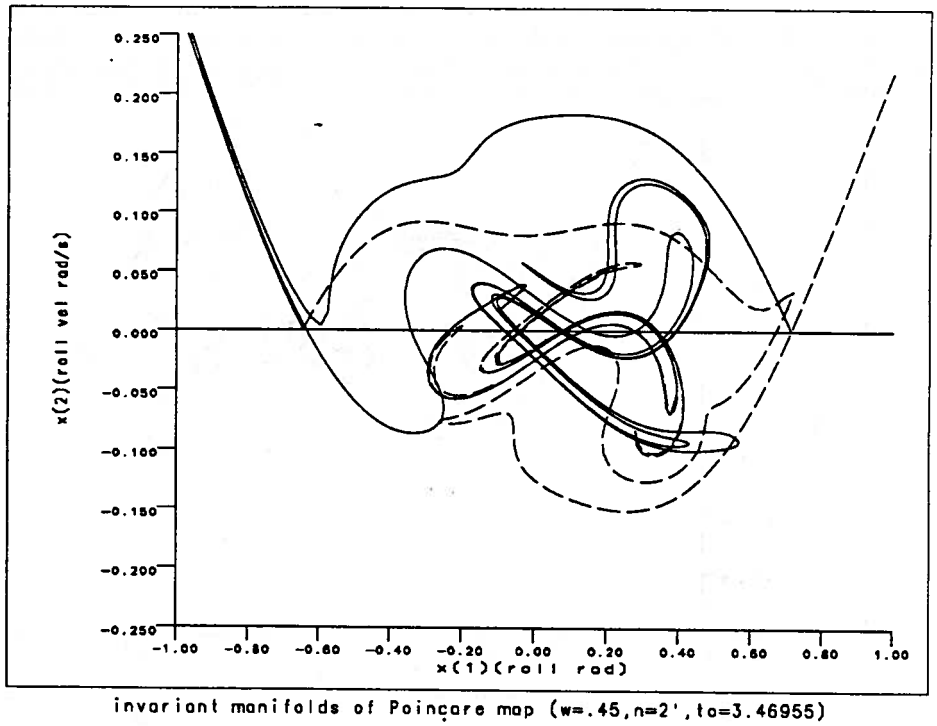

Figure 8.26: Search for totally unexpected capsize 1

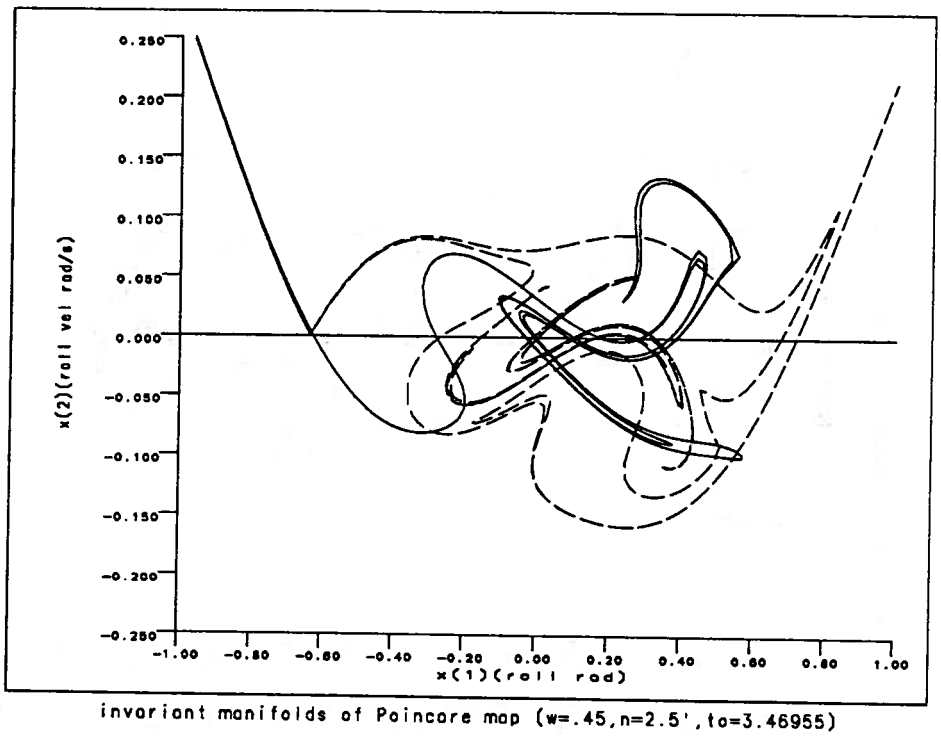

Figure 8.27: Search for totally unexpected capsize 2

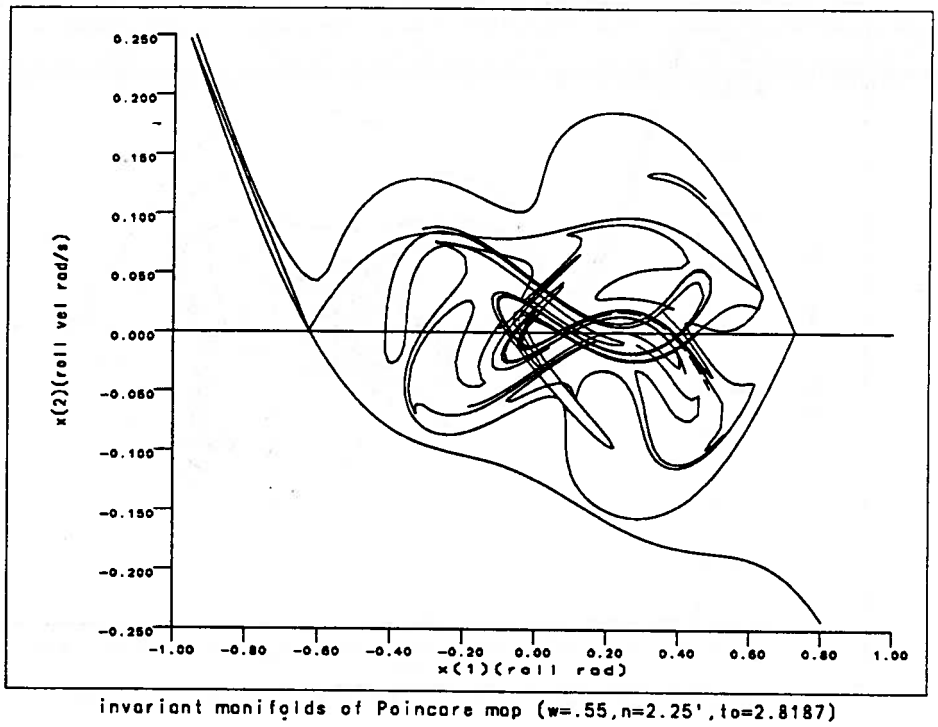

Figure 8.28: Search for totally unexpected capsize 3

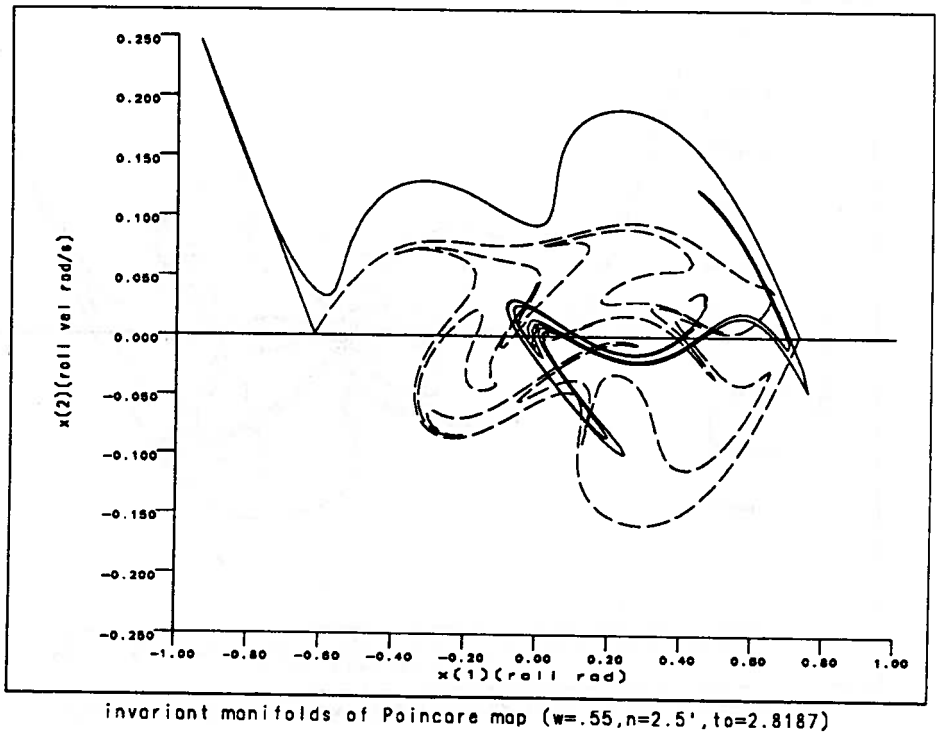

Figure 8.29: Search for totally unexpected capsize 4

Samples of Poincaré maps at different phases

The phrase that "two Poincaré maps at two different phases are C^r conjugate," and the explanation that "a C^r diffeomorphism exists between these two maps" may have been confusing to the more applications oriented reader. We, therefore, show two examples of Poincaré maps of the ship dynamical system which are the same except for their sampling phase. You can see in these two figures that the map is just a mirror image about the roll velocity axis (Figures 8.30 and 8.31). Figures 8.30 and 8.31 have sampling phases of $t_o = 3.1132$ seconds and $t_o = 8.4$ seconds respectively.

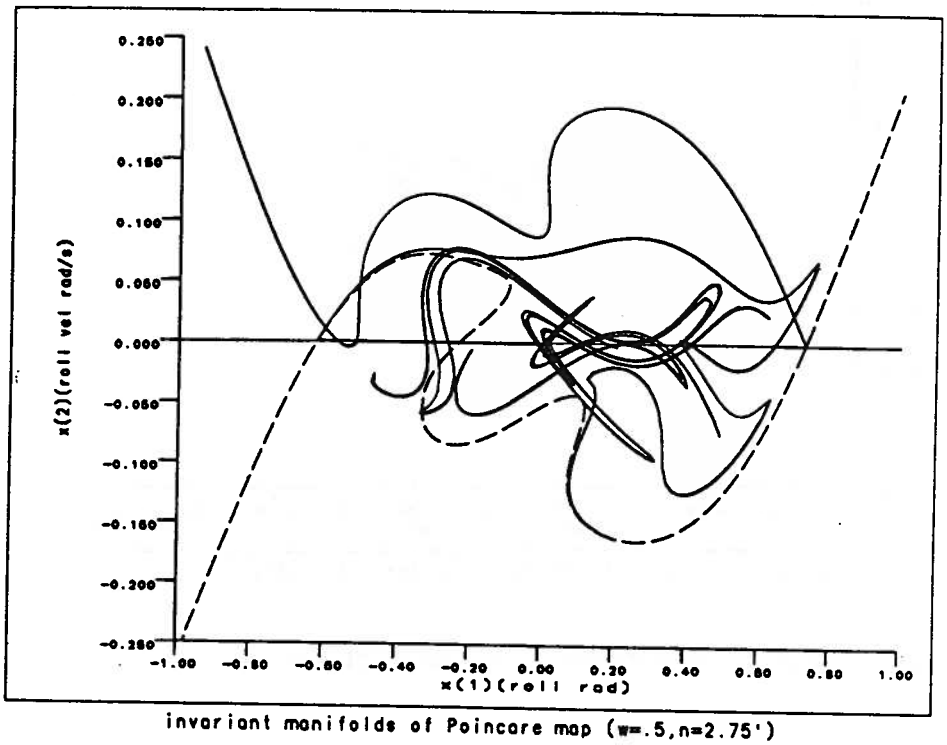

Figure 8.30: Poincaré maps at various phases

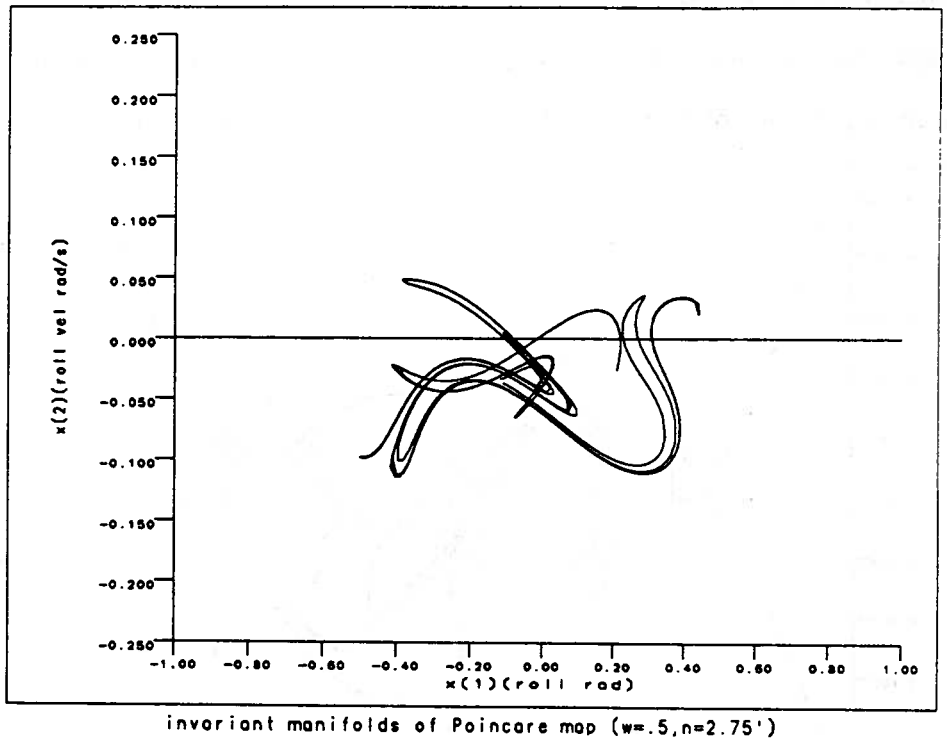

Figure 8.31: Poincaré maps at various phases

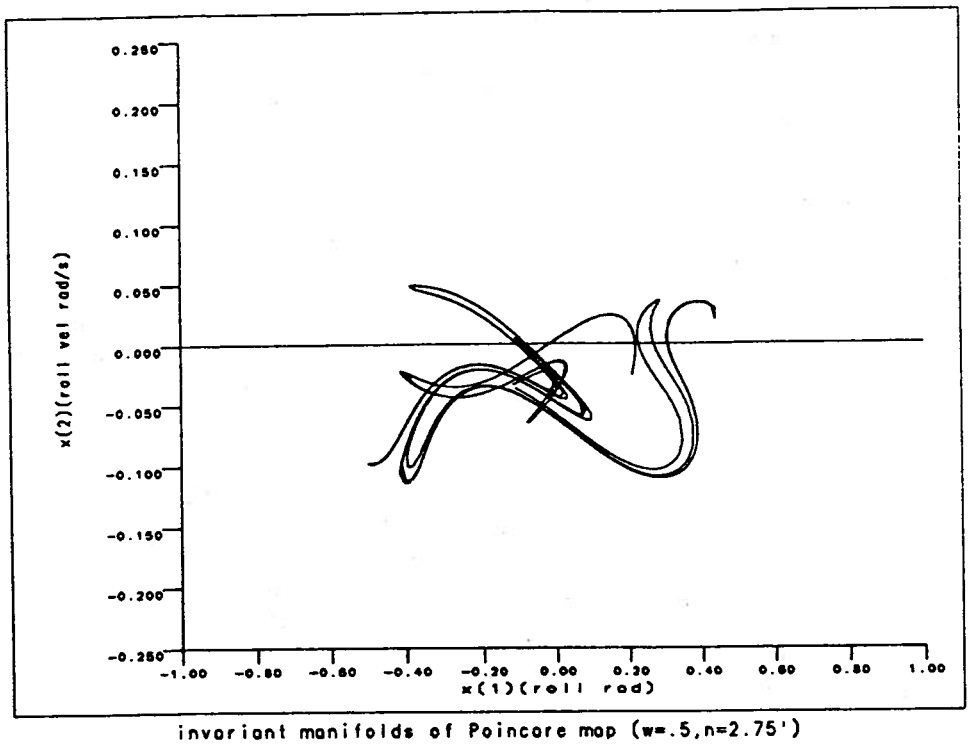

Figure 8.31: Poincaré maps at various phases

Comparative simulation studies

One of the important goals of this work was to minimize simulation by gaining a deeper understanding of the structure of the phase space or Poincaré map. With enough understanding and experience of what types of behavior to expect, under what circumstances, we may practically eliminate simulation for many nonlinear problems as we already can do with most linear problems. However, simulation is an analysis technique with which most engineers are familiar and have trust in. Therefore, in this section, we demonstrate with simulation some of the characteristics which our qualitative methods suggest. However, at the outset, we should be aware that we may still encounter phenomena and behavior that cannot be explained by our limited analysis techniques. When this occurs, we should not give up all faith in qualitative analysis and reject our techniques for all similar problems, but we should re-evaluate the assumptions and approximations inherent in our application of these techniques in order to explain their shortcomings. We carried out a few simulations in the previous subsection to demonstrate the eventual and initial behavior for the lobe dynamics problem. In this section, we will carry out a few additional simulations in order to demonstrate some further points.

Simulations of some aspects of the vessel turning problem

Using classical perturbation techniques, it can easily be shown (Schmidt and Tondl, (1986)) that the nonlinear magnification curve is unstable from the lower vertical tangent to the the vertical tangent at the peak (the dotted region in Figure 8.32). Since the saddle is not repelling or attractive, we refer to the saddle as nonstable (Parker and Chua, (1989)). Saddle manifolds are important in forming the boundaries between basins of attraction of other fixed points that are stable (Chapter V). What we do in these simulations is to start with an initial condition

slightly on one side or the other of the saddle and watch where they end up. Figure 8.32 shows the magnification curve with a vertical line at the simulation frequencies. Figure 8.33 shows a simulation slightly (about floating point accuracy; i.e., 1×10^{-8}) in the direction of the low amplitude solution. After a number of cycles, the curve eventually jumps down off the saddle to the low amplitude solution, the so-called "in phase branch". Figure 8.34 shows a simulation slightly (about floating point accuracy; i.e., 1×10^{-8}) in the direction of the high amplitude solution, the so-called "out of phase" branch. After a number of cycles, the curve eventually jumps up to the high amplitude solution. Although the jump up is not as dramatic as the jump down, it demonstrates the extreme sensitivity to initial conditions of motion near the saddle. Depending upon which side of the saddle the initial condition is on, it will go to one stable steady-state or the other.

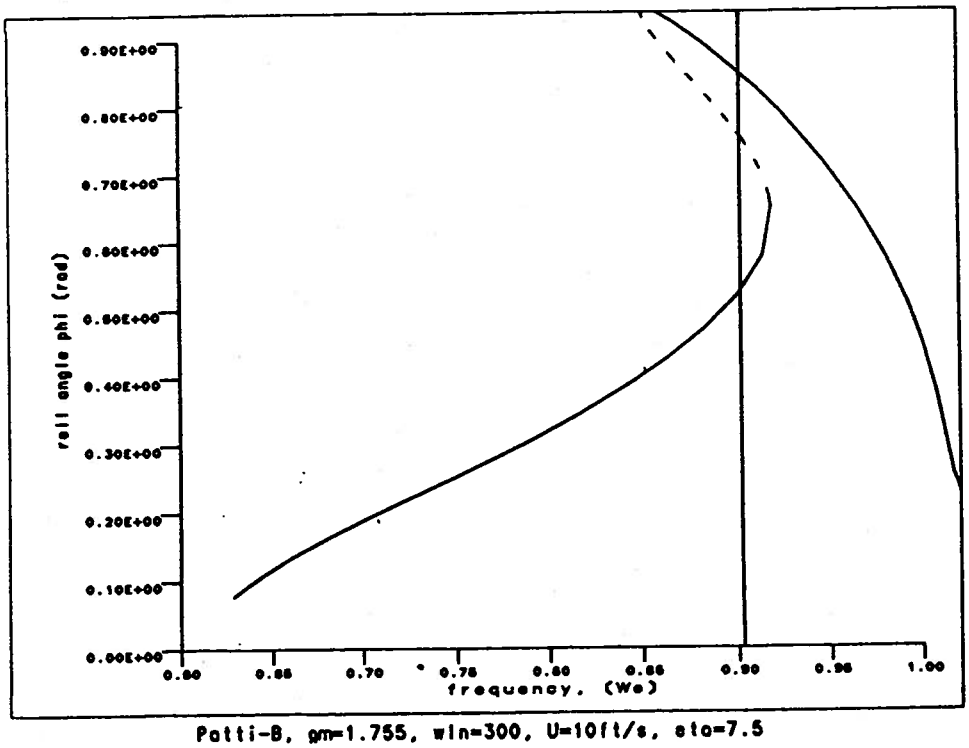

Figure 8.32: Magnification curve for simulation near the saddle

Another interesting phenomena we sought to investigate was the well-known jump phenomena. Initially, we rapidly swept from low to high frequency. The simulated

roll amplitude did not seem to follow the magnification curve. This behavior was quite perplexing until we evaluated our approximation. Although we assumed $\dot{\omega} \approx 0$ we actually had $\dot{\omega} \neq 0$. Such non-stationary phenomena are described in Mitropolsky, (1966). The $\dot{\omega} \neq 0$ phenomena is dominated by the transient behavior and thus, bears no resemblance to the assumed $\dot{\omega} = 0$ steady-state phenomena. Eventually, we started right at the vertical tangent and very slowly increased the frequency and did observe a jump as shown in Figure 8.35.

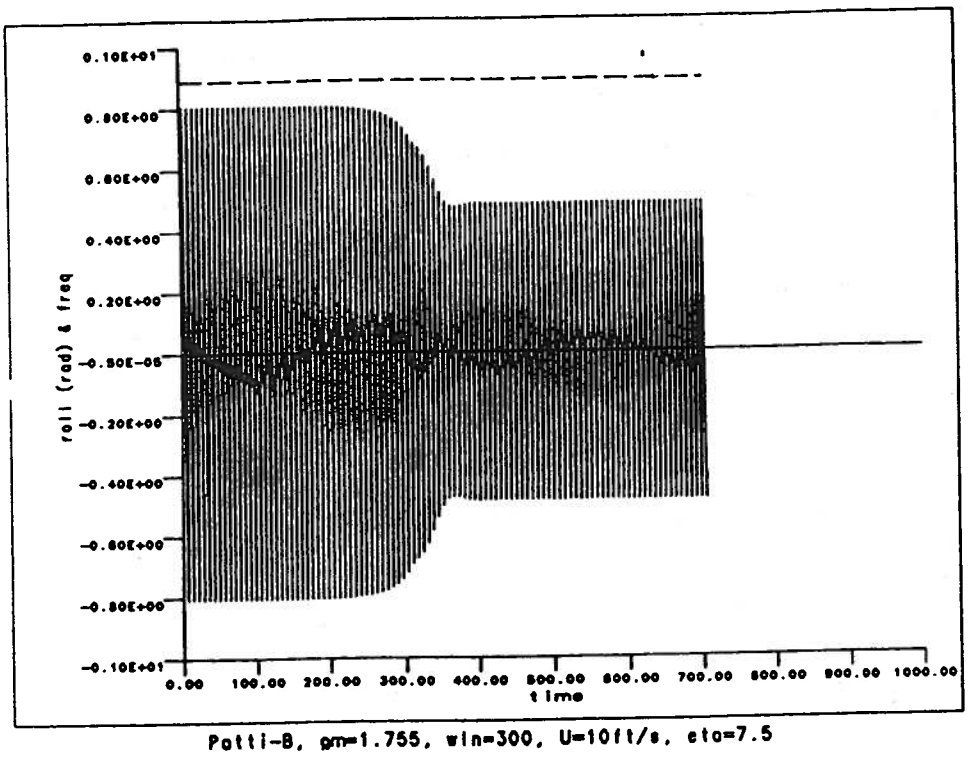

Figure 8.33: Simulation near the saddle (just in basin to lower branch)

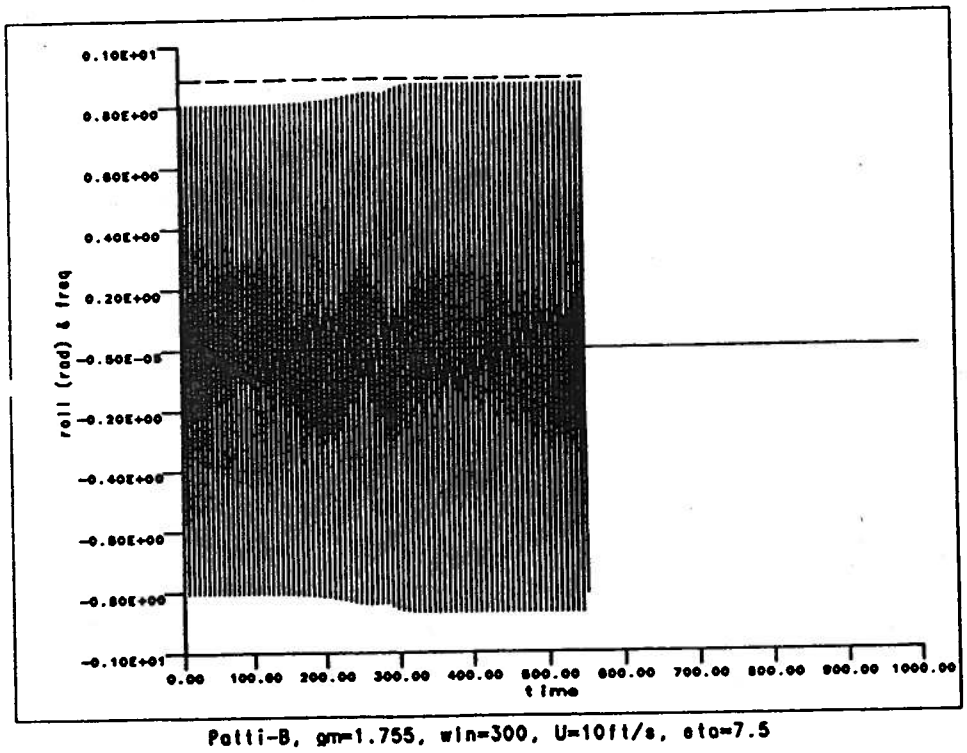

Figure 8.34: Simulation near the saddle (just in basin to upper branch)

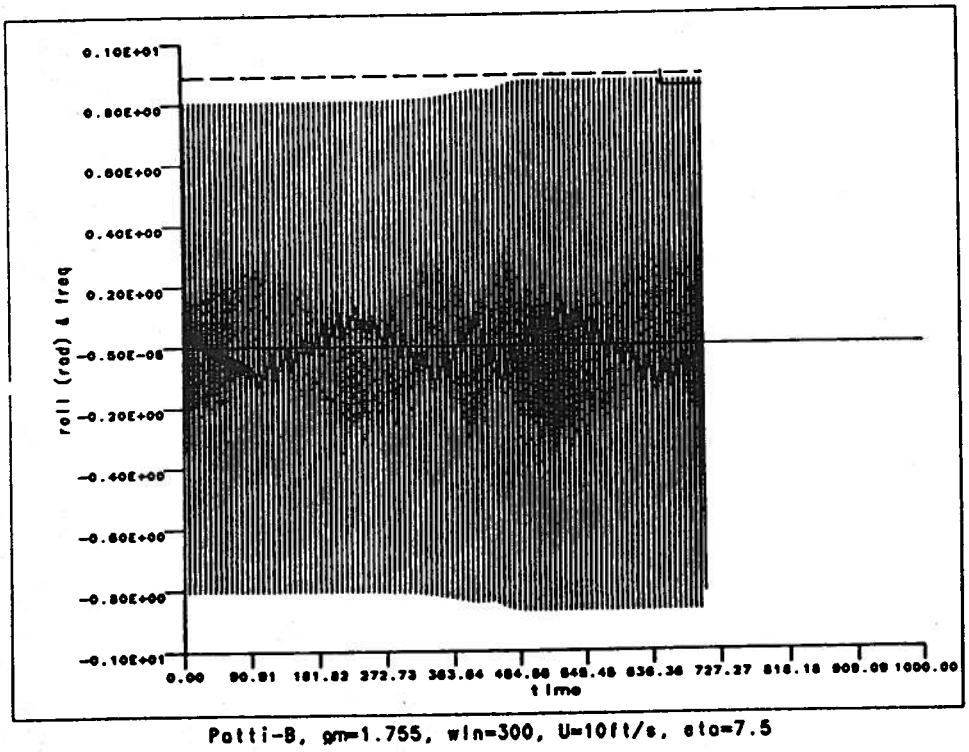

Figure 8.35: Simulation traveling through resonance

Some qualitatively different motions

In order to analyze the motion resulting from nonlinear systems, various qualitative and quantitative analysis techniques are required. Some of these tools are familiar to the ship dynamicist but uniquely applied, while others are very specialized. Most ship dynamicists are familiar with time histories, but not as familiar with the phase plane or Poincaré map. Although the time history is a useful visual technique to observe steady-state harmonic response, it quickly loses its usefulness for more general types of motion. For steady-state subharmonic motion, the motion may be viewed using the phase plane. In the phase plane, any two state variables may be plotted. For example, displacement versus velocity is most often plotted. From this plot, the order of the subharmonic response can be assessed. For steady-state aperiodic response, both the time history and the phase plane are insufficient. The dynamicist must then consider the Poincaré section. Since our system is time-varying, the trajectories in the phase plane may cross each other. In order to overcome this difficulty, an extended phase space with time added must be considered, or alternatively, the phase space may be sampled at integer multiples of the forcing period. The plot of the sampled phase variables is called a Poincaré section. For steady-state harmonic response, the Poincaré section is a single point. For subharmonic response, the Poincaré section is a finite number of points equal to the order of the subharmonic (number of periods to repeat). For the aperiodic response, there is an infinity of points in the Poincaré section. However, the infinitely many points describing the chaotic response often fall in an orderly or at least distinctive pattern. The resulting figure in the Poincaré section is called a *strange attractor.*

In the following figures, we give some examples of the three representations (time history, projected phase plane and Poincaré map) for the ship dynamical system for the three types of motion (harmonic, subharmonic and chaotic). In the figures, you

type of response	degrees of freedom	η_o
harmonic	single	4 ft
sub-harmonic	6-dof	2 ft
aperiodic	single	1 ft

Table 8.3: Qualitatively different motions ω_o= .4 rad/s, β = 90 deg

can see the periodic forcing and the various types of response. We note here that these are steady-state responses since the transients were not plotted. The figures are arranged as sets of time history, projected phase plane and Poincaré map for the harmonic response (Figures 8.36, 8.37, and 8.38); the same for subharmonic of order six (Figures 8.39, 8.40 and 8.41) and the same for the aperiodic response (Figures 8.42, 8.43, and 8.44). Finally, we let the aperiodic response evolve for about 300 periods and we begin to see the form of the strange attractor (Figure 8.45). Table 8.3 summarizes the ship and environmental data used in generating the data.

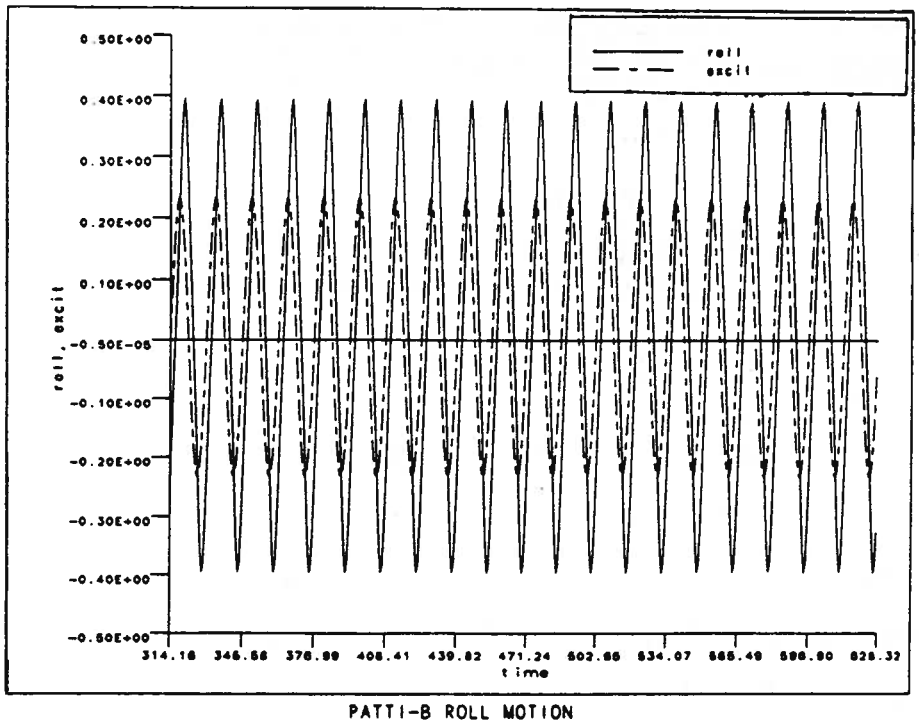

Figure 8.36: Time history of harmonic response

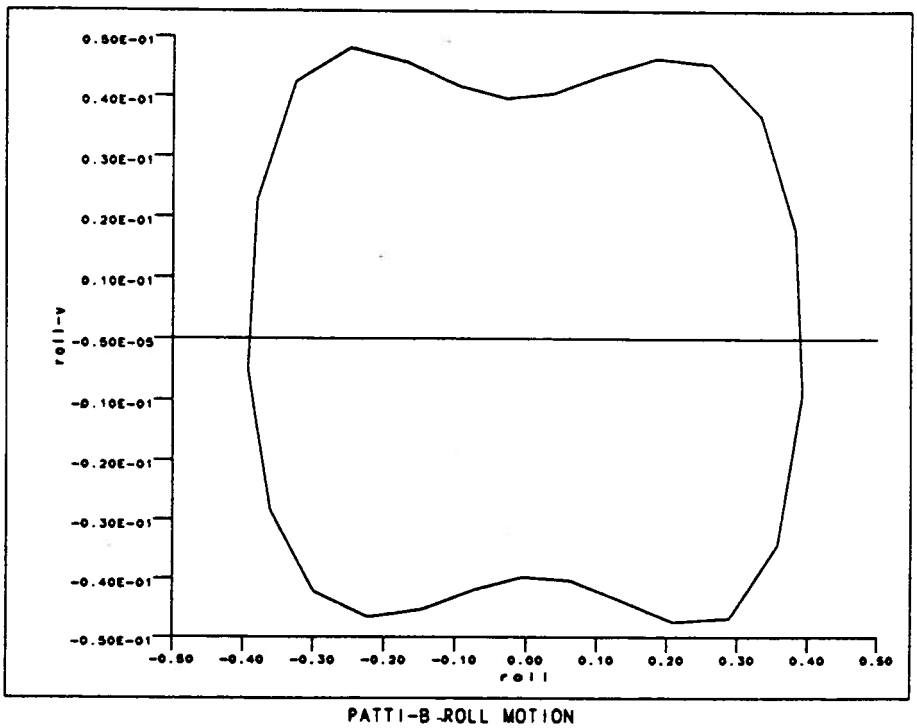

Figure 8.37: Projection of extended phase plane for harmonic response

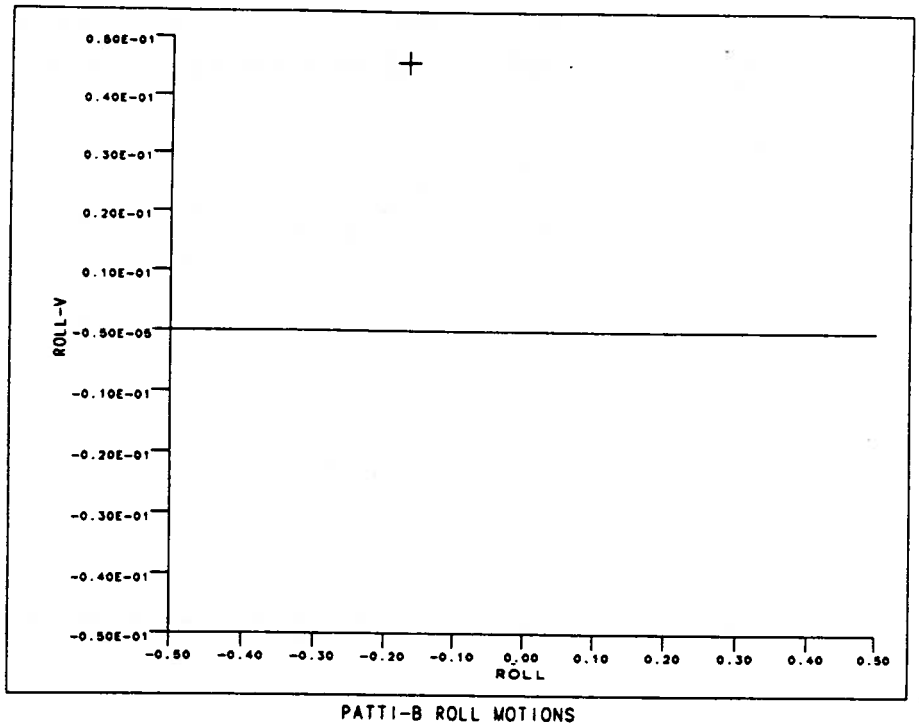

Figure 8.38: Poincaré map for harmonic response

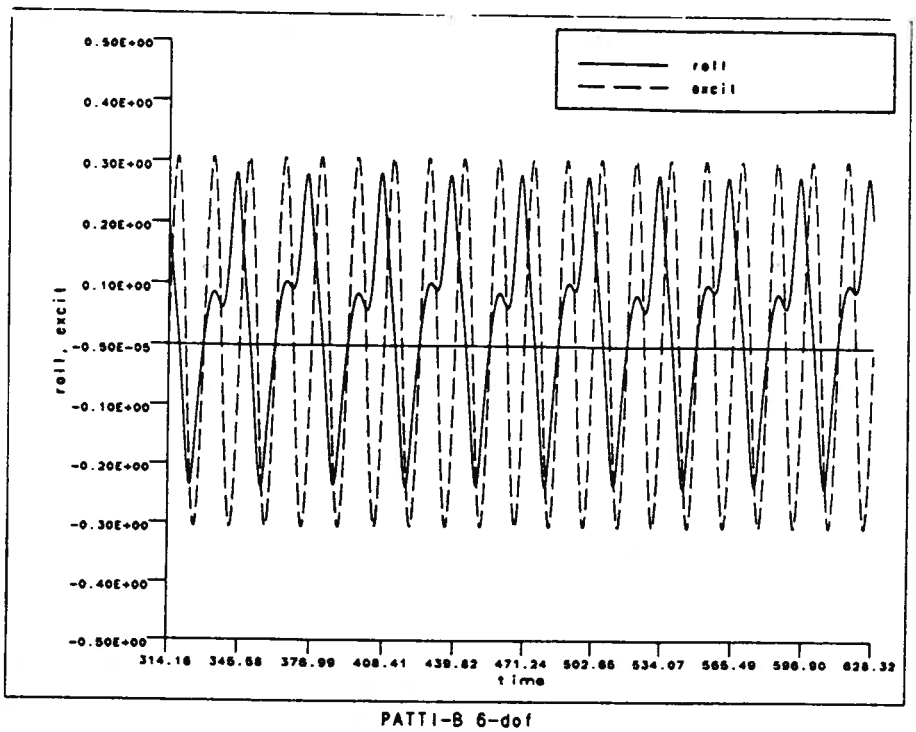

Figure 8.39: Time history of sub-harmonic response

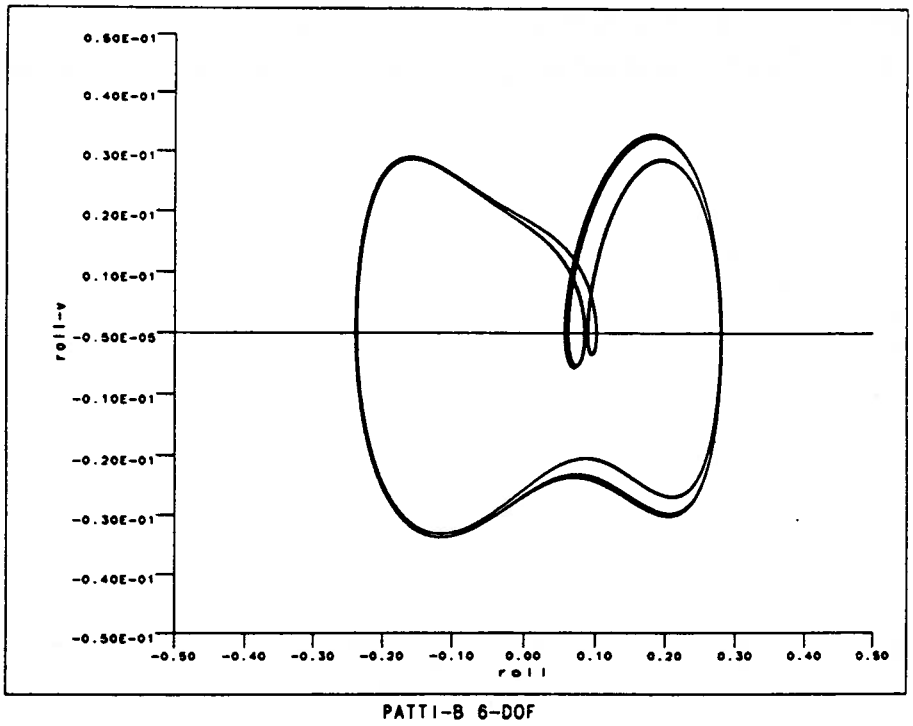

Figure 8.40: Projection of extended phase plane for sub-harmonic response

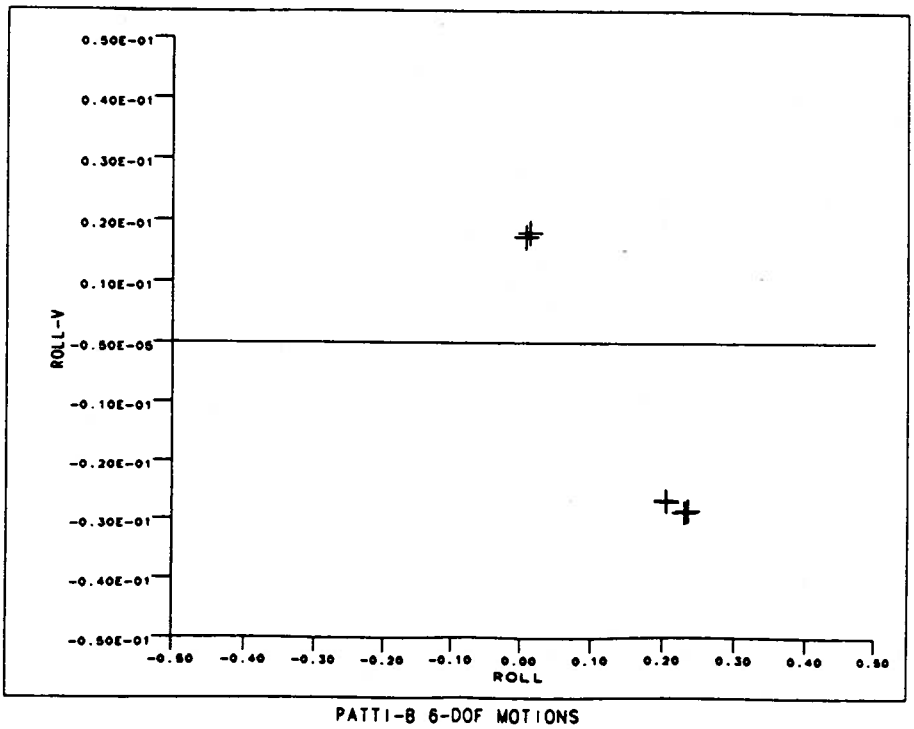

Figure 8.41: Poincaré map for sub-harmonic response

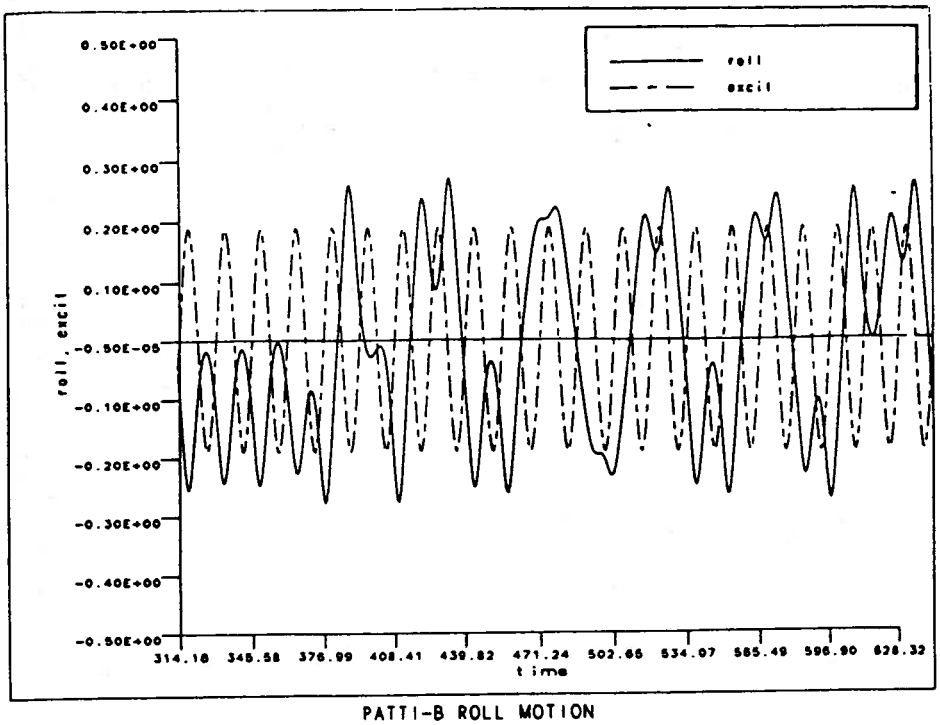

Figure 8.42: Time history of aperiodic response

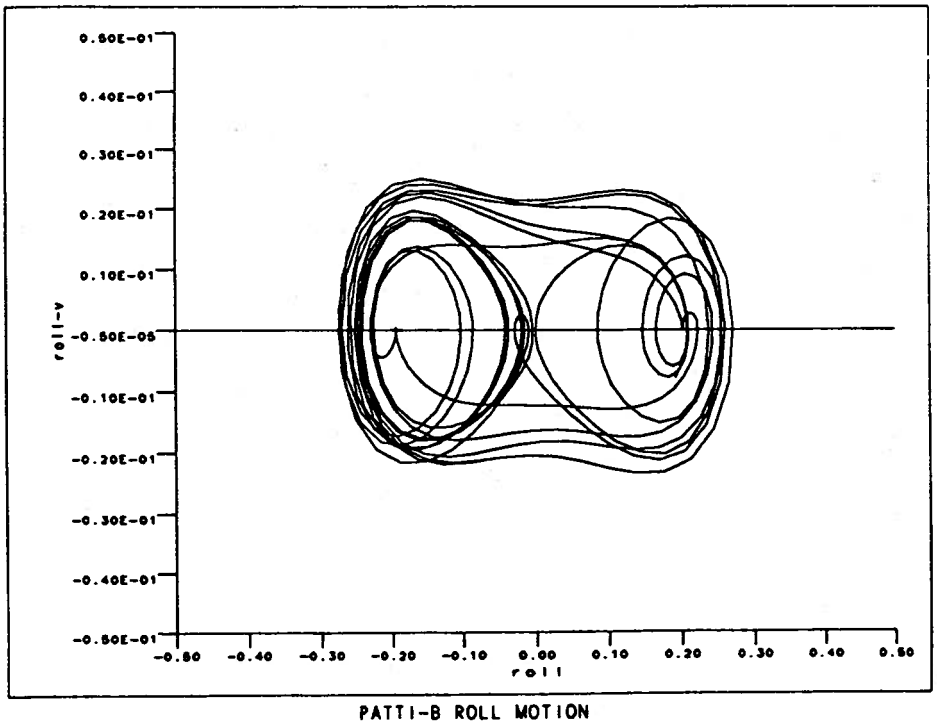

Figure 8.43: Projection of extended phase plane for aperiodic response

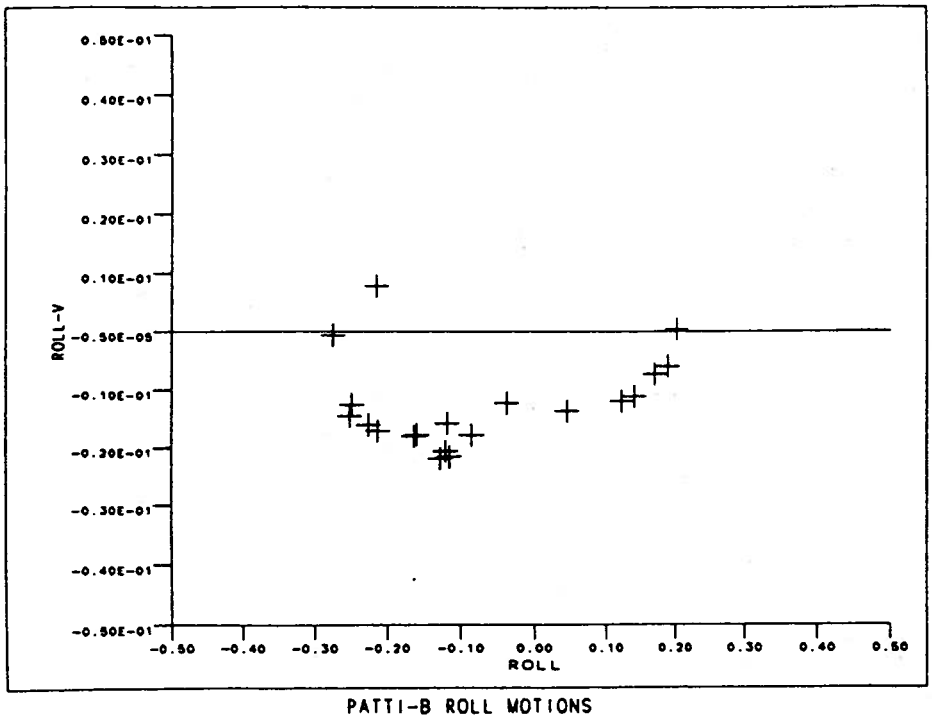

Figure 8.44: Poincaré map for aperiodic response

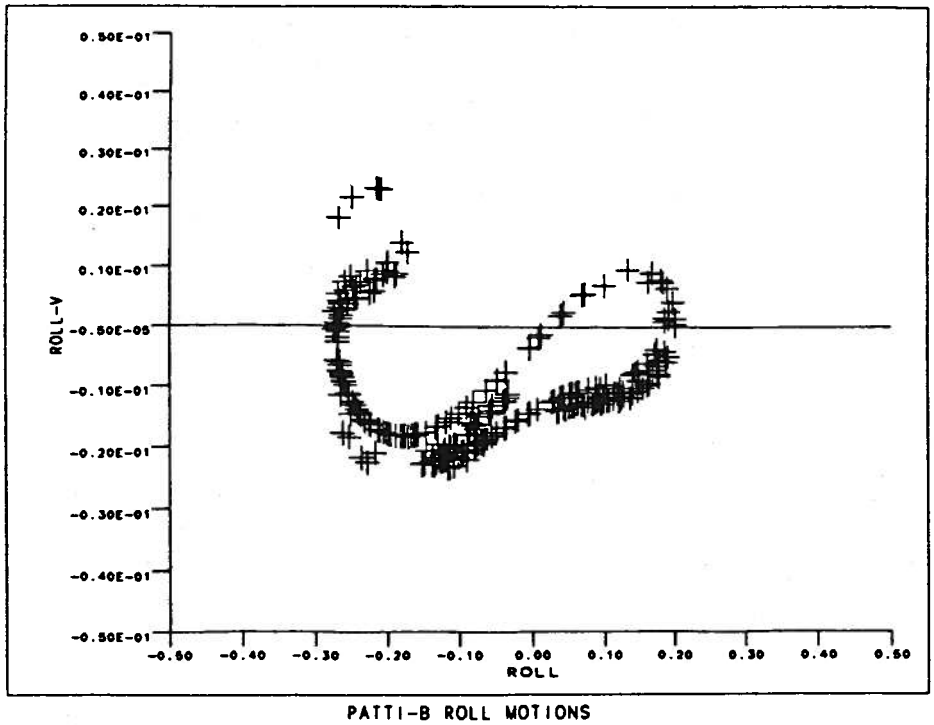

Figure 8.45: Poincaré map of strange attractor for aperiodic response

One specialized technique used to evaluate chaos is the determination of the Lyapunov exponent (Wolf, et al., (1985)) of the response. The Lyapunov exponent relates to the exponential divergence of neighboring trajectories, a characteristic of chaotic vibration. For motion converging to a fixed point like a stable node, all Lyapunov exponents must be negative. For periodic motion, at least one Lyapunov exponent must be zero. For chaotic motion, at least one Lyapunov exponent must be positive. It is required to have at least three independent phase variables or two phase variables and time available for chaotic vibration. For a continuous system (for a map), we must have one positive exponent (one multiplier greater than one) corresponding to the chaotic motion, one zero exponent (equal to one) corresponding to the periodic motion, and one negative exponent (one multiplier less than one) corresponding to the contracting motion. Since phase volume must contract for a dissipative system (with damping), it can be shown, that the sum of the Lyapunov exponents must be negative (Berge, Pomeau, and Vidal, (1984)). Further details of the technique of Lyapunov exponents, is contained in the appendix on Lyapunov exponents (Appendix D).

In order to demonstrate the practical utility of Lyapunov exponents, we present a set of figures for the *Patti-B* which includes a time history (Figure 8.46), a projected phase plane (Figure 8.47), a Poincaré section (Figure 8.48), and a time history of the Lyapunov exponent calculation (Figure 8.49). All these results are for over 850 periods and we begin to see the shape of this strange attractor even more clearly than the one in the previous section. We note that the Lyapunov exponent is a useful qualitative (a positive exponent implies chaos has occurred) and quantitative (we associate a number with the exponential expansion) measure of chaos. In addition, we can calculate a number which describes the dimensionality of the so-called strange

attractor. For a chaotic attractor, this number is not an integer as we expect for regular attractors. The dimension of a fixed point is zero and for a limit cycle the dimension is one. It has been conjectured by Yorke and Kaplan (Froehling, et al., (1980)) that the Lyapunov dimension is related to the Lyapunov exponents as follows:

$$d_f = j + \frac{\sum_{i=1}^{j} \lambda_i}{|\lambda_{j+1}|} \tag{8.14}$$

where j is defined as follows,

$$\sum_{i=1}^{j} \lambda_i > 0. \tag{8.15}$$

The exponents are ordered from largest to smallest (Appendix D). This means that j is the sum of positive (with zero defined to be positive) exponents divided by the next smallest. For the case considered, the steady-state Lyapunov exponents we calculate are $(+0.0415647, +0.0, -0.063931)$; plugging these into the above formula we obtain 2.64952 as the Lyapunov dimension of this attractor.

In addition to Lyapunov exponents, other techniques including double Poincaré sections (Wiggins, (1988)) and cell-to-cell mapping (Hsu, (1987)) exist to analyze and compare the nonlinear dynamics.

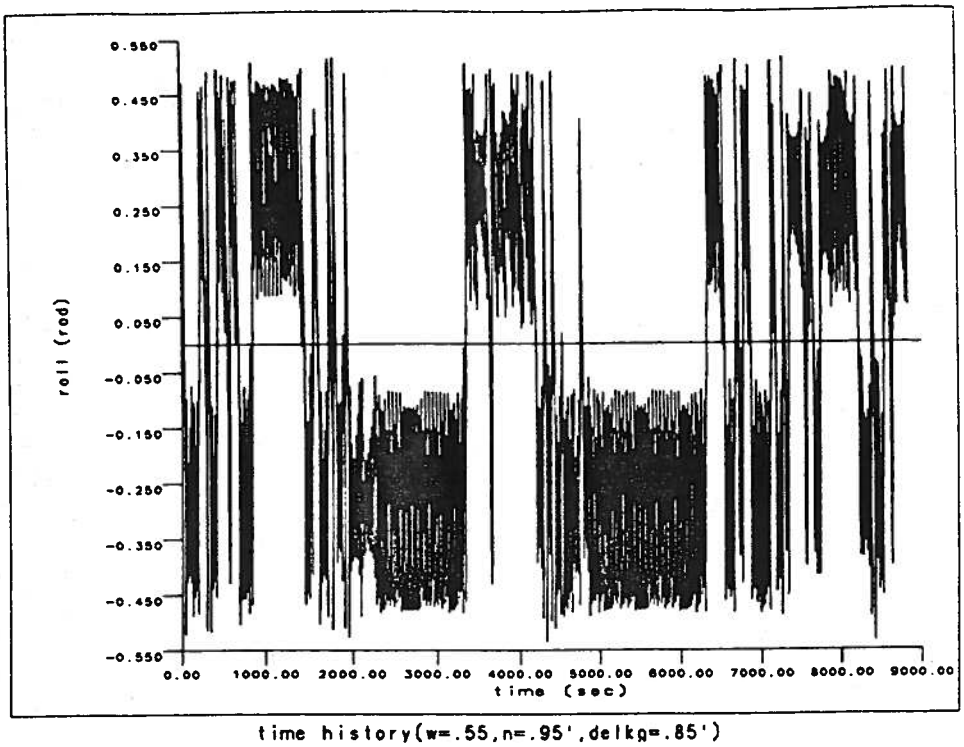

Figure 8.46: Time history of steady-state chaos

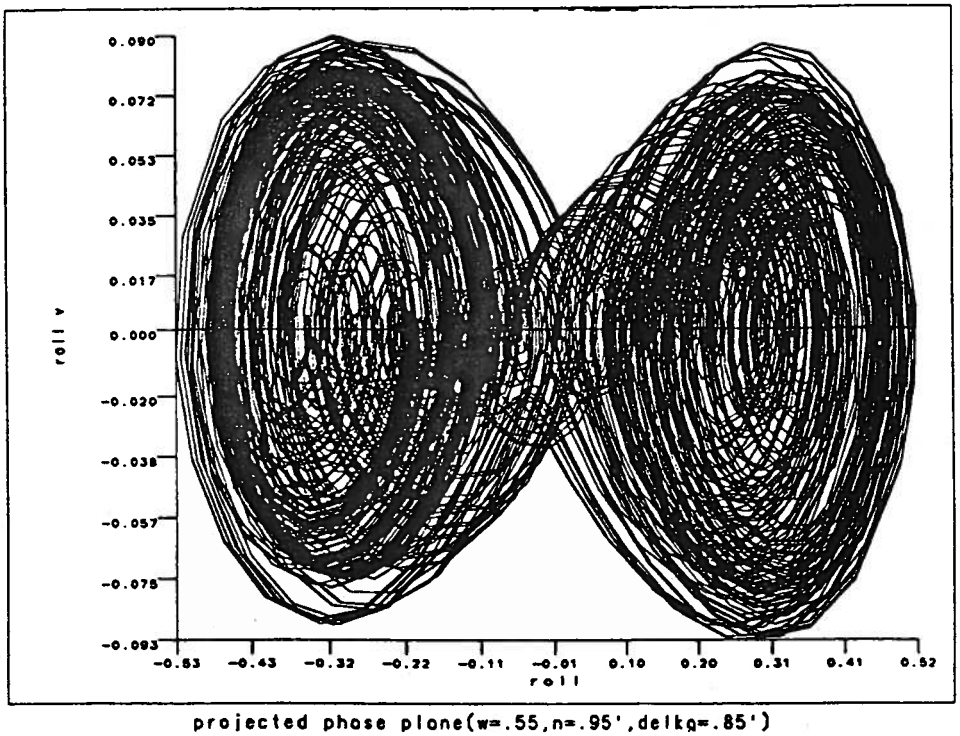

Figure 8.47: Projected phase plane of steady-state chaos

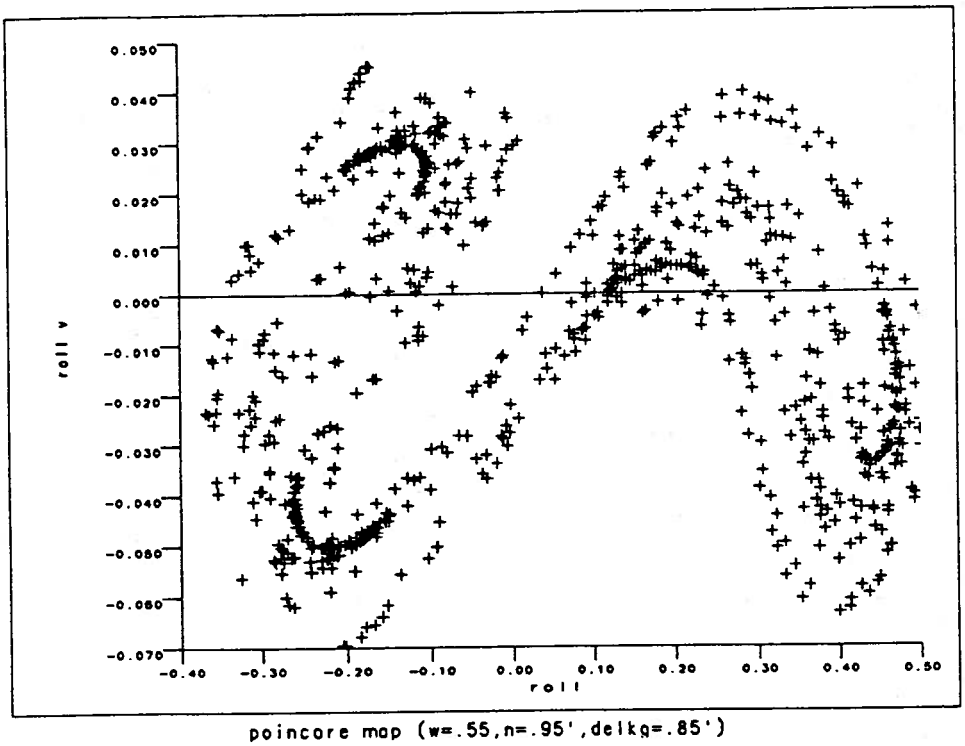

Figure 8.48: Poincaré map of steady-state chaos strange attractor

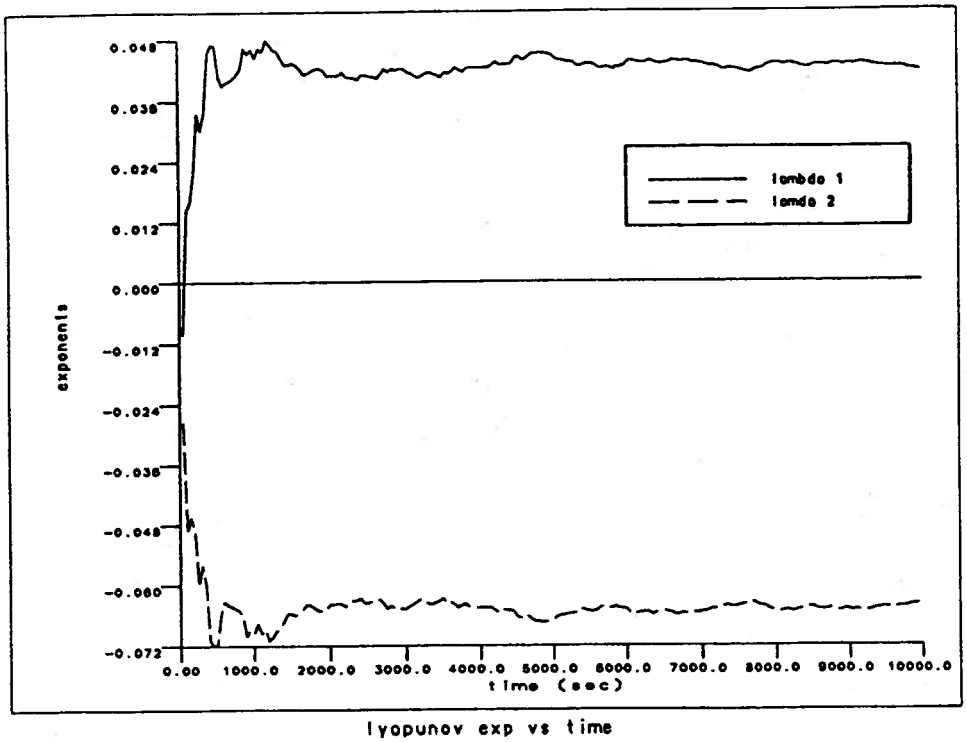

Figure 8.49: Time history of Lyapunov exponent calculations

Parametric excitation

Parametric excitation is an important dynamic effect in ship motions. As such, parametric excitation has been studied extensively in the ship dynamics field (e.g., Paulling and Rosenberg, (1959), Paulling,(1961), Blocki, (1980), and Kerwin, (1959)). Probably the most extensive experimental and computational study in this area was carried out during the 1970's at the University of California, Berkeley (Paulling, et al., (1979)). In addition to an extensive amount of experimental data, this project produced the nonlinear ship motion simulation computer program CAPSIZE. CAPSIZE is unique in that it calculates the exact hydrostatics at every time step. Recently, DeKat and Paulling, (1989) added to and improved the earlier program. This improved computer program is called KAPSIZE. KAPSIZE's most notable refinement is the addition of time domain hydrodynamics.

Although the experimental and simulation results are quite extensive in the Berkeley work, little theoretical analysis was included. Moreover, the theoretical analysis that was done, was for an undamped linear parametrically forced equation without external forcing. Relating this simplified analysis to a more exact treatment of the problem can be misleading and confusing for three reasons. First, when damping is considered, the region of instability decreases (Jordan and Smith, (1987)). Second, when the nonlinear spring is considered the previously unbounded motion often achieves a finite value (Minorsky, (1962)). Third, when external forcing is added to the parametric excitation, interesting interaction occurs (HaQuang, and Mook, (1987)).

Considering all these shortcomings, we undertook some preliminary analysis of the combined externally and parametrically forced nonlinear ship roll equation of motion with linear and nonlinear damping and an exact roll restoring spring. Our analysis includes an $O(\epsilon)$ approximation to the harmonic component of the time

varying restoring moment δGM which is determined by considering the slope at the waterline. This results in a time dependent righting moment curve as can be seen in the following equations and in Figure 8.50.

If we include parametric excitation we obtain the following single degree of freedom differential equation,

$$(I_{44} + A_{44})\ddot{\phi} + B_{44}\dot{\phi} + B_{44q}\dot{\phi} \mid \dot{\phi} \mid + GZ_m(\phi, t) = F_4 \cos(\omega t + \gamma_4) \tag{8.16}$$

where, $GZ_m(\phi, t) = \frac{(\overline{GM}_m + \delta GM \cos(\omega t))}{\overline{GM}_m} GZ_m(\phi)$.

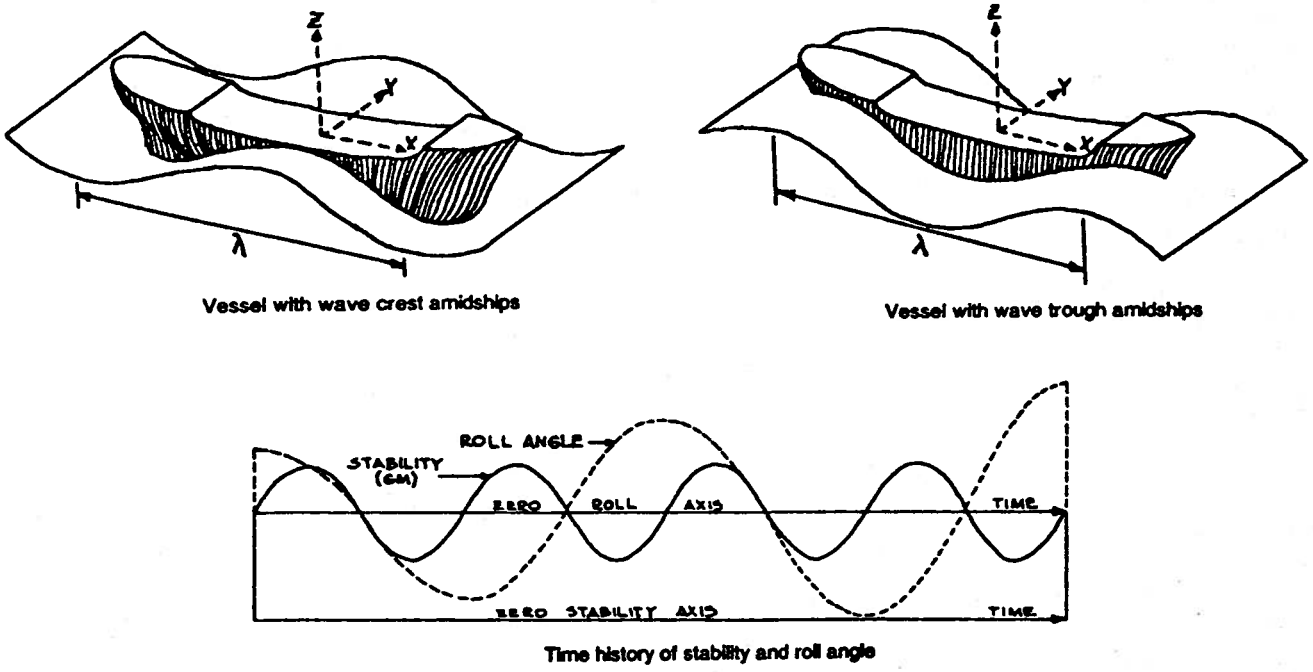

Figure 8.50: Parametric excitation (Bovet, (1974))

The large amplification of the combined externally and parametrically excited system versus the purely externally forced system is quite dramatic (see Figure 8.51). In addition, we obtain invariant manifolds (Figure 8.52) similar to those of the purely externally forced system (Figure 4.2). However, more importantly is the fact that the dynamic instability occurs long before static instability (Figure 8.51). We note

here that this dynamic loss of stability along the upper branch of the magnification curve may be the divergence instability described by Schmidt and Tondl, (1986).

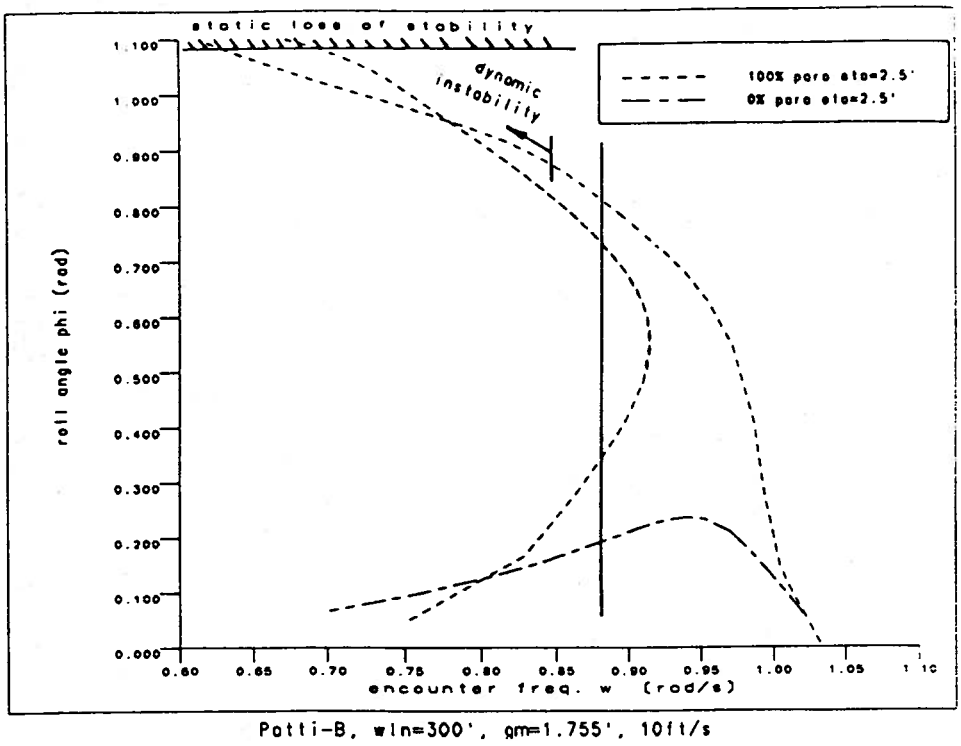

Figure 8.51: Parametric excitation magnification curve

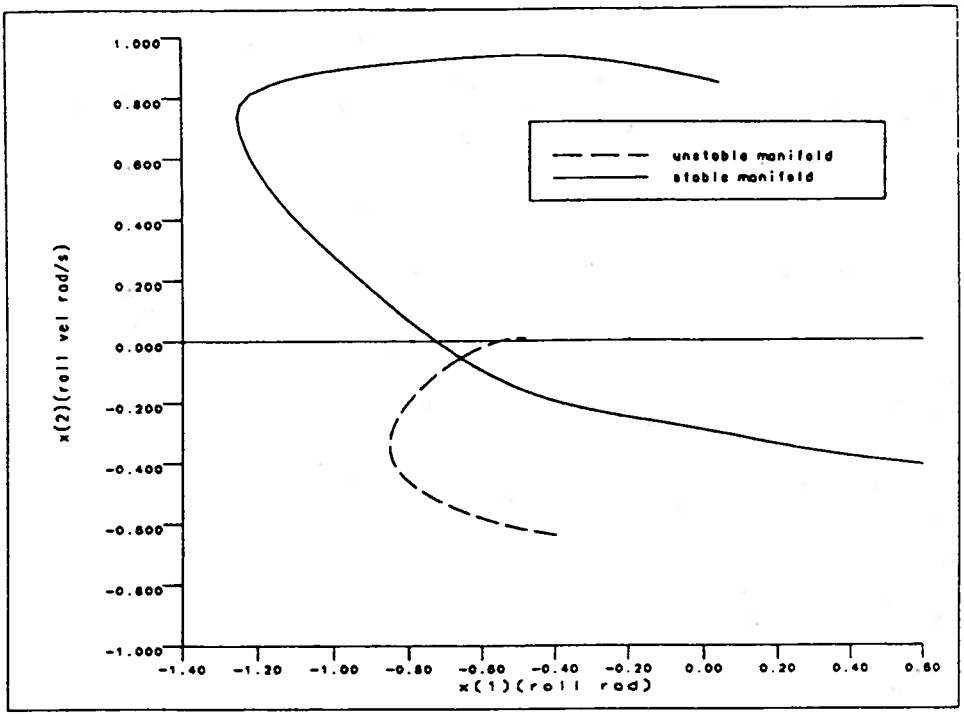

Figure 8.52: Parametric excitation Poincaré map

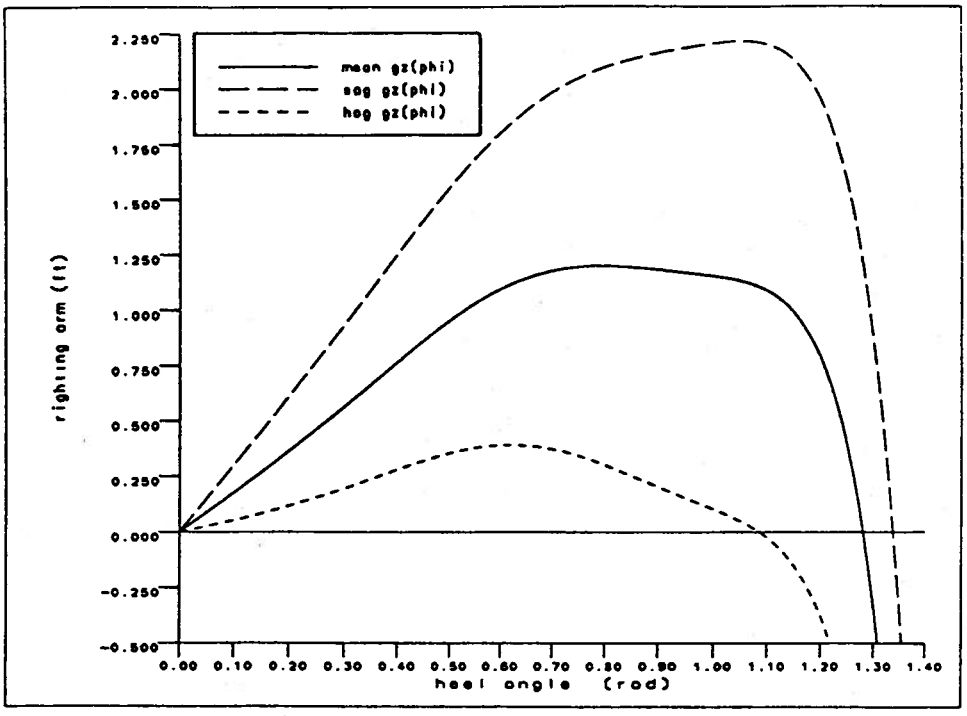

Figure 8.53: Range of static variation of righting arm curve

CHAPTER IX

OBSERVATIONS AND CONCLUSIONS

Considering the results if this thesis, we believe it is now clear how various important physical factors affect nonlinear ship dynamics and possibly capsizing. This thesis considered the effect of the static roll restoring moment, nonlinear damping, and external wave excitation on the resulting dynamics. In addition, we also saw what characteristics of the vessel righting arm are most important. These include the angle of vanishing stability, the loll angle, and the magnitude and slope of the righting arm curve at any point. Away from zero roll angle, the nonlinear terms in the roll restoring moment are important. We can also see from the lobe dynamics analysis the extreme importance of initial conditions in assuring vessel safety. We note how slight changes in the parameters of the system can result in dramatic changes in the character of the resulting dynamics. Examples of this include the pinching off of the upper branch of the magnification curve as the metacentric height is increased and the intersection of the manifolds as the forcing is increased beyond a certain threshold value, and the surprisingly complex dynamics which may result. We also see how important the parametric excitation is in both increasing the magnitude of the vessel response and also introducing new types of behavior which were not previously observed.

Importance of initial conditions without manifold intersections

By far, the most important practical result of this work is the application of the idea of invariant manifolds of the Poincaré map to analyze the boundedness of large amplitude ship rolling motion. The invariant manifolds are the boundaries between qualitatively different dynamics, for that phase of the Poincaré map. By using the Poincaré mapping technique, we can consider the entire phase space of interest for highly nonlinear, damped and periodically time-varying differential equations, which the forced roll equation of motion is. Before these manifolds intersect, the boundary between capsizing (unsafe region due to unbounded eventual solutions) and non-capsizing (safe region due to bounded eventual solutions) behavior is clear (see Figure 5.6). Given a particular ship configuration (inertia, added mass and linear and quadratic damping coefficients), operating condition (described by a particular righting arm curve) and environmental condition (regular wave forcing), we can determine the corresponding invariant manifolds and easily determine whether a given initial condition of roll angle and roll velocity at a particular phase of the forcing (i.e., $(\phi_o, \dot{\phi}_o, t = t_p)$) will capsize (eventually become unbounded) or will not capsize (remain bounded).

Importance of initial conditions with manifold intersections

Once the manifolds intersect, we can still determine the eventual fate of the motion originating from given initial conditions. This can be done easily for a few periods of the forcing but becomes more difficult for longer times because of the complicated re-intersection of the manifolds. We can determine at what value of the forcing the manifolds intersect using the Melnikov method. After the manifolds intersect, we must study the initial conditions inside the resulting intersections called

lobes. Although it is not difficult to determine where initial conditions inside the lobes will iterate to after a few iterates (time integrations for integer periods of the external forcing) of the map, because of the eventual re-intersection of the lobes, it is more difficult to predict the eventual state (after many iterates) of the motion (see Figure 7.5). However, for lobes near the so-called turnstile (see Figure 7.3), we are able to predict whether an initial condition $(\phi_o, \dot{\phi}_o, t = t_p)$ inside one of the lobes will iterate from inside to outside or vice versa (see Figures 8.23, 8.24 and 8.25).

Importance of hetroclinic and homoclinic intersections

A vessel with an initial loll angle will have two sets of invariant manifolds. One set originating from the saddle corresponding to zero roll angle and two sets of saddles corresponding to the positive and negative loll angles. The manifolds are called, respectively, homoclinic and hetroclinic intersections. Intersection of the hetroclinic manifolds separate the boundary between the safe and unsafe regions into lobes. Some inside (safe) lobes may eventually iterate outside (unsafe); we refer to this event as *an unexpected capsizing* (see Figures 8.23 and 8.24 condition (2)). Another possible event that can occur is when the unstable homoclinic manifolds intersect the stable hetroclinic manifolds. This capsizing mechanism could force initial conditions near the origin to iterate outside the safe region (see Figure 8.21). We refer to this capsizing mechanism as *a totally unexpected capsizing.*

Conditions necessary to reduce degrees of freedom

In order to be able to simply analyze (in the plane) whether initial conditions are safe or not requires reducing the linearly coupled, damped and forced multiple degree of freedom system to an equivalent single degree of freedom system, but this

is not always possible. Although it is possible to analytically decouple an unforced and undamped system, it is not possible for even the linear damped and forced system to exactly decouple the modes of interest (Shahruz and Ma, (1988)). However, we have determined conditions which must be met in order to approximately obtain an equivalent single degree of freedom system corresponding to the more complete multiple degree of freedom system. These conditions require reducing the sway velocity while assuring the eigenvectors still lie in a plane for the most stable and least stable eigenvalues. We recall that the global (nonlinear) manifolds are tangent to the eigenvectors at the fixed points.

Importance of physical parameters

- *effect of nonlinear roll restoring moment curve*

  The character of the nonlinear roll restoring moment curve was the single most important physical parameter studied. This is reassuring since current ship static stability criteria consider only the righting arm curve. The zeroes of the nonlinear roll restoring moments correspond to the fixed points for the damped system. Once forcing is added, these fixed points become periodic orbits or fixed points in the Poincaré map. Therefore, the character of the static roll restoring moment is also important in determining fixed points for the forced and damped system.

- *effect of roll damping*

  The effect of including nonlinear roll damping versus solely linear roll damping was found to be important quantitatively and not qualitatively. Including nonlinear roll damping resulted in a decrease in the amplitude of the roll motion, but did not cause any qualitative changes. The magnitude of the forcing and damping will determine the area in the Poincaré map for safety. By consider-

ing the Melnikov function, the damping will also determine the required wave amplitude for intersections.

- *effect of forcing magnitude and frequency*

  The effect of the forcing was most important in periodically perturbing the differential equation. As stated above, the magnitude of the forcing determined the area in the Poincaré map for safety and whether or not intersections will occur.

- *single degree of freedom versus multiple degrees of freedom*

  The results of the bifurcation and stability analysis of the harmonic solutions suggested that consideration of the multiple versus single degree of freedom problem was qualitatively very important (see Figures 8.3 and 8.4). Studying the quantitative effect of the multiple degrees of freedom versus the single degree of freedom was not as clear when the invariant manifolds were studied. This was because the Poincaré maps for the multiple degree of freedom system are four dimensional and more difficult to study than the two dimensional system, (Appendix B).

- *effect of frequency dependence in the hydrodynamic coefficients*

  The bifurcation and stability analysis of the harmonic solutions suggested that the frequency dependence of the hydrodynamics (A_{ij} and B_{ij}) was not very important (see Figure 8.5).

- *effect of water-on-deck*

  The effect of considering water-on-deck or damage was to substantially reduce the magnitude of the static roll restoring moment curve and possibly change its character and result in a loll angle. This loll angle resulted in the unperturbed homoclinic connection and an additional type of complicated dynamics.

- *effect of adding parametric excitation*

  Combined external and parametric excitation is important in both increasing the magnitude of the vessel response and also introducing new types of behavior which were not previously observed.

Generality of techniques

Finally, the techniques described in this thesis are more general then the specific application of a vessel rolling with an initial loll angle would suggest. An obvious generalization would be to analyze a righting arm curve without a loll angle. In this case, we would have only the hetroclinic intersections and would not have the possibility of the combined homoclinic and hetroclinic intersections occurring. All the previous analysis would be applicable. Another more general problem would be to consider a static heel bias due to a steady wind force for example. This is the case considered in existing ship stability weather criteria and it would be interesting to compare the dynamics with and without this bias. For this case we would have to calculate a new Melnikov function but one has already been calculated for a similar system (Namachchivaya and Hilton, (1987)). Another application would be to further study parametric excitation. Although we have already started the bifurcation study of the combined externally and parametrically forced system and calculated one set of invariant manifolds (Figure 8.52), we might continue our analysis by calculating the Melnikov function. Again a mathematically similar system with only parametric excitation has already been analyzed (Ariaratham and Xie, (1989)), and a system with combined external and parametric with incommensurate frequencies has also been analyzed by Yagasaki, Sakata and Kimura, (1990).

CHAPTER X

FUTURE WORK

In this thesis a preliminary attempt was made to evaluate the effect of various approximations. In the various areas some work has been done but the complexities of the most general ship dynamical system may prove these problems to be unsolvable.

Multi-frequency forcing

A possibly more realistic analytical model of the system dynamics would include multi-frequency forcing. Since sea waves are irregular, the single frequency excitation although tractable may be unrealistic. Wiggins, (1988) has applied the Melnikov method to a single degree of freedom nonlinear oscillator with multi-frequency excitation and has found the resulting quasi-periodic motion to exhibit larger regions of chaotic dynamics. Recall, it is well-known that the linear hydrodynamics (added mass and damping) coefficients are frequency dependent. If the frequency dependence of the hydrodynamics is found to be important for multiple frequency forcing, the idea of an extended phase space as proposed by Schmiechen, (1973) and used by other ship dynamics researchers in the United States (McCrieght, (1986)) and in Germany (Sharma, Jiang and Schellin, (1988)) could be applied.

Parametric excitation and a bias

Parametric excitation is interesting both dynamically and practically. Preliminary results of a single case indicate many new and interesting phenomena may occur when combined external and parametric excitation are present. Although much experimental and simulation work has been done by other investigators (e.g., Paulling, (1979)) only the linear parametric instability without external forcing or damping has been analytically studied. We suggest addressing these shortcomings of the previous analysis in more detail. We suggest studying additional aspects and the additional phenomena that may occur.

Physically, parametric excitation may be due to the time-varying hydrostatic forces or because of water moving onto and off the vessel's aft deck as suggested by Troger (Troger, 1989). If the external wave excitation and water-on-deck forces are occurring at different frequencies additional analysis is required. A system with combined external and parametric excitation with incommensurate frequencies has been analyzed using perturbation techniques (HaQuang, and Mook, (1987)). The solely parametrically forced system has been analyzed using modern methods (e.g., Melnikov) by Ariaratnam and Xie, (1989). The combined parametric and externally excited system with incommensurate frequencies has been analyzed by using averaging and Melnikov by Yagasaki, Sakata, and Kimura, (1990) and shown to have chaotic dynamics.

It is well-known to naval architects that ships with a bias may be most vulnerable to capsize. This bias may be due to a steady force as a result of wind acting or a cargo shift. Further investigation should evaluate this effect upon the safe basins of attraction, escape from a potential well (capsize), and lobe dynamics. In the biased case, the saddle connections are no longer symmetric. Previous investigators (e.g., Nayfeh and Khedir, (1986) and Virgin, (1987)) have found complex dynamics in a

similar system by the period doubling route. In addition, Namachchivaya and Hilton, (1987) have used Melnikov methods to analyze the dynamics of mathematically similar systems.

Development of a probabilistic stability criteria

In order to eventually apply these techniques to vessel design, we must incorporate them into some sort of probabilistic criteria (e.g., Gilbert and Card, (1990)) which considers the randomness of the seaway. Troesch (1990) has suggested using modified linear ship motion theory or nonlinear simulation in order to determine the probability of achieving a certain initial condition. Further, we could use the results of this work as the conditional probability (Parsons, (1990)) of capsize given a joint probability describing the initial conditions. Integrating these two numbers over a large but finite area of the phase plane, we could determine some measure of vessel safety and risk.

Other vessel types

Finally, these techniques are not limited to the study of extreme rolling motion of a displacement hull form. Using experimentally determined coefficients, Troesch (1990) has recently applied the stability and bifurcation methods we describe here to analyze the strongly coupled heave-pitch porpoising instability experienced by planing hulls. In a region where linear stability analysis predicts a single stable solution, he determined a similar stable nonlinear solution but also discovered a nonstable saddle type solution. Numerical simulation showed the saddle to be associated with the boundary between the bounded stable motion corresponding to the linear solution and a previously unobserved unbounded motion!

APPENDICES

APPENDIX A

The Mathematical Details of the Melnikov Function

Derivation of the Melnikov function

As described in the main text, the Melnikov method is used to calculate a distance (the Melnikov function) between the stable and unstable manifolds of a perturbed dynamical system. Zeroes of the Melnikov function correspond to crossings of these manifolds. According to the Smale Birkhoff Theorem (Guckenheimer and Holmes, (1986)), crossings of these manifolds are a necessary but not sufficient condition for complicated dynamics to occur. Following (Guckenheimer and Holmes, (1986)), the derivation of the Melnikov function is as follows:

We begin with a periodically time-varying dynamical system of the form,

$\dot{x} = f(x) + \epsilon g(x,t)$;

$x = (u,v) \in R^2$.

Where, $f(x)$ is a known autonomous vector field (usually but not always a Hamiltonian vector field) and $g(x,t)$ is a periodically time varying perturbation of fixed period, $f(x) = (f_1(x), f_2(x))$ and $g(x,t) = (g_1(x,t), g_2(x,t))$.

Using the result of a Lemma from (Guckenheimer and Holmes, (1986)), we know that the perturbed manifolds, q_ϵ, may be uniformly approximated to $O(\epsilon^2)$ as the sum of the unperturbed manifold, q^0, (see Figure A.1) a yet to be determined $O(\epsilon)$ term, ϵq_1, as follows,

$q_\epsilon^s(t,t_0) = q^0(t-t_0)+\epsilon q_1^s(t,t_0)+O(\epsilon^2)$ and $q_\epsilon^u(t,t_0) = q^0(t-t_0)+\epsilon q_1^u(t,t_0)+O(\epsilon^2)$.

This implies that,

$|q_\epsilon^u(t,t_0) - q^0(t-t_0)| \sim O(\epsilon^2)$ and

$|q_\epsilon^s(t,t_0) - q^0(t-t_0)| \sim O(\epsilon^2)$.

Using the above results, it can easily be shown that solutions lying in the stable manifold can be uniformly approximated by a solution to the following variational equation (Jordan and Smith, (1987)),

$\dot{q}_1^s(t,t_0) = Df(q^0(t-t_0))q_1^s(t,t_0) + g(q^0(t-t_0),t)$,

and a similar result holds for $\dot{q}_1^u(t,t_0)$.

Next define the separation of the manifolds as

$d(t_0) = q_\epsilon^u(t_0) - q_\epsilon^s(t_0)$.

where $q_\epsilon^u(t_0)$ and $q_\epsilon^s(t_0)$ in the above equations are the unique closest points lying on the normal to $q^0(t-t_0)$ given by,

$f^\perp(q^0(0)) = (-f_2(q^0(0)), f_1(q^0(0)))$.

Using this we define the unique signed [1] distance between the closest points on the perturbed manifolds as,

$$d(t_0) = \epsilon\frac{f(q^0(0)) \wedge (q_1^u(t_0) - q_1^s(t_0))}{|f(q^0(0)|} + O(\epsilon^2) \qquad \text{(A.1)}$$

Alternatively, (Rom-Kedar, Wiggins, and Leonard, (1990)) derive a possibly more useful form which is as follows,

$$d(t_0) = \epsilon\frac{f^\perp(q^0(0)) \cdot (q_1^u(t_0) - q_1^s(t_0))}{|f(q^0(0)|} + O(\epsilon^2). \qquad \text{(A.2)}$$

The $\wedge$ is the usual vector cross-product in $\mathbf{R}^2$ and $\cdot$ is the dot-product.

---

[1] The sign of distance function describes the relative orientation of the manifolds. It measures the distance between the stable and unstable manifolds. A positive distance implies the stable manifold is inside the unstable while a negative distance implies the opposite. Therefore, it is obvious that a zero distance implies that the manifolds have intersected.

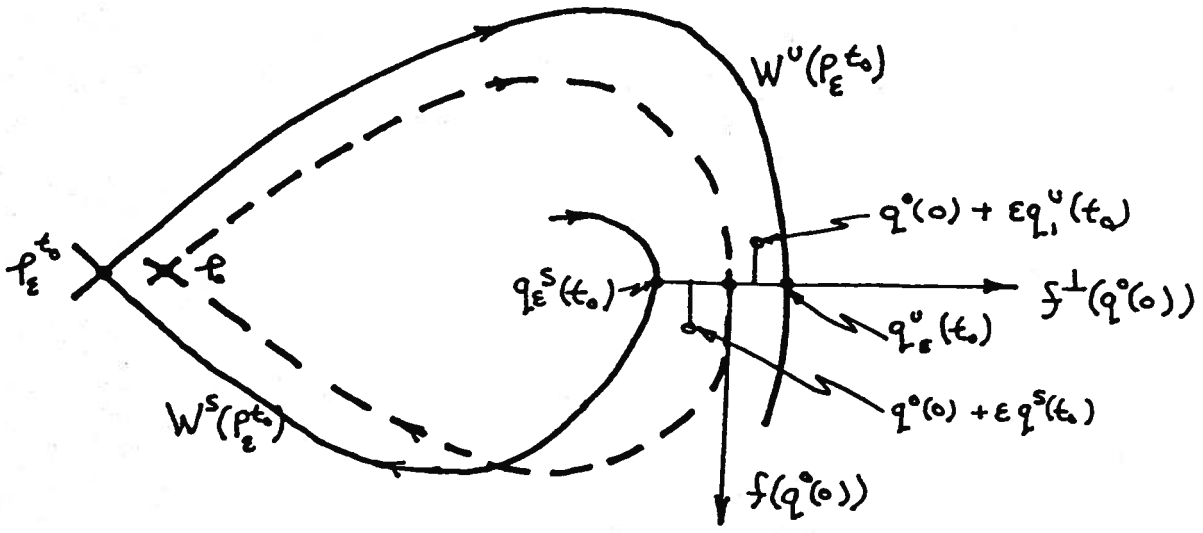

Figure A.1: Notation for intersecting manifolds

Finally, we define the Melnikov function as follows

$$M(t_0) = \int_{-\infty}^{+\infty} f(q^0(0)) \wedge g(q^0(t-t_0), t)dt. \tag{A.3}$$

In order to show that the Melnikov function represents the distance between the two perturbed manifolds, we again follow (Guckenheimer and Holmes, (1986)) and consider the time dependent distance function,

$\Delta(t, t_0) = f(q^0(t-t_0)) \wedge (q_1^u(t, t_0) - q_1^s(t, t_0))$

$\Delta(t, t_0) \equiv \Delta^u(t, t_0) - \Delta^s(t, t_0)$.

Alternatively, we may define the scaled distance between the manifolds in terms of the above quantity as,

$$d(t_0) = \frac{\epsilon \Delta(t, t_0)}{|f(q^0(0))|} + O(\epsilon^2). \tag{A.4}$$

To start the derivation, we take the time derivative of both sides of the time dependent distance function and obtain,

$$\frac{d\Delta^s(t, t_0)}{dt} = Df(q^0(t-t_0))\dot{q}^0(t-t_0) \wedge q_1^s(t, t_0) + f(q^0(t-t_0) \wedge \dot{q}_1^s(t, t_0). \tag{A.5}$$

Recalling that $\dot{q^0} \equiv f(q^0)$, we obtain,

$$\dot{\Delta}^s(t,t_0) = Df(q^0)f(q^0) \wedge q_1^s + f(q^0) \wedge (Df(q^0)q_1^s + g(q^0,t)).$$

Simplifying, we obtain,

$$\dot{\Delta}^s(t,t_0) = traceDf(q^0)\,\Delta^s + f(q^0) \wedge g(q^0,t).$$

If the unperturbed system is Hamiltonian then the $traceDf(q^0) \equiv 0$. Integrating the remaining term from t_0 to ∞ we get,

$$\Delta^s(\infty,t_0) - \Delta^s(t_0,t_0) = \int_{t_0}^{+\infty} f(q^0(t-t_0) \wedge g(q^0(t-t_0,t)dt. \qquad \text{(A.6)}$$

Here, we note that as $t \to \infty, \Delta^s$ goes to p (the saddle point). Repeating the above procedure for the unstable manifold, we obtain,

$$\Delta^u(t_0,t_0) - \Delta^u(-\infty,t_0) = \int_{-\infty}^{t_0} f(q^0(t-t_0) \wedge g(q^0(t-t_0),t))dt. \qquad \text{(A.7)}$$

Combining the above two results, we obtain,

$$d(t_0) = \frac{\epsilon M(t_0)}{|f(q^0(0))|} + O(\epsilon^2). \qquad \text{(A.8)}$$

□

It is now clear that the perturbed trajectories of the differential equation need never be calculated. All that is required is to know the unperturbed trajectories along which the perturbed differential equation is evaluated. Being able to analyze the perturbed dynamics without ever having to calculate the perturbed trajectories is the benefit of using the Melnikov method. Using Melnikov's method allows us to never calculate the perturbed dynamics, even though we obtain a simple expression describing the characteristics of the perturbed system in terms of the equation parameters.

Using the Melnikov function to study lobe size

One of the results of Wiggin's lobe dynamics theory (Rom-Kedar, Leonard, and Wiggin's, (1990)) is to use the Melnikov function to approximately ($O(\epsilon)$) determine the lobe area. The simplest case is a lobe bounded by two primary intersection points (pip's) of the perturbed stable and unstable manifolds. We note here that it is the primary intersection points that correspond to the zeroes of the Melnikov function.

The lobe might look like Figure A.2. The area of the lobe $\mu(L)$ can be obtained by integrating (ds) along the unstable manifold between the two primary intersection points q_1 and q_2. This is,

$$\mu(s) = \int_{q_1}^{q_2} l(s)ds. \tag{A.9}$$

The height of the normal from the stable manifold to the unstable manifold, $l(s)$ is approximately equal to the distance between the stable and unstable manifolds measured normal to the unperturbed manifold; i.e.,

$$l(s) = |d(t_0, \epsilon)| + O(\epsilon^2). \tag{A.10}$$

Recall, this distance $d(t_0, \epsilon)$ is just the unscaled distance used in the derivation of the Melnikov function in the previous section. Therefore, we can express the height between the two manifolds in terms of the Melnikov function, $M(t_0)$ as follows,

$$l(s) = \frac{|M(t_0)|}{|f(q_u(-t_0)|} + O(\epsilon^2). \tag{A.11}$$

Using the chain rule for derivatives, to redefine the differentials, we rewrite the differential distance (ds) along the unstable manifold in terms of a differential time (dt_0) along the unperturbed manifold as follows,

$$ds = \frac{ds}{dt_0} dt_0 = [|f(q_u(-t_0)| + O(\epsilon)]dt_0. \tag{A.12}$$

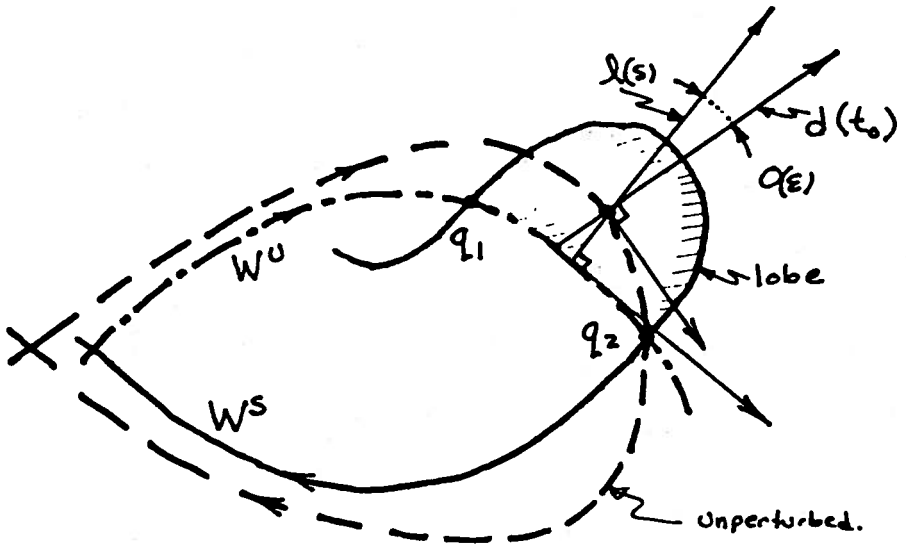

Figure A.2: Lobe created by intersecting manifolds

We also need to determine the new limits of integration in terms of the new time variable, these are $q_u(-t_{01}) = q_1$ and $q_u(-t_{02}) = q_2$ (see figure). Substituting, all of the above into the area integral, we obtain,

$$\mu(s) = \int_{t_{01}}^{t_{02}} [\frac{|M(t_0)|}{|f(q_u(-t_0)|} + O(\epsilon^2)][|f(q_u(-t_0)| + O(\epsilon)]dt_0 \qquad \text{(A.13)}$$

Simplifying, we obtain

$$\mu(s) = \int_{t_{01}}^{t_{02}} |M(t_0)|dt_0 + O(\epsilon^2). \qquad \text{(A.14)}$$

The above integral is approximately ($O(\epsilon)$) the lobe area determined using the Melnikov function. Although the lobe arrangement is usually not so simple when there are other than primary intersections, we can determine the area in those cases too. In addition, this adds another powerful interpretation of the Melnikov function. In the non-dissipative system, knowing the area and behavior of one lobe allows you to determine its and all other lobes behavior for all time. This is so because of area preservation, (i.e., every lobe is a forward and backward iterate of another). However, in the dissipative system where area is not preserved such is not the case

and we need to study all lobes for all times. For an example application of this technique see Wiggins, Rom-Kedar, (1990). In this work, they calculate the escape rate for a non-dissipative Duffing's equation.

APPENDIX B

Discussion of the Melnikov Vector

Following Wiggins, (1988), we determine the effect of multiple degrees of freedom upon the Melnikov calculation. This formulation is called a Melnikov vector and is a generalization of the Melnikov function calculation in two dimensions. In order to determine the effects of the additional degrees of freedom upon the dynamics, we follow an extension of the original Melnikov theory described in Appendix A. The multiple degree of freedom theory is explained in a number of references including Wiggins and Holmes, (1987), Wiggins, (1988) and Wiggins and Shaw, (1988). The general theory for a variety of classes of systems is completely discussed in Wiggins, (1988). However, Wiggins and Holmes, (1987) and Wiggins and Shaw, (1988) describe the theory applicable to our specific case, the case of a slowly-varying oscillator. The determination of the Melnikov vector (i.e., the multiple degree of freedom analogue to the Melnikov function) is essentially the single degree of freedom system (two phase variables) with the addition of two slowly varying terms.

In order to reduce our multiple degree of freedom system to the form described by the slowly varying oscillator we transform our coordinate system in two steps. First, we move our coordinate origin to the location where the roll-sway and sway-yaw inertial and added mass coupling are eliminated. This translation is analogous to an origin at the center of gravity for a system without hydrodynamic cross-coupling. Second, we rotate our axis system so that the roll-yaw inertial and added mass cross product of inertia are eliminated. Again, this rotation is analogous to rotating

to a principle axis system if the added mass is ignored. Upon carrying out these coordinate system transformations, our system is now in a form required for the theory of slowly varying oscillators described in the preceding references.

The theory of slowly varying oscillators, described by Wiggins and Shaw, (1988), is very similar to the simple Melnikov function calculation described in Appendix A with some subtle modifications. Because of the slowly varying terms, instead of a single homoclinic or heteroclinic orbit in the unperturbed system, we now have a family of such orbits parametrized by the slowly varying coordinates. What is required to determine is which member or members of this family is or are the one or ones of interest. This is determined by applying Theorem 2.2 from Wiggins and Shaw, (1988). This theorem states that by averaging the perturbations to the slowly varying coordinates and determining for what value or values this is equal to zero while evaluating the homoclinic or heteroclinic variables at the fixed points will determine the family member(s) of interest. According to equation 2.13 of Wiggins and Shaw, (1988), two terms appear in the Melnikov vector for the slowly varying oscillator. The expression for the slowly varying Melnikov vector is as follows,

$$M(t_0) = \int_{-\infty}^{+\infty} \nabla H(q_0^{z_0}(t_0)) \cdot g(q_0^{z_0}(t_0), t + t_0)dt - \frac{\partial H}{\partial z}(\gamma(z_0)) \int_{-\infty}^{+\infty} g_z(q_0^{z_0}(t_0), t + t_0)dt \tag{B.1}$$

where, $\nabla H = (\frac{\partial H}{\partial x}, \frac{\partial H}{\partial y}, \frac{\partial H}{\partial z_1}, \frac{\partial H}{\partial z_2})$.

The first term is analogous to the terms for the single degree of freedom Melnikov function while the second term considers the effect of the slowly varying coordinates. It turns out for our case, we get a linear system for our reduced perturbation, and that, when averaged, this becomes zero for zero values of both sway and yaw velocity. In addition, our Melnikov vector is a scalar due to dot products of trivial functions. As a result of all of this, our multiple degree of freedom Melnikov function is just the single degree of freedom Melnikov function with the previously mentioned coordinate

system transformations carried out.

We note here that Wiggins and Shaw, (1988) contains a concise discussion of the relationship between transverse homoclinic (heteroclinic) intersections and the Smale horseshoe for a three phase variable system. Although, our problem is four dimensional we believe the extension is completely analogous.

In order to understand the multiple degree of freedom problem it is useful to visualize the geometry of our system. The problem with our system is that the Poincaré maps are four dimensional and we cannot express this graphically. Therefore, we must rely on a three dimensional graphical representation, drawn on a two dimensional sheet of paper, and the concepts of co-dimension (Arnold, (1988), and Guckenhiemer and Holmes, (1986)) used in local bifurcation theory. As a result of a brief discussion with Professor VI Arnold the exact arrangement of our system is clear. To illustrate these ideas we draw a three dimensional figure before and after intersection and annotate it so as to reflect the additional dimension, (see Figure B.1).

Although for theoretical reasons it is often desirable to reduce a multiple dimensional system to the so-called center manifold (Carr, (1981))(Guckenhiemer and Holmes, (1986)), for our system this is not practical or maybe even possible. This is so because the center manifold is a local idea that is borrowed from local bifurcation theory and our interest is in the global behavior of the system. In order to apply center manifold theory, we must determine the stable, unstable and center subspaces and extract the center subspace. Once we divide the spectrum into these three subspaces, we know from the center manifold theorem that a center manifold exists. Although, the stable and unstable subspaces are unique the center manifold is not. Our problem is similar, yet not the same as center manifold problems in two respects. First, in center manifold problems we often have all eigenvalues less than one and study the behavior of those equal to one (i.e., the center manifold), in our

problem we are interested in the most stable and least stable eigenvalues and the center manifold is not as important to us. Second, center manifold theory is part of local bifurcation theory, and applies to the behavior at or very near fixed points. We know that the global manifolds are tangent to the local manifolds which can be approximated by the eigenvectors. However, we are interested in behavior far from the fixed points and cannot be sure how the manifolds evolve.

Since we are unable to numerically determine anything but a one dimensional trajectory using our modified software (Parker and Chua, (1989)), we can not detemine general intersections of the stable and unstable manifolds. However, we might want to consider whether an intersection is even possible for a given geometry. Since we have a one rapidly expanding eigendirection (unstable), one rapidly contracting eigendirection (stable), and two slowly evolving directions, it seems as though we have a three dimensional stable and a three dimensional unstable manifold evolving from a two dimensional homo(hetero)clinic "point" (Arnold, (1990)). Therefore, considering the idea of co-dimension (Guckenhiemer and Holmes, (1986)), the intersection of these two three dimensional manifolds in our four dimensional space will be two dimensional (i.e., $3+3-4=2$). The other possible cases are summarized in Table B.1, if the sum of the dimensions is less than that of the space, then no intersections will likely occur (Guckenhiemer and Holmes, (1986)). In the table $dim(W^1)$ is the dimension of one manifold, $dim(W^2)$ is the dimension of the other manifold, while $dim(inter)$ is the dimension of the intersection. However, since our multiple degree of freedom system has only one unstable mode corresponding to the single degree of freedom unstable mode, we have a three-dimensional stable manifold and a one dimensional unstable manifold. Therefore, we have a zero dimensional (points) intersection in the Poincaré map (i.e., $3+1-4=0$).

$dim(W^1)$	$dim(W^2)$	$dim(inter)$
3	1	0
2	2	0
3	2	1
3	3	2

Table B.1: Possible intersections of two manifolds in R^4

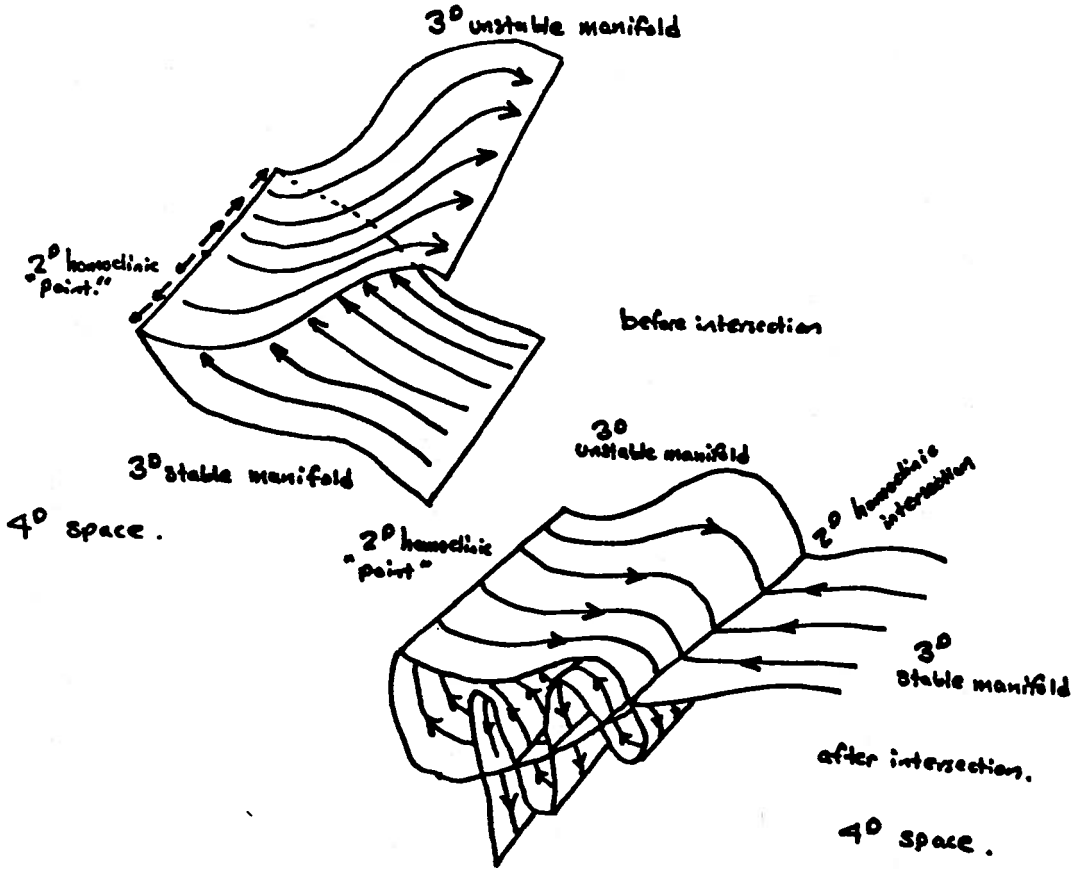

Figure B.1: Multi-dimensional manifolds a) before and b) after intersection

APPENDIX C

Stability of Periodic Solutions and the Monodromy Matrix

Following Seydel, (1988), we study the stability of periodic solutions. In order to study the stability of a given periodic solution we investigate the stability of neighboring trajectories.

If we begin with a differential equation [1]as follows,

$$\dot{\mathbf{y}} = \mathbf{f}(\mathbf{y}, \lambda) \tag{C.1}$$

with initial conditions $\mathbf{y}(0) = \mathbf{z}$ and solution trajectory $\varphi(t; \mathbf{z})$.

In order to examine the stability of this equation, we consider slight deviations (d_0) from the initial conditions ($\mathbf{z}^*$) and study whether this deviation grows or decays with respect to time (see Figure C.1),

$$d(t) = \varphi(t; \mathbf{z}^* + d_0) - \varphi(t; \mathbf{z}^*). \tag{C.2}$$

Since we are considering periodic solutions, we study the solution after one period ($T = 2\pi/\omega$) as follows[2],

---

[1] Recall, although we have a nonautonomous differential equation, we may consider an extended differential equation (adding time as a independent variable) and eventually considering a map.

[2] For autonomous differential equations, the period of the periodic solution is often unknown and part of the solution. However, we study harmonic solutions of

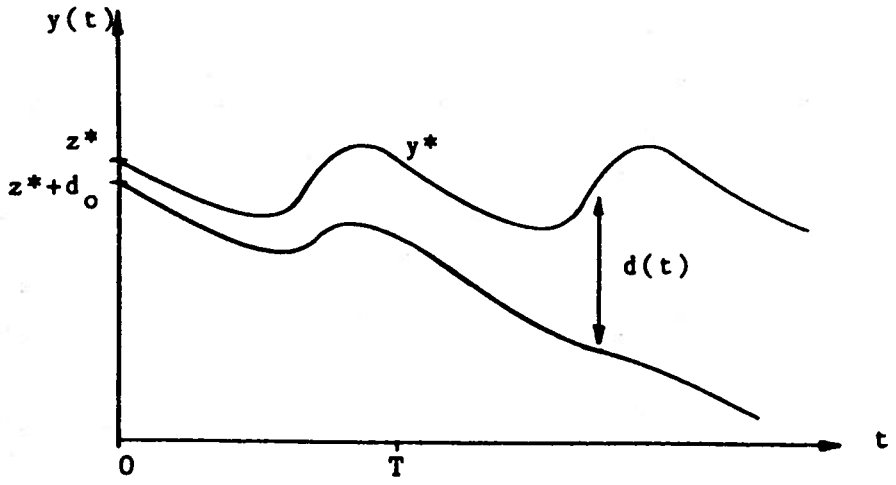

Figure C.1: Deviation of known solution with respect to time (Seydel, (1988))

$$d(T) = \varphi(T; \mathbf{z}^* + d_0) - \varphi(T; \mathbf{z}^*) \tag{C.3}$$

We begin by expanding $d(T)$ in a Taylor series about the known (given) initial value as follows,

$$d(T) = \frac{\partial \varphi(T; \mathbf{z}^*)}{\partial \mathbf{z}} d_0 + \text{ higher order terms}, \tag{C.4}$$

and study the linearized Jacobian matrix,

$$\frac{\partial \varphi(T; \mathbf{z}^*)}{\partial \mathbf{z}}. \tag{C.5}$$

This linearized matrix is called the monodromy matrix and studying its properties will determine if $(d_0(t))$ grows or decays with respect to time. In order to better understand the properties of the monodromy matrix, we continue to manipulate it. Since, φ solves the differential equation, the following is an identity,

---

periodically forced differential equations with time periodicity T. Although it may happen that subharmonic solutions arise by the flip or period doubling bifurcation as the parameter λ is varied, we only found this to occur for the combined externally and parametrically forced case we studied.

$$\frac{d\varphi(T;\mathbf{z})}{dt} = \mathbf{f}(\varphi(t;z),\lambda) \text{ for all t .} \tag{C.6}$$

Continuing, we differentiate the above equation with respect to z to obtain,

$$\frac{d}{dt}\frac{\partial\varphi(T;\mathbf{z})}{\partial\mathbf{z}} = \frac{\partial\mathbf{f}(\varphi(t;\mathbf{z}),\lambda)}{\partial\varphi}\frac{\partial\varphi(t;,\mathbf{z})}{\partial\mathbf{z}}. \tag{C.7}$$

Since $\varphi(0;\mathbf{z}) = \mathbf{z}$, we know,

$$\frac{\partial\varphi(0;\mathbf{z})}{\partial\mathbf{z}} = \mathbf{I}. \tag{C.8}$$

Considering the above results, we are able to infer that the monodromy matrix (the above expression evaluated at time T) is the fundamental solution matrix $\Phi(T)$ at time T. Recall, that the fundamental matrix Φ is the solution to the following initial value problem,

$$\dot{\Phi} = \mathbf{f_y}(\mathbf{y}^*,\lambda)\Phi, \text{ with initial condition matrix } \Phi(0) = \mathbf{I}. \tag{C.9}$$

Summarizing the above manipulations, we obtain the following definition from (Seydel, (1988)),

Definition *The n^2 monodromy matrix M of the periodic solution $y^*(t)$ with period T and initial value vector $\mathbf{z}^*$ is given by the following,*

$$M = \Phi(T) = \frac{\partial\varphi(T;\mathbf{z})}{\partial\mathbf{z}} \tag{C.10}$$

with φ and Φ defined by the above manipulations.

From Floquet theory, the stability of the periodic solution y^* can be studied by considering the eigenvalues of the monodromy matrix. We note here that by considering the stability after one period we have reduced the given extended (add time) continuous differential system to that of a discrete map (take time away again).

The stability of the system is now based upon whether or not the remaining n-1 eigenvalues (the periodic time eigenvalue is one) are less than one (stable) or if any one of them is greater than one (unstable).

Change in stability with respect to the parameter (Bifurcation)

Recall bifurcation theory is how the number and stability properties of solutions change as a parameter is varied. Of most interest to us for application to the ship turning problem is how the stability properties change. Using classical methods, we can calculate the stability properties of the single degree of freedom problem with fixed parameters (hydrodynamic coefficients). However, for the generalized problem with multiple degrees of freedom and frequency dependent hydrodynamic coefficients stability cannot easily be determined. For such generalized problems BIFPACK is well suited. What type of singular points we can have for a two-dimensional map is illustrated in Seydel, (1988) and for continuous time three-dimensional systems in Tondl and Schmidt, (1986).

The mechanism for losing stability in a map is determined by where one or more of the eigenvalues of the map are when they cross the unit circle. Losing stability occurs when an eigenvalue crosses the unit circle from inside ($|\mu(\lambda_0)| < 1$) to outside ($|\mu(\lambda_0)| > 1$), while gaining stability is accomplished by the reverse. The three ways of losing (gaining) stability, determined by the location of the eigenvalue as it crosses the unit circle, are as follows (see figure),

a) Divergence bifurcation where $\mu(\lambda_0) = 1$,

b) Flip or period doubling bifurcation where $\mu(\lambda_0) = -1$,

c) Hopf bifurcation where $\Im(\mu(\lambda_0)) \neq 0$.

In all our studies to date, (with one exception) the mechanism for gaining or losing stability has been by the divergence bifurcation. In the single case where

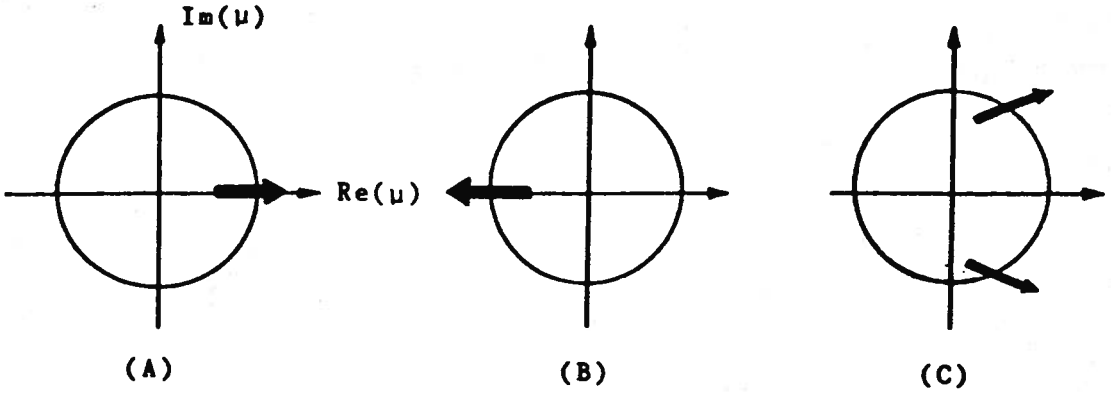

Figure C.2: Mechanisms for losing stability (Seydel, (1988))

parametric excitation due to time-varying hydrostatics was included, a series of flip or period doubling bifurcations were observed.

APPENDIX D

Quantifying Complicated Ship Dynamics with Lyapunov Exponents

In the previous chapters, we have described the occurrence of chaotic dynamics in ship dynamical systems. One characteristic of nonlinear dynamical systems exhibiting chaotic dynamics is an extreme sensitivity to initial conditions. This extreme sensitivity to initial conditions is quantified using the Lyapunov characteristic exponent. The Lyapunov exponent is just a generalization of the eigenvalues of a fixed point in an autonomous system and the Floquet characteristic exponent that describes the stability of periodic orbits (Parker and Chua, (1989)).The Lyapunov exponent characterizes the exponential divergence of neighboring trajectories in a general dynamical system.

Lyapunov Exponent from Governing Equation

The Lyapunov spectrum of exponents is physically the long term evolution of an infinitesimal n-sphere of initial conditions (Wolf, et al., (1985)). This n-sphere will evolve into a n-ellipsoid because of expansion and contraction of the phase space with time (see Figure D.1).

The Lyapunov exponents expressed in terms of the lengths of the various principal axes $p_i(t)$ is as follows,

for the continuous time system, we have

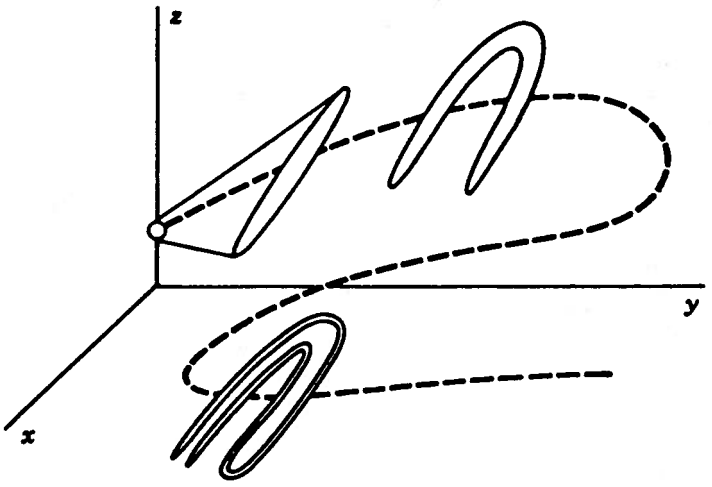

Figure D.1: Evolution of an initial condition sphere with time (Moon, (1988))

$$\lambda_i = \lim_{t\to\infty} \frac{1}{t} \log_2 \frac{p_i(t)}{p_i(0)} \tag{D.1}$$

and for the discrete time system,

$$m_i = \lim_{k\to\infty} \frac{1}{k} \left|\frac{p_i(k)}{p_i(0)}\right|^{\frac{1}{k}}. \tag{D.2}$$

The exponents λ_i are ordered from largest to smallest. In order for chaotic dynamics to occur we must have at least one positive exponent. We note here that $2^{\lambda_1 t}$ is the linear growth of the first principle axis, $2^{(\lambda_1+\lambda_2)t}$ is the area growth of the first two principle axes and $2^{(\lambda_1+\lambda_2+\lambda_3)t}$ is the volume growth. Since the sum of the exponents must be negative for a dissipative system and since it can be shown (Parker and Chua, (1989)) that any continuous time system will have a zero exponent, it takes at least three dimensions (one may be time) in order have chaotic dynamics. For a three-dimensional chaotic system, the signs of the exponents will be $(+, 0, -)$. Although the nearby trajectories will exponentially diverge, since motion

is often bounded over time the phase volume becomes folded (see Figure D.1).

The exponential divergence of nearby trajectories reflects the reason we have extreme sensitivity to initial conditions. We may also think of the positive Lyapunov exponent as an exponential expansion and eventual folding to be a way of destroying information. That means we may consider the exponents to reflect the number of bits/second gained (-) and destroyed (+) (Chua and Parker, (1989)). Bits per second is the reason for the base two logarithm. Given a finite numerical precision and a positive exponent, it is easy to calculate the time interval required to lose all information about the initial state of a trajectory.

Numerical Implementation Problems and Cautions

In the numerical implementation of an algorithm to calculate the spectrum of Lyapunov exponents, two problems arise. First, is the problem of exponential growth of the trajectory of interest (i.e., the one with positive exponent). Second, is the problem that the integration path eventually lines up with the largest trajectory making the calculation of the remaining exponents unreliable.

The first concern may be addressed by defining the Lyapunov exponent as a product,

$$\lambda_1 \approx \frac{1}{kT} \ln \parallel \delta x(KT; \delta x_0, x_0) \parallel \tag{D.3}$$

$$\lambda_1 = \frac{1}{kT} \ln \prod_{k=1}^{k} \parallel \delta x^{(k)} \parallel \tag{D.4}$$

$$\lambda_1 = \frac{1}{kT} \sum_{k=1}^{k} \ln \parallel \delta x^{(k)} \parallel . \tag{D.5}$$

Using the above equations, the exponent is always renormalized to unity at the beginning of each time step.

The second concern may be handled by repeatedly reorthogonalizing the vectors using the Gram-Schmidt orthogonalization procedure, as often as needed. This is as follows,

$$v_1' = \frac{v_1}{\| v_1 \|} \tag{D.6}$$

$$v_2' = \frac{v_2 - \langle v_2, v_1' \rangle v_1'}{\| v_1 - \langle v_2, v_1' \rangle v_1' \|} \tag{D.7}$$

$$v_3' = \frac{v_3 - \langle v_3, v_2' \rangle v_2' - \langle v_3, v_1' \rangle v_1'}{v_3 - \langle v_3, v_2' \rangle v_2' - \langle v_3, v_1' \rangle v_1'}. \tag{D.8}$$

The above procedure seems to address the reasonable concerns of numerically estimating the Lyapunov exponents from a differential equation or map. This calculation may be used as an additional way to prove that chaos is present in a dynamical system. In addition it can be used to quantify the exponential divergence of neighboring trajectories and sensitivity to initial conditions. Yet the technique should not be applied in isolation or blindly since it may lead to incorrect conclusions. We have used this technique only to verify the prescence of chaotic dynamics and to estimate the exponential divergence of neighboring trajectories.

Reconstruction of an attractor from a time-series

Using the above ideas and the idea of attractor reconstruction due to Ruelle (Eckmann and Takens, (1985)), one can in theory reconstruct an attractor and its properties from a time history of a single phase variable. This technique has been extensively studied and developed by Wolf, et al., (1985). In practical applications of this technique a large amount of data from numerical simulations or physical experiments is required. In order to apply this technique we start by choosing a point on a reference trajectory called a fiducial trajectory and a nearby point. We

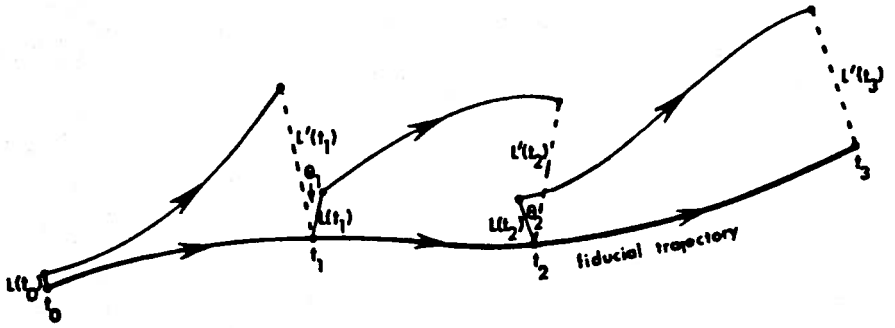

Figure D.2: Lyapunov exponent from a time series replacement (Wolf, et al., (1985))

follow these points until they have sufficiently diverged. We then search the data file for a replacement point and trajectory. The replacement must be sufficiently close to the first points current position along the fiducial trajectory and have a minimum orientation error (see Figure D.2). The formula to estimate the largest Lyapunov exponent is as follows (Wolf, et al., (1985)),

$$\lambda_1 \approx \frac{1}{t_m - t_0} \sum_{k=1}^{M} \log_2 \frac{L'(t_k)}{L'(t_{k-1})}. \tag{D.9}$$

The figure (Figure D.2) shows how the points evolve with time and how replacements are selected.

Relationship to Lyapunov dimension

As stated previously, the repeated stretching and folding of a given phase volume due to the presence of Smale horseshoes in the phase space or Poincaré map results in a fractal like character of basin boundaries to maps of initial conditions. A way to characterize the fractal nature of the non-simple basin boundaries is the so-called fractal dimension. While simple objects have integer dimensions, fractal objects

have non-integer dimensions. For example, a point has dimension zero, a line has dimension one, an area has dimension two and a volume dimension three. However, a fractal object may densely but not completely fill a given area or volume. The fractal dimension measures how filled a certain volume is with trajectories. A simple geometric construction and formula to determine fractal dimension is

$$d = \lim_{\epsilon \to 0} \frac{\log(N(\epsilon))}{\log(1/\epsilon)}. \tag{D.10}$$

Where N is the number of square boxes with dimension on the side of ϵ required to cover a given attractor. As the boxes get smaller and smaller the ratio converges to an accurate measure of the fullness of the attractor.

It has been conjectured by Kaplan and Yorke (Froehling, et al., (1980)) that the relationship between the dynamic Lyapunov spectrum of exponents and the static information or fractal dimension is as follows,

$$d_f = j + \frac{\sum_{i=1}^{j} \lambda_i}{|\lambda_{j+1}|} \tag{D.11}$$

Where is j is defined as follows,

$$\sum_{i=1}^{j} \lambda_i > 0. \tag{D.12}$$

Recall that the exponents are ordered from largest to smallest. This means that, j is the sum of positive (with zero defined to be positive) exponents divided by the next smallest.

APPENDIX E

Modification to the Righting Arm Curve

From hydrostatics, we know that the height of the center of gravity is related to the initial slope of the righting arm curve GM and the shape of the righting arm curve $GZ(\phi)$ (Rawson and Tupper, (1978)). For a constant displacement [1] and only changes in the height of the center of gravity, we can derive any righting arm curve from the reference righting arm curve as follows,

$$GZ_{new}(\phi) = GZ_{ref}(\phi) - G_{new}G_{ref}sin(\phi). \tag{E.1}$$

In order to modify the vessel's righting arm curve, we determine the static effect of the water-on-deck by using the classical hydrostatic approximation to the effect of slack liquid tanks. This approximation is exact, at the zero frequency limit. It neglects the effect of water on flow or off flow either through the scuppers or over the bulwark tops. This approximation also neglects the effect of deck exposure. Considering all the approximations, the amount of water is small so that its weight is small with respect to the vessel's displacement. The motion is slight (infinitesmally small) so that the nonlinear effects of water over the bulwark top or deck exposure are neglected.

First, we determine the decrease in metacentric height due to the added weight of the water-on-deck. From hydrostatics (Rawson and Tupper, (1978)), it is as follows,

---

[1] This is approximately true when a small quantity water comes aboard

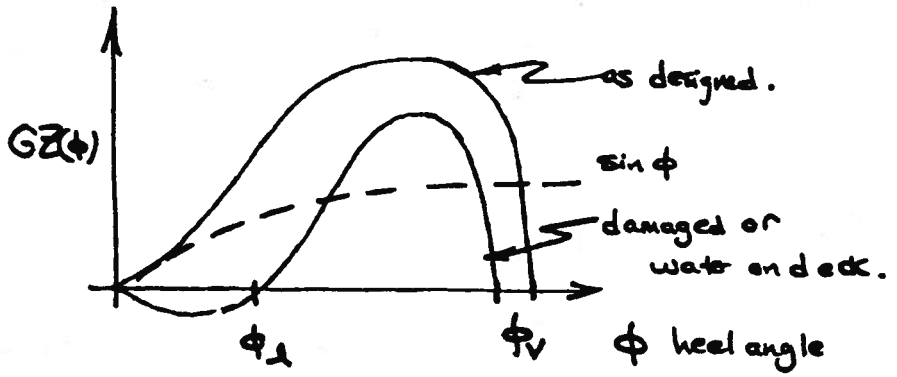

Figure E.1: Derivation of modified righting arm curve from reference

$$\delta GM_w = \frac{gw}{\Delta + w} \tag{E.2}$$

where g is the distance of the water centroid above the vessel center of gravity.

Second, we determine the decrease of metacentric height due to the water-on-deck's off-center moment as the vessel heels. Recall, this linear approximation neglects water spilling over the bulwark top and the water exposing the deck. This decrease in metacentric height is,

$$\delta GM_I = \frac{I_l}{\nabla_s}, \tag{E.3}$$

where I_l is the transverse area moment of inertia of the planform of the water-on-deck.

BIBLIOGRAPHY

BIBLIOGRAPHY

[1] Abkowitz, MA, *Stability and Motion Control of Ocean Vehicles*, MIT Press, Cambridge, 1969.

[2] Adee, HB and Pantazopoulos, MS, "Experimental Study of a Vessel Response in Waves with Water Trapped on Deck," *Third International Conference on the Stability of Ships and Ocean Vehicles*, Sept. 1986, Gdansk, Poland.

[3] Alligood, KT and Yorke, JA,"Fractal Basin Boundaries and Chaotic Attractors", in *Chaos and Fractal: the Mathematics behind the Computer Graphics*, ed. Devany and Keen, American Mathematical Society, 1988.

[4] Andronov, AA, Vitt, AA and Khaikin, SE, *Theory of Oscillators*, Pergamon, New York, 1966, (re-published by Dover, 1980).

[5] Ariaratnam, ST and Xie, WC,"Chaotic Motion under Parametric Excitation", *Dynamics and Stability of Systems*, Vol.4, No.2, 1989.

[6] Arnold, VI *Geometrical Methods in the Theory of Ordinary Differential Equations, Second Edition*, Springer Verlag, New York, 1988.

[7] Arnold, VI, Lectures on Singularity and Bifurcation Theory at the University of Michigan, and prior private discussion, April 3-4, 1990.

[8] Beck, RF, "Ship Motions in Regular Waves," *Principles of Naval Architecture*, Chapter VII, SNAME, New York, 1989.

[9] Beck, RF and Troesch, AW, "Department of Naval Architecture and Marine Engineering Student's Documentation and User's Manual for the Computer Program SHIPMO," Report No. 89-2, Ann Arbor, MI. 1989.

[10] Berge, P, Pomeau, Y and Vidal, C, *Order within Chaos*, John Wiley, New York,1984.

[11] Bishop, RED., Bucher, RK and Price, WG,"The Use of Functional Analysis in Ship Dynamics," *Proceedings of the Royal Society of London*, Series A, Vol.232., 1973.

[12] Blocki, W, "Ship Safety in Connection with Parametric Resonance of the Roll," *International Shipbuilding Progress*, February 1980.

[13] Bovet,, DM, Johnson, RE and Jones, EL, "Recent Coast Guard Research into Vessel Stability", *SNAME Marine Technology*, October 1974

[14] Braathen, A, *Application of a Vortex Tracking Method to the Prediction of Roll Damping of a Two-dimensional Floating Body*, PhD Dissertation, Division of Marine Hydrodynamics, The Norwegian Institute of Technology, The University Of Tronheim, 1987.

[15] Brook, K, "The Role of Simulation in Determining the Roll Response of a Vessel in an Irregular Seaway," *Proceedings of the Second International Conference on the SAFESHIP Project: Ship Stability and Safety* London, June 9 and 10, 1986.

[16] Caglayan, IH, "Water-on-deck: A Theoretical and Experimental Study," *SNAME, Texas*, 1985.

[17] Caldeira-Savaiva, F, "The Boundedness of a Lienard Equation Arising in the Theory of Ship Rolling," *IMA Journal of Applied Mathematics*, Vol. 36, 1986.

[18] Carr, J., *Applications of Centre Manifold Theory*, Applied Mathematical Sciences Series, No. 35, Springer-Verlag, New York, 1986.

[19] Cardo, A, Francescutto, A, and Nabergoj, R, "On the Maximum Amplitudes in Nonlinear Rolling" *Second International Conference on the Stability of Ships and Ocean Vehicles*, Sept. 1982, Tokyo.

[20] Cardo, A, Francescutto, A, and Nabergoj, R, "Ultaharmonics and Subharmonics in the Rolling Motion of a Ship Steady state Solution" *International Shipbuilding Progress*, Vol. 28,.

[21] CCMemo407, *Numerical Analysis and Applications Software Abstracts (NAAS)*, The University of Michigan Computing Center, Ann Arbor, September, 1979.

[22] Coast Guard, *Marine Casuality Report M/V Joan La Rie* , US Coast Guard (USCG), June 1984, p.14.

[23] Dahle, E and Kjaerland, O, "The Capsizing of the M/S Helland-Hansen (The Investigation and Recommendations for Preventing Similar Accidents)," *RINA Transactions*, 1979.

[24] Dahle, E and Kjaerland, O, "Probability of Capsizing in Steep Waves from the Side in Deep Water," *Third International Conference on the Stability of Ships and Ocean Vehicles*, Sept. 1986, Gdansk, Poland.

[25] Dalzell, JF "A Note on the Form of Ship Roll Damping," *SNAME Journal of Ship Research*, September 1978.

[26] DeKat,JO and Paulling, JR, "The Simulation of Ship Motions and Capsizing in Severe Seas", *SNAME 1989 Annual Meeting*, New York, November 1989.

[27] Dillingham, JT, *Motion Prediction of a Vessel with Shallow water-on-deck*, PhD Dissertation, Dept. of Naval Architecture, University of California, Berkeley, 1979.

[28] Dillingham, JT, "Motion Studies of a Vessel with water-on-deck," *SNAME Marine Technology*, vol. 18, No. 1, Jan 1981.

[29] Dillingham, JT, and Falzarano, JM, "A Numerical Method for Three-Dimensional Sloshing," *SNAME STAR*, May 1986, Portland, OR.

[30] Dillingham, JT and Falzarano, JM, "Three-Dimensional Simulation of Green water-on-deck," *Third International Conference on the Stability of Ships and Ocean Vehicles*, Sept. 1986, Gdansk, Poland.

[31] Doedel, E, *AUTO: Software for Continuation and Bifurcation Problems in Ordinary Differential Equations*, Pasadena, 1986.

[32] Eckmann, JP and Ruelle, "Erogodic Theory of Chaos and Strange Attractors," *Review of Modern Physics*, Vol.57 No.3, part I, July 1985.

[33] Elsimaillaway, N and Miller, NS, "Time Simulation of Ship Motions a Guide to Factors Degrading Stability," *SNAME Transactions*, 1987.

[34] Falzarano, JM, *NA625 Seminar: Predicting Complicated Dynamics Leading to Vessel Capsizing*, University of Michigan, February, 14, 1989.

[35] Falzarano, JM, *Nonlinear Aspects of Ship Dynamic Stability Phase I Final Report*, Department of Naval Architecture, University of Michigan, December 1988.

[36] Falzarano, JM, *Nonlinear and Coupled Aspects of Ship Dynamic Stability*, PhD Prospectus, Department of Naval Arcitecture and Marine Engineering, the University of Michigan, September 1987, pp.3-6, pp.15-16.

[37] Froehling, H, Chrutchfield, JP, Farmer, D, Packard, NH, and Shaw, R, "On Determining the Dimension of Chaotic Flows," *Physica 3D*, 1981.

[38] Gilbert, RR and Card, JC, "The New International Standard for Subdivsion and Damage Stability of Dry Cargo Ships," *SNAME Marine Technology*, Vol 27, No. 2, March 1990.

[39] Grochowalski, S, "Investigation into the Physics of Ship Capsizing by Combined Captive and Free-running Model Tests," *SNAME Annual Meeting*, New York, November 1989.

[40] Grebogi, Ott and Yorke, "Chaotic Attractors in Crises," *Physical Review Letters*, Vol.48, No.22, 1982.

[41] Grebogi, Ott and Yorke, "Crises, Sudden Changes in Chaotic Attractors and Transient Chaos," *Physica 8D*, 1983.

[42] Grebogi, Ott and Yorke, "Basin Boundary Metamorphasis: Changes in Accessible Boundary Orbits," *Physica 24D*, 1987.

[43] Greenspan, B.D. and Holmes, P.J. "Homoclinic Orbits, Subharmonic and Global Bifurcations in Forced Oscillations," *Nonlinear Dynamics and Turbulence*, ed. Iooss and Joseph, Pitman, 1982.

[44] Guckenheimer, J and Holmes, P, *Nonlinear Oscillations, Dynamical Systems and Bifurcations of Vector Fields*, Applied Mathematical Sciences Series, No. 54, Springer-Verlag, New York, 1986.

[45] Hale, J *Ordinary Differential Equations*, Wiley, New York, 1969, (re-published by Krieger, 1980).

[46] HaQuang, N. and Mook, D.T., "A Nonlinear Analysis of the Interactions Between Parametric and External Excitations", *Journal of Sound and Vibration*, Vol. 118, No. 3, 1987.

[47] Hayashi, C,*Nonlinear Oscillations in Physical Systems*, McGraw-Hill, New York, 1964, (re-published by Princton Univerity Press, 1985.

[48] Himeno, Y, "Prediction of Ship Roll Damping: State-of-the-Art," The University of Michigan, *Department of Naval Architecture and Marine Engineering, Report number 239*, Ann Arbor, MI, September 1981.

[49] Holmes, P.J., "Nonlinear Oscillations and the Smale Horseshoes Map", in *Chaos and Fractal: the Mathematics behind the Computer Graphics*, ed. Devany and Keen, American Mathematical Society, 1988.

[50] Holmes, C and Holmes, PJ "Second Order Averaging and Bifurcations to Subharmonics in Duffing's Equation", *Journal of Sound and Vibration*, Vol. 78, 1981.

[51] Holmes, P and Whitley, D "On the Attracting Set for Duffing's Equation I: Analytical Method for Small Force and Damping," *Research Notes in Mathematics #101, Partial Differential Equations and Dynamical Systems*, Longman, 1983.

[52] Holmes, P and Marsden, J, "A Partial Differential Equation with Infinitely Many Periodic Orbits: Chaotic Oscillations of a Forced Beam," *Archives of Rational Mechanics and Analysis*, Vol. 76, 1981.

[53] Hsu, CS, *Cell to Cell Mapping: A Method of Global Analysis for Nonlinear Systems*, Applied Mathematical Sciences Series, No. 64, Springer-Verlag, New York, 1986.

[54] InterCAD, *STAAF (Stability Analysis of Arbitrary Forms) User's Manual*, Annapolis, MD, 1983.

[55] Jons, O, Fuller, G and Letorneau, R, "Fishing Vessel Stability: A Case Study for Operator Guidance and Involvement," *SNAME Transactions*, 1987.

[56] Jordan, DW and Smith, P, *Ordinary Differential Equations (Second Edition)*, Oxford University Press, New York, 1987.

[57] Kerwin, JE, "Notes on Rolling in Longitudinal Waves," *International Shipbuilding Progress*, Vol.2, No.16, 1955.

[58] Li, GX and Moon, FC"Criteria for Chaos of a Three-well Potential Oscillator with Homoclinic and Heterclinc Orbits," *Journal of Sound and Vibration* Vol. 136, 1990.

[59] Ling, FH, "On the Melnikov's Method," *Zeitschrift Fur Angewandte Mathematik Und Mechanik*, 1987, p. T107.

[60] Marsden, J, *EECS 760 Seminar: Nonlinear Dynamics Fundamentals and Open Problems*, University of Michigan, Jan 17, 1989, and prior private discussion.

[61] McCrieght, WC, "Ship Maneuvering in Waves," *Sixteenth Symposium on Naval Hydrodynamics*, Berkeley, 1986.

[62] Melnikov, VK, "On the Stability of the Center for Time-Periodic Perturbations," *Transactions of the Moscow Mathematical Society*, 1963.

[63] Minorsky, N, *Nonlinear Oscillations*, Van Nostrand, Princton, 1962, (re-published by Krieger, 1983).

[64] Mitropolsky, YA, *Problems of the Asymptotic Theory of Nonstationary Vibrations*, Israel Program for Scientific Translations, Jerusalem, 1965, (published in the United States by Daniel Davey and Co., New York).

[65] Moon, FC, "Experimental Models for Strange Attractors Vibrations in Elastic Systems," *New Approaches to Nonliner Problems in Dynamics*, ed. PH Holmes, SIAM, Pacific Grove, 1980.

[66] Moon, FC, *Chaotic Vibrations: An Introduction for Applied Scientists and Engineers*, Wiley, 1988.

[67] Morozov, A.D., "Approach to a Complete Qualitative Study of Duffing's Equation", *USSR Computational Mathematics and Mathematical Physics*, Vol. 13, No. 5, 1973.

[68] Morozov, A.D., "A Complete Qualitative Investigation of Duffing's Equation", *Differential Equations*, Vol. 12, 1976.

[69] Mosley, H, "On the Dynamical Stability and the Oscillations of Floating Bodies" *Philosophical Transactions of the Royal Society of London*, 1850.

[70] Marshall, L.R., Nayfeh, A.H. and Mook, D.T., "Forward Speed Effects in the Equations of Ship Motion," *Journal of Sound and Vibration*, Vol.85, No.5, 1982.

[71] The Mathlab Group,*MACSYMA Reference Manual:Version Ten*, Laboratory for Computer Science MIT, Cambridge, 1983.

[72] Namachchivaya, NS and Hilton, HH, "Chaotic Motion of a Forced Nonlinear Oscillator," *Canadian Mathematical Society Conference Proceedings*, Vol.8, 1987.

[73] National Transportation Safety Board (NTSB), "Grounding and Capsizing of the Clam Dredge Patti-B," *NTSB Marine Accident Report*, 1979.

[74] Marshall, LR, Nayfeh, AH and Mook, DT, "Forward Speed Effects in the Equations of Ship Motion," *Journal of Sound and Vibration*, Vol. 85, 1973.

[75] Nayfeh, AH and Khedir, AA, "Nonlinear Rolling of Biased Ships in Regular Beam Waves," *International Shipbuilding Progress*, April 1986.

[76] Nayfeh, AH and Khedir, AA, "Nonlinear Rolling of Biased Ships in Regular Beam Waves," *Dynamical Systems Approaches to Nonliner Problems in Systems and Circuits*, ed. Salamm and Levi, SIAM, Henniker,1988.

[77] Nayfeh, AH and Sanchez, NE, "Chaos and Dynamic Instability in the Rolling Motion of Ships," *Seventeenth Symposium on Naval Hydrodynamics*, The Hague, 1988.

[78] Nayfeh, AH and Sanchez, NE "Stability and Complicated Rolling Responses of Ships in Regular Beam Seas", to be published in *International Shipbuilding Progress*, 1990.

[79] Newman, JN, *Marine Hydrodynamics*, MIT Press, Cambridge, MA, 1977,

[80] Odabassi, AY, "Ultimate Stability of Ships," *RINA Transactions*, 1977.

[81] Ozkan, IR, "Total (Practical) Stability of Ships," *Ocean Engineering* Vol. 8, No. 6, 1981.

[82] Papoulias, FA and Bernitsas, MM, "Stability of Motions of Moored Ocean Vehicles," *Dynamics and Stability of Systems,* Vol.1, No.4, 1986.

[83] Papoulias, FA and Bernitsas, MM, "Autonomous Oscillations, Bifurcations, and Chaotic Response of Moored Vessels," *SNAME Journal of Ship Research,* Vol.32, No.3, 1988.

[84] Papoulias, FA, "A Qualitative and Quantitative Study of Steady-State Response of Towed Floating Bodies," *Dynamics and Stability of Systems,* Vol.3, No.3 & 4, 1986.

[85] Parker, TS, "Overview of INSITE," Berkeley, California, 1989

[86] Parker, TS and Chua, LO, "Chaos: A Tutorial for Engineers," *Proceedings of the IEEE Special Issue on Chaotic Systems*, ed. Chua, Vol. 75, No.8, 1987.

[87] Parker, TS and Chua, LO, "INSITE: A Software Toolkit for the Analysis of Nonlinear Dynamical Systems," *Proceedings of the IEEE Special Issue on Chaotic Systems*, ed. Chua, Vol. 75, No.8, 1987.

[88] Parker, TS and Chua, LO, *Practical Numerical Algorithms for Chaotic Systems*, Springer-Verlag, New York, 1989.

[89] Parsons, MG, *Deparment of Naval Architecture and Marine Engineering, The Univerity of Michigan*, private discussion, Ann Arbor, 1990.

[90] Paulling, JR, and Rosenberg, RM, "On Unstable Ship Motions Resulting From Nonlinear Coupling," *SNAME Journal of Ship Research*, June 1959.

[91] Paulling, JR,, "The Transverse Stability of a Ship in a Longitudinal Seaway," *SNAME Journal of Ship Research*, March 1961.

[92] Paulling, JR, et al., "Ship Motions and Capsizing in Astern Seas," *Tenth ONR Symposium on Naval Hydrodynamics*, Cambridge, 1974.

[93] Paulling, JR, et al., "Model Tests and Numerical Simulations of Ship Capsizing in Following Seas," Final Report to US Coast Guard, 1979.

[94] Rawson, KJ and Tupper, EC, *Basic Ship Theory, Volume I*, Longman, New York, 1976.

[95] Rom-Kedar, V and Wiggins, S, "Transport in Two-dimensional Maps", *Archives of Rational Mechanics*, Vol. 109, Number 3.

[96] Rom-Kedar, V, Leonard, A. and Wiggins, S., "An Analytical Study of Transport, Mixing and Chaos in an Unsteady Vortical Flow," to be published in *Journal of Fluid Mechanics*, 1990.

[97] Rudowski, J and Szemplinska-Stupnicka, W, "On an Approximate Criterion for Chaotic Motion in a model of a Buckled Beam," *Ingenieur-Archives*, Vol.57, 1987.

[98] Schmidt, G and Tondl, A *Nonlinear Oscillators*, Cambridge University Press, Cambridge, 1986.

[99] Sharma, SD, Jiang, JT, and Schellin, TE, "Dynamic Instability and Chaotic Motion of a Single-Point-Moored Tanker," *Seventeenth Symposium on Naval Hydrodynamics*, The Hague, 1988.

[100] Schmiechen, M, *On State Space Models and Their Application to Hydromechanic Systems*, Department of Naval Architecture, University of Tokyo, 1973.

[101] Schuster, HG, *Deterministic Chaos*, Physik-Verlag, Weinheim, FRG, 1984.

[102] Seydel, R, *From Equilibrium to Chaos: Practical Bifurcation and Stability Analysis*, Elsevier, New York, 1988.

[103] Seydel, R, *BIFPACK:A Program Package for Continuation, Bifurcation and Stability Analysis*, University of Wuezburg, 1988a.

[104] Shahruz, S.M. and Ma, F "Approximate Decoupling of the Equations of Motion of Linear Underdamped Systems," *Transactions of ASME, Journal of Applied Mechanics*, September, 1988.

[105] Shaw, S. and Wiggins, S., "Chaotic Motion of a Whirling Pendulum," *Physica 31D*, 1988.

[106] Shaw, S., *Mechanical Engineering Department, Michigan State University*, private discussion, East Lansing, 1989-90.

[107] Stiendl, A., *Institute for Mechanics, Vienna Technical University*, private discussion, Vienna, May and June, 1989.

[108] Szemplinska-Stupnicka, W., "Chaotic and Regular Motion in Nonlinear Vibrating Systems," in *Chaotic Motions in Nonlinear Dynamical Systems*, ed. Szemplinska-Stupnicka, Iooss, and Moon, Springer-Verlag, 198X.

[109] Szemplinska-Stupnicka, W., "Bifurcations of Harmonic Solutions Leading to Chaotic Motion in Softening Type Duffing's Oscillator," *International Journal Of Nonlinear Mechanics*, Vol.23, No.4.

[110] Takezawa, S and Hirayama, T, "On the Dangerous Complex Environmental Conditions to the Safety of a Moored Semi-Submersible," *Third International Conference on the Stability of Ships and Ocean Vehicles*, Sept. 1986, Gdansk, Poland.

[111] Thelander, J.A., *Aircraft Motion Analysis*, USAF Flight Dynamics Laboratory, Wright-Patterson Air Force Base, 1964.

[112] Thompson, JMT, and Stewart, HB, *Nonlinear Dynamics and Chaos*, Wiley, New York, 1986.

[113] Thompson, JMT, Bishop, SR and Leung, LM, "Fractal Basin Boundaries and Chaotic Bifurcations Prior to Escape From a Potential Well," *Physics Letters A*, Vol. 121, No. 3, 1987.

[114] Thompson, JMT, "Chaotic Phenomena Triggering the Escape from a Potential Well," *Proceedings of the Royal Society of London*, Vol. A, 421, 1989.

[115] Thompson, JMT, "Loss of Engineering Integrity due to the Erosion of Absolute and Transient Basin Boundaries", *IUTAM Symposium, Nonlinear Dynamics in Engineering Systems*, August 1989.

[116] Thompson, JMT, and Ueda, Y, "Basin Boundary Metamorphasis in the Canonical Escape Equation," *Dynamics and Stability of Systems*, Vol. 4, No. 3 and 4, 1989.

[117] Troesch, AW, *Naval Architecture 440, Ship Dynamics II: Course Notes*, The University of Michigan, Department of Naval Architecture and Marine Engineering, Ann Arbor, MI, September 1986.

[118] Troesch, AW, *Department of Naval Architecture and Marine Engineering, The Univerity of Michigan*, private discussion, Ann Arbor, 1989-90.

[119] Troger, H., *Institute for Mechanics, Vienna Technical University*, private discussion, Vienna, May and June, 1989.

[120] Troger, H. and Stiendl, A., *Nonlinear Stability and Bifurcation Theory: An Introduction For Engineers and Scientists*, to be published Springer-Verlag, Vienna, 1990.

[121] Vinge, T and Brevig, P "Nonlinear Two-dimensinal Ship Motions," *RINA Ocassional Publication No. 5, Seminar on the Norwegian Ships in Rough Seas Project*, London, 1982.

[122] Virgin, LN, "The Nonlinear Rolling Response of a Vessel Including Chaotic Motions Leading to Capsize in Regular Seas," *Applied Ocean Research*, Vol. 9, No. 2, 1987.

[123] Virgin, LN, "Approximate Criterion for Capsize Based on Deterministic Dynamics" *Dynamics and Stability of Systems,* Vol.4, No.1, 1989.

[124] Vugts, JH, *The Hydrodynamic Forces and Ship Motion in Waves*, Ph.D. Dissertation at The Technical University of Delft, Ship Building Department, Delft, October 1970.

[125] Webster, W, "The Transverse Motions," *Principles of Naval Architecture*, Chapter VII, SNAME, New York, 1989.

[126] Wiggins, S, *Global Bifurcations and Chaos (Analytical Methods)*, Applied Mathematical Sciences Series, No. 73., Springer-Verlag, New York, 1988.

[127] Wiggins, S, *Introduction to Applied Nonlinear Dynamical Systems and Chaos*, to be published Springer-Verlag, Texts in Applied Mathematics, Vol. 2, New York, 1990.

[128] Wiggins, S. and Shaw, S., "Chaos and Three-dimensional Horseshoes in Slowly Varying Oscillators," *Transactions of ASME, Journal of Applied Mechanics*, December, 1988.

[129] Wolf, A, Swift, JB, Swinney, HL, and Vastano, JA, "Determining Lyapunov Exponents from a Time-Series," *Physica 17D*, 1985.

[130] Yagasaki,K., Sakata, M. and Kimura, K., "Dynamics of a Weakly Nonlinear System Subjected to Combined Parametric and External Excitation," *Transactions of ASME, Journal of Applied Mechanics*, March, 1990.

[131] Zeeman, EC, *Catastrophe Theory: Selected Papers*, Reading, MA, Addison-Wesley, 1977, pp.441-493.